THE EFFECT OF PORE DIMENSION OF ZEOLITES ON THE SEPARATION OF GAS MIXTURES

A Dissertation
Presented to
The Academic Faculty

by

SANG EUN JEE

In Partial Fulfillment
of the Requirements for the Degree of
DOCTOR OF PHILOSOPHY in the
School of Chemical and Biomolecular Engineering

Georgia Institute of Technology
May, 2010

THE EFFECT OF PORE DIMENSION OF ZEOLITES ON THE SEPARATION OF GAS MIXTURES

Approved by:

Dr. David S. Sholl Advisor
School of Chemical & Biomolecular Engineering
Georgia Institute of Technology

Dr. Sankar Nair
School of Chemical & Biomolecular Engineering
Georgia Institute of Technology

Dr. Ronald Chance
School of Chemical & Biomolecular Engineering
Georgia Institute of Technology

Dr. Seung Soon Jang
Materials Science and Engineering
Georgia Institute of Technology

Dr. Martha Grover
School of Chemical & Biomolecular Engineering
Georgia Institute of Technology

Date Approved: March 31, 2010

ACKNOWLEDGEMENTS

First and foremost I offer my sincerest gratitude to my supervisor, Dr. David Sholl who has supported me throughout my thesis with his patience and knowledge. I attribute the level of my research during PhD to his encouragement and effort and this thesis would not have been completed or written without him.

I also want to thank to our group members, who helped me to develop technical skills and supported my research through helpful discussion. I appreciate technical help from David Newsome, Haibin Chen and helpful discussion with Seda Keskin, Ji Zhang and Taku Watanabe. Most of all, I wish to express my gratitude to the group members came from Carnegie Mellon together, who shared most of the meaningful time together.

Because I have moved following my advisor, I could make good friends at two distant cities, Pittsburgh and Atlanta. I would like to appreciate the emotional support from my classmates at CMU, Jing Cho, Wingki Lee, Jas Cheong, who shared most of the time until I finish coursework and other friends at Pittsburgh, Ildoo Kim, Minkyung Lee, Jueun Lee, Nayoung Kim, Jaewon Kang, Byungeun Yoo and Joshua Foster who supported me to overcome challenging moment in my graduate school life.

Special thanks to Hyewon and Hyea, who have supported me in every aspect in Atlanta. Without their effort to comfort me especially before my defense, I could not successfully finish the phD. From my heart, I want to say thanks to my sister-like friends.

I want to send many thanks to my parents in South Korea who has been supporting me with love. At last, I owe my deepest gratitude to my husband, Yunseong Song, who was with me at the most difficult time in my life and helped me to overcome the biggest challenges.

TABLE OF CONTENTS

LIST OF TABLES

LIST OF FIGURES

SUMMARY

We examined the effect of the pore dimension of zeolites on the separation of gas mixtures using atomistic simulation methods. We studied two categories of the zeolites with small pores: pore modified silicalite for H_2/CH_4 separation and small pore silica zeolites for CO_2/CH_4 separation. The effect of pore modification of silicalite on the H_2/CH_4 separation was examined. Under some degrees of surface modification, the CH_4 flux was reduced much more than the H_2 flux, resulting in high ideal selectivities. The use of small pore zeolites for CO_2/CH_4 separations was studied. In DDR, we showed that CO_2 diffusion rates are only weakly affected by the presence of CH_4, even though the latter molecules diffuse very slowly. Consequently, therefore, the permeance of CO_2 in the equimolar mixtures is similar to the permeance for pure CO_2, while the CH_4 permeance in the mixture is greatly reduced relatively to the pure component permeance. The calculated CO_2/CH_4 separation selectivities are higher than 100 for a wide range of feed pressure, indicating excellent separation capabilities of DDR based membranes. Inspired by the observation in DDR we also examined the separation capabilities of 10 additional pure silica small pore zeolites for CO_2/CH_4 separations. From these considerations, we predict that SAS, MTF and RWR will exhibit high separation selectivities because of their very high adsorption selectivities for CO_2 over CH_4. CHA and IHW, which have similar pore structures to DDR, showed comparable separation selectivities to DDR because of large differences in the diffusion rates of CO_2 and CH_4.

CHAPTER 1

INTRODUCTION

1.1 SEPARATION PROCESS USING ZEOLITES

Separation is a process that transforms a mixture of substances into two or more products that differ in chemical properties or some physical properties, such as size[1]. Separation processes are essential to the specialty chemical industries, petroleum refining, and materials processing industries and development of the advanced separation technologies are critical for reducing waste, improving energy efficiency, and increasing the efficiency of raw material use.[2]

Membranes are competitive chemical separation technology in many applications. Membranes require low energy consumption compared to other separation methods such as distillation[3]. Membrane based separation is an ideal candidate for an environmentally friendly and energy efficient separation process. Membranes use different adsorption and diffusion rates of permeating molecules to permit size and shape selectivity. Porous membranes have been fabricated using many materials, including polymers, zeolites, carbon nanotubes and metal organic frameworks.

In this thesis, we will consider the zeolites as a separation membrane. Zeolites are common class of inorganic materials that possess ordered atomic-scale porous networks.[4] Natural zeolites form where volcanic rocks and ash layers react with alkaline groundwater but they are rarely pure and are frequently contaminated by other minerals, metals, quartz, or other zeolites[5]. For this reason, naturally occurring zeolites are excluded from many important commercial applications. There are a large number of synthetic zeolites. Synthetic zeolites are formed under hydrothermal conditions with sol-gel crystallization from alumino-silicalite solutions with organic substances.

Zeolites have several beneficial properties as a separation membrane. They have ordered crystalline structures with pore diameters less than a nanometer. Zeolites are typically thermally, mechanically very stable. For these reasons and others, membranes made from zeolites have been extensively studied as attractive devices for gas and liquid phase separations[6]. In this thesis, we will examine the separation ability of specific zeolite topologies using atomistic simulation methods.

1.2 ZEOLITES WITH VARIOUS TOPOLOGIES

The structure of the zeolites plays a key role in the separation procedure of the gas mixtures. In molecular transport, through a membrane, adsorption and diffusion both contribute to determining the flux of the given species. Therefore, to achieve high separation selectivities, it would be useful to find out the specific zeolite topologies among the large number of zeolites that are known for which the adsorption and diffusion rates of the permeating molecules differ significantly. One significant factor that can make a big difference in the diffusion rates of two species is the pore size of the zeolite structures.

Table 1.1 shows a classification of zeolite frameworks based on their biggest oxygen member ring sizes. The pore size depends on the number of rings and the shape of the pores. Among the various frameworks, the MFI structure, which has 10-membered rings, has been the most widely studied [7-12]. However, the pore size of this framework is ~5.5 Å[13], which is too large to separate small molecules with similar sizes such as H_2/CH_4 or CO_2/CH_4. Thus, studies of small pore zeolites are critical for light gas separation. The use of the small pore frameworks such as surface modified zeolites or smaller pore zeolites have been explored by several studies [14-20] but their separation ability has not been fully understood. Therefore, in this thesis, we consider the pore modified MFI and small pore zeolite structures with 8 membered oxygen rings.

Biggest Ring	Second biggest ring				
	none	7-ring	8-ring	10-ring	12-ring
6-ring	AFG,AST,DOH,LIO, LOS,LTN,MEP,MTN, NON,SGT,SOD				
8-ring	ABW,AFT,ATN,ATV, AWW,BIK,CAS,EAB, JBW,LEV,ANA,ERI, ESV,KFI,PAU,RHO, ERI,UFI,MTF,RTE DDR,RWR,SAS,CHA LTA IHW	STT	AEI,APC,APD,ATT, BRB,EDI,GIS,GOO, MER,MON,PHI,THO, YUG,NAT,KFI,PAU, TSC,RHO,EPI,ITE, ITW		
9-ring	CHI		LOV		
10-ring	AEL,AFO,EUO,LAU, MTT,NES,PAR,TON, MEL		DAC,EPI,FER,HEU, MFS,STI,WEN	MFI	
12-ring	AFI,ATO,ATS,CAN, LTL,MTW,ROG,FAU	MEI	AFR,AFS,AFY,BPH, GME,MAZ,MOR,OFF	BOG	EMT, BEA
14-ring	AET				
18-ring	VFI				
20-ring			CLO		

Table 1.1: Pore size classification of the zeolite structure types using data from the overview of the pore sizes of the different structure types[21]

Pore modification of the widely used zeolites could be one good way to achieve high separation selectivities for small size molecules such as H_2. In chapter5, we use silicalite, which is pure silica form of ZSM-5(structure code MFI, space group Pnma). As mentioned before, the pore of the silicalite is too large to block the other small molecules mixed with H_2. Moreover, H_2 adsorption in zeolites is generally weaker than CO_2 or CH_4, two typical gases present during H_2 production. For this reason, various methods to reduce the pore openings can be considered to block the other small molecules from a membrane by increasing the membrane's surface resistances. In chapter 5 we present an atomistic model of this situation.

Small pore zeolites are materials consists of cages interconnected with narrow 8 membered oxygen rings with 3~4 Å diameters as shown in Table 1.1. One typical small pore zeolite is DDR[22]. The key characteristic of these small pore zeolites is that their very narrow windows could cause a large difference in diffusivities of two given species, resulting in high selectivities.

In this thesis, we consider 11 pure silica forms of small pore zeolites including DDR for CO_2/CH_4 separations. All of the zeolite forms were obtained from the XRD experimental data[23-31] and their window diameters vary from 2.2~4.2 Å. DDR is examined in detail in chapter 4 and 5 since it has been reported as a good material as a separation membrane. Additionally, based on the methodologies developed modeling in DDR, we examine the separation selectivities of all 11 small pore zeolites for CO_2/CH_4 separation in chapter 6.

1.3 TRANSPORT PROPERTIES OF GASES IN THE ZEOLITES USING MOLECULAR SIMULATION

Despite the large number of known synthetic zeolite structures, reproducible membranes can be synthesized and used only for a handful of different zeolite structures. Synthesizing and studying a zeolite membrane made of an arbitrary crystal structure is very difficult due to cost and time constraints. Thus, there is currently no experimental way to find which from the hundreds of different zeolite structures would perform optimally for a given separation. As a result, molecular simulation methods could play an important role in the examination of the separation abilities of the given zeolite structures.

For the extensive study of the separation abilities of nanoporous membranes, understanding the trends in the permeabilities and the selectivities of specific system is essential. The most widely used approaches for this outcome uses the well established methods of Grand Canonical Monte Carlo (GCMC) and Molecular Dynamics (MD) to measure the adsorption isotherm and molecular diffusivities of the species of interest.

These quantities are then used as parameters into a macroscopic transport model based on Fick's Law to make quantitative predictions of the permeance of membranes under practical conditions. Using this approach, there have been extensive studies of the separation selectivities in various nanoporous membranes such as large pore zeolites (silicalite, ZSM-5)[32-37], carbon nanotubes (CNTs)[38,39], metal organic frameworks (MOFs)[40-44] and alumino silicate materials[45].

Although the modeling approach outlined above has provided the reasonable predictions for variety of large pore membranes, it invoked a critical assumption regarding the interfaces between a nanoporous membrane and the surrounding bulk phases, that no mass transfer resistances for the adsorption into or desorption from the porous material[9,46]. In reality, however, the net transfer resistance for the molecules permeating through a crystalline membrane is a combination of the resistance arising from intracrystalline diffusion and the surface resistances associated with entering and leaving the membrane material. Moreover, for the pore modified silicalite, the key element to achieve high H_2/CH_4 separation selectivity is the blocking of the CH_4 molecules at the pore mouth, namely, high surface resistances.

To study pore modified silicalite, we used the Local Equilibrium Flux Method (LEFM) to measure the flux considering surface resistances. This method has provided the good predictions of the surface resistances of the silicalites[47,48]. To model the modified membranes, a modifying layer was constructed near the surface by adding the Si and O atoms with the specific criteria[49,50]. With given structures, the permeability and the ideal selectivities for H_2/CH_4 separation in the various pore modified silicalites have been calculated to examine the effect of the pore modification on the separation selectivities.

In the examination of the CO_2/CH_4 separation in the small pore zeolites, we have followed the modeling approaches outlined above but with modification to address two important issues. As we discussed in the previous section, the small size of the 8MR

windows in small pore zeolites lead too strong difference in the diffusivities of two species[51]. We show that the force-field currently used in the previous zeolites does not give accurate predictions of the single-component diffusion rates when compared to available experimental measurements. Therefore, for the reasonable predictions of the separation abilities of the entire small pore zeolites, the development of new forcefield is necessary which can describe all available experimental data. In this thesis we will present a new forcefield transferrable for small pore silica zeolites derived from the experimental single component adsorption isotherm and single component self diffusivities of the CH_4 and CO_2 molecules in the DDR structure.

Molecular Dynamics (MD) can readily predict the diffusivities of light gases for larger pore zeolites such as silicalite. However, for the small pore zeolites, the diffusivities of CH_4 molecules are slower than 10^{-8} cm^2/sec, meaning that this situation cannot be described properly using MD simulations. To address this issue, we formulated new Kinetic Monte Carlo (KMC) methods for the CO_2/CH_4 binary mixtures transport in the DDR structures. Hopping rates used as parameters in binary KMC are derived from Transition State Theory (TST) based calculations and the MD calculations for CH_4 and CO_2 at arbitrary loadings.

The overall aim of the entire thesis is to examine the transport properties of zeolites structures with different topologies to suggest if they are good separation materials for the specific gas mixtures. Our calculations point to the physical origin and characteristic factors that bring high separation selectivities, and ultimately help in charting a path for fabrication of the high selective membranes.

1.3 THESIS OUTLINE

In chapter 2, we explain the general computational methods used to measure transport properties of the gas mixtures in the zeolites in the thesis. This chapter describes the potential energy surface that defines the interaction between molecules and zeolite, measurement methods for the adsorption isotherm and diffusivities, and methods to calculate flux of the given species will be presented.

In chapter 3, the effect of pore modification of the silicalite on H_2/CH_4 separation is examined. The pore modified structures are described at various degree of modification using molecular simulation methods. With given structures, ideal selectivities and permeabilities of H_2/CH_4 are examined with the effect of the surface resistances on to the each species.

The separation ability of the small pore zeolites for CO_2/CH_4 separation will be discussed in the chapter 4 to chapter 6. First in chapter 4, a new forcefield which can reproduce all available experimental data for adsorption and diffusion will be introduced for CO_2 and CH_4 in DDR. The single and mixture component adsorption and single component diffusion properties are calculated using detailed calculation in the chapter 4. In chapter 5, we discuss the mixture component diffusion properties with new binary KMC methods formulated for this system. By calculating the flux and the selectivities, the separation abilities of DDR structures are addressed. From these examinations, we find which characteristic of the zeolite structures brings the high selectivities for CO_2/CH_4 separation.

With the observations from the study of the DDR, the separation selectivities for CO_2/CH_4 for 11 small pore zeolites are examined in the chapter 6. Chapter 7 summarizes our main findings.

REFERENCES

(1) Yang, R. T. *Gas Separation by Adsorption Processes*; Academic press: New York, 1997.

(2) Panel on Separation Technology for Industrial Reuse and Recycling; Committee on Industrial Technology Assessments; Commission on Engineering and Technical Systems; National Research Council *Separation Technologies for the Industries of the Future*; National Academies Press: New York, 1999.

(3) Baker, R. W. *Ind. Eng. Chem. Res.* **2002**, *41*, 1393.

(4) King, C. J. *Separation process*; Mcgraw-Hill College: Columbus, 1980.

(5) Auerbach, S. M.; Carrado, K. A.; Dutta, P. K. *Handbook of zeolite science and technology*; CRC Press: New York, 2003.

(6) McLeary, E. E.; Jansen, J. C.; Kapteijn, F. *Micropor. Mesopor. Mater.* **2006**, *90*, 198.

(7) Julbe, A.; Motuzas, J.; Arruebo, M.; Noble, R. D.; Beresnevicius, J. *Stud. Surf. Sci. Catal.* **2005**, *158*, 129.

(8) Motuzas, J.; Julbe, A.; Noble, R. D. *Microporous Mesoporous Mater.* **2006**, *92*, 259.

(9) Bowen, T. C.; Falconer, J. L.; Noble, R. D.; Skoulidas, A. I.; Sholl, D. S. *Ind. Eng. Chem. Res.* **2002**, *41*, 1641.

(10) Bowen, T. C.; Noble, R. D.; Falconer, J. L. *J. Membr. Sci.* **2004**, *245*, 1.

(11) Motuzas, J.; Julbe, A.; Noble, R. D.; Guizard, C.; Beresnevicius, Z. J.; Cot, D. *Microporous Mesoporous Mater.* **2005**, *80*, 73.

(12) Poshusta, J. C.; Noble, R. D.; Falconer, J. L. *J. Membr. Sci.* **1999**, *160*, 115.

(13) Olson, D. H.; Kokotailo, G. T.; Lawton, S. L.; Meier, W. M. *J. Phys. Chem.* **1981**, *85*, 2238.

(14) Hong, M.; Falconer, J. L.; Noble, R. D. *Ind. Eng. Chem. Res.* **2005**, *44*, 4035.

(15) Masuda, T.; Fukumoto, N.; Kitamura, M.; Mukai, S. R. *Microporous Mesoporous Mater.* **2001**, *48*, 239.

(16) Krishna, R.; van Baten, J. M. *Chem. Phys. Lett.* **2007**, *446*, 344.

(17) Krishna, R.; van Baten, J. M. *Sep. Purif. Technol.* **2008**, *61*, 414.

(18) Li, S. G.; Falconer, J. L.; Noble, R. D. *J. Membr. Sci.* **2004**, *241*, 121.

(19) Li, S. G.; Falconer, J. L.; Noble, R. D. *Adv. Mater.* **2006**, *18*, 2601.

(20) Poshusta, J. C.; Tuan, V. A.; Pape, E. A.; Noble, R. D.; Falconer, J. L. *Ind. Eng. Chem. Res.* **1998**, *37*, 3924.

(21) http://www.biw.kuleuven.be/pers/tomr/zeostruc.htm; Remans, T.: 1998.

(22) Gies, H. *Z. Kristallogr.* **1986**, *175*, 93.

(23) Calligaris, M.; Nardin, G.; Randaccio, L. *Zeolites* **1983**, *3*, 205.

(24) Cantin, A.; Corma, A.; Leiva, S.; Rey, F.; Rius, J.; Valencia, S. *J. Am. Chem. Soc.* **2005**, *127*, 11560.

(25) Camblor, M. A., Corma, A., Lightfoot, P., Villaescusa, L.A. and Wright, P.A. *Angew. Chem. Int. Ed.* **1997**, *36*, 2659.

(26) Yang, X. B.; Camblor, M. A.; Lee, Y.; Liu, H. M.; Olson, D. H. *J. Am. Chem. Soc.* **2004**, *126*, 10403.

(27) Gramlich, V.; Meier, W. M. *Z. Kristallogr.* **1971**, *133*, 134.

(28) Barrett, P. A.; Diaz-Cabanas, M.-J.; Camblor, M. A. *Chem. Mater.* **1999**, *11*, 2919.
(29) Marler, B.; Grunewald-Luke, A.; Gies, H. *Zeolites* **1995**, *15*, 388.
(30) Patinec, V., Wright, P.A., Lightfoot, P., Aitken, R.A. and Cox, P.A. *J.CHem.Soc.* **1999**, 3909.
(31) Camblor, M. A.; Diaz-Cabanas, M.-J.; Perez-Pariente, J.; Teat, S. J.; Clegg, W.; Shannon, I. J.; Lightfoot, P.; Wright, P. A.; Morris, R. E. *Angew. Chem. Int. Ed.* **1998**, *37*, 2122.
(32) Skoulidas, A. I.; Sholl, D. S. *J. Phys. Chem. B* **2001**, *105*, 3151.
(33) Skoulidas, A. I.; Sholl, D. S. *J. Phys. Chem. B* **2002**, *106*, 5058.
(34) Skoulidas, A. I.; Sholl, D. S. *J. Phys. Chem. A* **2003**, *107*, 10132.
(35) Skoulidas, A. I.; Sholl, D. S. *J. Phys. Chem. B* **2005**, *109*, 15760.
(36) Skoulidas, A. I.; Sholl, D. S.; Johnson, J. K. *J. Chem. Phys.* **2006**, *124*, 054708.
(37) Skoulidas, A. I.; Sholl, D. S.; Krishna, R. *Langmuir* **2003**, *19*, 7977.
(38) Chen, H.; Sholl, D. S. *J. Am. Chem. Soc.* **2004**, *126*, 7778.
(39) Skoulidas, A. I.; Ackerman, D. M.; Johnson, J. K.; Sholl, D. S. *Phys. Rev. Lett.* **2002**, *89*, 185901.
(40) Keskin, S.; Liu, J.; Johnson, K.; Sholl, D. S. *Langmuir* **2008**, *24*, 8254.
(41) Keskin, S.; Sholl, D. S. *J. Phys. Chem. C* **2007**, *111*, 14055.
(42) Keskin, S.; Sholl, D. S. *Energy Environ. Sci.* **2010**, *3*, 343.
(43) Keskin, S.; Liu, J.; Johnson, J. K.; Sholl, D. S. *Micropor. Mesopor. Mater.* **2009**, *125*, 101.
(44) Keskin, S.; Sholl, D. S. *Langmuir* **2009**, *25*, 11786.
(45) Zang, J.; Konduri, S.; Nair, S.; Sholl, D. S. *ACS Nano* **2009**, *3*, 1548.
(46) Takaba, H.; Koshita, R.; Mizukami, K.; Oumi, Y.; Ito, N.; Kubo, M.; Fahmi, A.; Miyamoto, A. *Journal of Membrane Science* **1997**, *134*, 127.
(47) Newsome, D. A.; Sholl, D. S. *J. Phys. Chem. B* **2005**, *109*, 7237.
(48) Newsome, D. A.; Sholl, D. S. *Microporous Mesoporous Mater.* **2008**, *107*, 286.
(49) Mukhopadhyay, A. B.; Oligschleger, C.; Dolg, M. *Phys. Rev. B* **2003**, *67*, 014106.
(50) Mukhopadhyay, A. B.; Oligschleger, C.; Dolg, M. *J. Phys. Chem. B* **2004**, *108*, 16085.
(51) Hedin, N.; DeMartin, G. J.; Roth, W. J.; Strohmaier, K. G. *Micropor. Mesopor. Mater.* **2008**, *109*, 327.

CHAPTER 2

COMPUTATIONAL METHODS

2.1 POTENTIAL ENERGY SURFACE

The fundamental quantity underlying an atomically-detailed description of molecules interacting with a nanoporous adsorbent is the potential energy surface. The potential energy surface for an adsorbed molecule is defined as the total potential energy felt by the guest molecule at a given position. In all of our calculations, the total potential energy is taken as the summation of individual pair-wise interactions between a guest molecule and all host atoms and other guest molecules. Usually the van der Waals interactions between adsorbate molecules are described using the Lennard-Jones (LJ) pair-wise potential:

$$U_{ij} = 4\varepsilon\left[\left(\frac{\sigma}{r_{ij}}\right)^{12} - \left(\frac{\sigma}{r_{ij}}\right)^{6}\right] \qquad (2.1)$$

Here, U_{ij} is the pair-wise potential energy, ε is an energy parameter that measures the well depth, σ is a distance parameter that characterizes the spacing between molecules, and r_{ij} is the distance between particles *i* and *j*. Figure 2.1 shows the shape of the LJ pair-wise potential as a function of the interparticle distance r_{ij}. As shown in this figure, a steep repulsive region is present at low intermolecular spacing while the minimum value of the potential occurs at intermediate r_{ij}. In Eq. (2.1), the first term describes the repulsive region while the second term shows the attractive region, making the overall well shape of the interacting potential. It is useful to note that the second term is derived from theoretical expressions of the London potential but the first term is chosen primarily for computational convenience to model the repulsive force. This potential has been used to model the adsorption and diffusion of the light gases in the silica zeolites[1-15], CNTs[16,17]

and MOFs[18-22]. In our molecular simulation, we treat CH_4 and H_2 molecules as spherical molecules defined by a single interaction center. CO_2 molecules are defined as linear molecule[23]. To describe the interactions between CO_2 molecules and zeolites, long distance electrostatic interactions are defined by

$$U_{ij}^{electro} = \frac{q_1 q_2}{r_{ij}^2} \qquad (2.2)$$

where $U_{ij}^{electro}$ is the pair-wise electrostatic interaction energy, q_i is the electrostatic charge of the *i* species. For CO_2-CO_2 interaction, q_i is chosen to reproduce the experimental quadrupole moment. The forces acting on a molecule due to pairwise potentials are defined by $\vec{F} = -\nabla U_{ij}$.

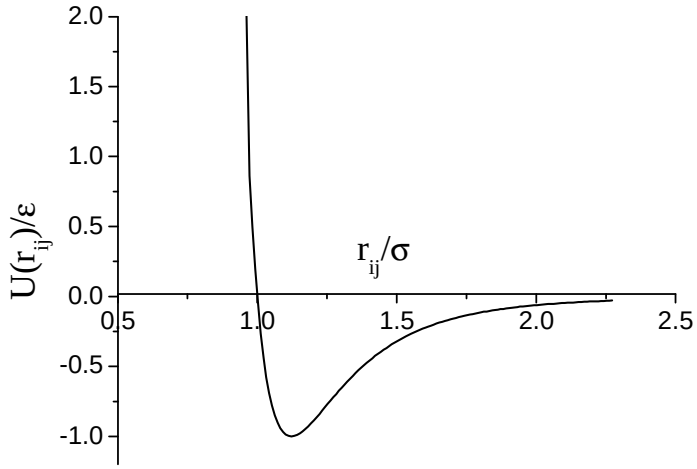

Figure 2.1: The Lennard-Jones pairwise potential as a function of the interparticle distance.

In molecular simulation, the most important underlying assumption is that potential energy surface can describe the molecular interactions, in other words, it can reproduce the all available experimental properties. Typically, the potential parameters are fitted to an experimental adsorption isotherm in an iterative scheme so that the entire

adsorption was matched with the simulation values. For CH_4, H_2 and CO_2, the parameters fitted on the silicalite structures have been widely used[5,24]. However, for small pore zeolite like DDR, these parameters are not transferrable because of its narrow 8MR windows. We will show in subsequent chapters that new potential parameters had to be developed to allow molecular simulations to agree with experimental data for this specific type of zeolite. We developed a new potential that can reproduce experimental Henry's constant, the heats of adsorption, the adsorption properties and diffusion properties. The details of force field parameterization will be discussed in the chapter 4.

In our calculations, the van der Waals interactions between the adsorbate molecules and the zeolite frameworks only included the framework O atoms of the zeolites. This simplification is possible because the interior of zeolites' pores closest to the adsorbate molecules are only O atoms[5,24]. In all calculation in this thesis, the zeolite was assumed to be rigid. This physically reasonable assumption greatly improves the computational efficiency of molecular simulations of these materials. Specifically, we used a pretabulated table and an interpolation scheme to rapidly compute the potential and forces due to adsorbate-zeolite interactions for each zeolite we studied.

2.2 MODELING ADSORPTION ISOTHERMS USING SIMULATION

Adsorption isotherms are calculated from atomistic simulations using Grand Canonical Monte Carlo (GCMC). This is well known as a successful method to describe the adsorption of the molecules in many materials, showing good agreement with the experiments[25-27]. This section will briefly review the concepts of GCMC and its implementation in molecular simulation of molecules in zeolites.

Monte Carlo simulations are a class of computational algorithms that rely on repeated random sampling to compute the results. We are interested in using MC to solve the physical problem of finding the average density of adsorbate molecules defined by some specified chemical potential and temperature. To calculate the adsorption isotherm,

we use Grand Canonical Monte Carlo, which simulates the $\{\mu VT\}$ ensemble, for this method allows the total number of guest molecules to fluctuate in response to some applied state point's chemical potential.

The GCMC method generates a chain of random events that move the system from an old state to a new state. Once a possible move has been generated, it must be determined if this move is possibly performed or not. In GCMC, three distinct moves are defined: insertion, deletion and translation. In an insertion move, a molecule is inserted into a random position in the simulation volume. In a deletion move, a randomly chosen molecule is removed from the system. In a translation move, a randomly chosen molecule is moved some random distance within the simulation volume. The acceptance of these three movements is calculated from the potential energies of the old and new states[28,29].

$$Acc(Insertion) = \min\left(1, \frac{\left[V \exp(\beta(\mu - U_{Tot}^{New}))\right]}{\Lambda^3 (N+1)}\right) \qquad (2.3)$$

$$Acc(Deletion) = \min\left(1, \frac{\left[\Lambda^3 N \exp(-\beta(\mu - U_{Tot}^{Old}))\right]}{V}\right) \qquad (2.4)$$

$$Acc(Translation) = \min(1, \exp(-\beta(U_{Tot}^{New} - U_{Tot}^{Old}))) \qquad (2.5)$$

Here μ is the chemical potential, V is the volume of the simulation box, N is the total number of molecules in the simulation volume, Λ is the de Broglie wavelength of the molecule, $\beta = 1/k_B T$, U_{Tot} is the total potential energy of the molecules in the simulation volume for the current and the trial configurations.

In GCMC simulations for the adsorption calculation, a pressure was defined and the corresponding activity was calculated from an equation of state. For all of our calculations, we used ideal equation of state. At each state point, some number of GCMC steps is applied to equilibrate the system under the equilibrium, before collecting data over another set of GCMC moves at the same state point.

2.3 MODELING DIFFUSIVITIES USING SIMULATION

2.3.1 SINGLE COMPONENT DIFFUSION

To describe the different aspects of mass transport for single component and mixture transport, several types of diffusion coefficients were calculated in this thesis. To describe the single component transport, three types of diffusivities are used to characterize the motion of the pure gases in the zeolites. First, self diffusion is the diffusion of the individual, "tagged" *i* molecules among otherwise identical species. The self diffusion coefficient D_s, also known as a tracer diffusion coefficient, is defined in the isotropic system as the mean square displacement of the individual molecules through

$$D_s = \lim_{t\to\infty} \frac{1}{t} \left\langle \frac{1}{6N} \sum_{l=1}^{N} \left\| r_l\ (t) - r_l(0) \right\|^2 \right\rangle \qquad (2.6)$$

Here, $\langle ... \rangle$ denotes an ensemble average and *N* is the number of adsorbed molecules in the simulation. The expression inside $\langle ... \rangle$ is mean square displacement of the particle i.

A more macroscopic definition of diffusion is based on the fact that net flux occurs if a concentration gradient exists. This flux, $\vec{J}$, is given by the Fick's law

$$\vec{J} = -D_t(c)\nabla c \qquad (2.7)$$

where ∇c is the concentration gradient of the adsorbed species and $D_t(c)$ is the concentration dependent single component Fickian diffusion coefficient. This diffusion coefficient is directly involved in describing the net mass transfer of material through amembrane.

The last important diffusion coefficients in single component diffusion is the corrected diffusivity, which can be written as

$$D_t = D_o \left(\frac{\partial \ln f}{\partial \ln c} \right)_T \qquad (2.8)$$

Using this definition, once the adsorption isotherm relating the adsorbed concentration, c ,

to the bulk fugacity of the adsorbing species, f, is known, then the transport diffusivity can be obtained from the corrected diffusivity. This corrected diffusivities also could be measured using Equilbrium MD simulations (EMD) with[30,31]

$$D_o = \frac{1}{6N}\lim_{t\to\infty}\frac{1}{t}\left\langle \sum_{l=1}^{N}\left\| r_l\ (t) - r_l(0)\right\|^2 \right\rangle \qquad (2.9)$$

Similar to the self-diffusivity, the equations above are written for diffusion in a three-dimensional isotropic medium. It can be helpful to think Eq. (2.9) as describing the diffusive motion of the center of the mass of the molecules relative to the reference frame of the adsorbent.

To describe single component diffusivities, we introduced three diffusion coefficients: the self diffusivity D_s, the corrected diffusivity D_o and the Fickian diffusivity D_t. D_s and D_o can be measured from the trajectories of the particles, while D_t could be calculated from the corrected diffusivities and the adsorption isotherms. Since the diffusion in zeolites is generally anisotropic the diffusion equation can be generalized by using a factor of 2 instead of 6 in Eq. (2.6) and (2.9). The orientationally averaged diffusivities are calculated with the individual component of the diffusivities by $D = (D_x + D_y + D_z)/3$. Usually, all of these coefficients are concentration dependent and are are not equal. There is only one limit where these coefficients coincide[32,33]. At low concentrations, the self, corrected and Fickian diffusivities are all equal, so that

$$\lim_{c\to 0} D_s(c) = \lim_{c\to 0} D_o(c) = \lim_{c\to 0} D_t(c) = D(0) \qquad (2.10)$$

where $D(0)$ is dilute concentration diffusivity.

2.3.2 MIXTURE DIFFUSION

Diffusion properties of binary mixtures are important for separation of the two species using zeolite membranes. Self diffusivities of the mixtures can be calculated from

the mean square displacement of individual particles as in the single component case. However, to calculate the mixture flux, macroscopic transport coefficients are required. In the diffusion of the mixtures, the flux of *i* species can be expressed in terms of chemical potential gradients.

$$\vec{J}_i = -\sum_{j=1..N} L_{ij}(\mu_1,...,\mu_N)\nabla\mu_j \qquad (2.11)$$

Here, L_{ij} are the Onsager transport coefficients, which forms symmetric matrix$[L]$. It is possible to determine these Onsager coefficients using the trajectories from an Einstein expression[34]:

$$L_{ij} = \frac{1}{6Vk_BT}\lim_{t\to\infty}\left\langle \sum_{l=1}^{N_i}(r_{li}(t)-r_{li}(0))\cdot\sum_{k=1}^{N_j}(r_{kj}(t)-r_{kj}(0))\right\rangle \qquad (2.12)$$

In this expression, V is the simulation volume, N_i is the number of molecules of species i and $r_{li}(t)$ and is the position of molecule l of species i at any time t.

Equation (2.11) can also be expressed in terms of concentration gradients:

$$\vec{J}_i = -\sum_{j=1..N} D_{ij}(c_1,...,c_N)\nabla c_j \qquad (2.13)$$

Here the Fickian diffusion coefficients form the nonsymmetric matrix$[D]$. Since Eq. (2.11) and Eq. (2.13) are completely equivalent, the Fickian diffusivities can be calculated from the Onsager coefficients measured in molecular simulation. In Eq. (2.11) the chemical potential gradients can be transformed as[35,36]

$$\nabla\mu = k_BT[\Gamma]\nabla c \qquad (2.14)$$

where $[\Gamma]$ is the matrix of thermodynamic correction factors defined by

$$\Gamma_{ij} = \left(\frac{\partial \ln f_i}{\partial \ln c_j}\right) \qquad (2.15)$$

f_i denotes the fugacity of i species and c_i is its intracrystalline concentration. Therefore, from Eq. (2.11), (2.13) and (2.14), the elements of the Fickian diffusivities can be

expressed in terms of the Onsager coefficients and thermodynamic correction factors as follows:

$$D_{ii} = \frac{k_B T}{c_i} \sum_{j=1}^{N} L_{ij} \left(\frac{\partial \ln f_j}{\partial \ln c_i} \right) \qquad (2.16)$$

$$D_{ij} = \frac{k_B T}{c_j} \sum_{k=1}^{N} L_{ik} \left(\frac{\partial \ln f_k}{\partial \ln c_j} \right) \qquad (2.17)$$

Here, the thermodynamic correction factors are calculated from the binary adsorption isotherms.

If we examine one-dimensional transport of a binary gas mixture through a zeolite membrane, the description above leads to

$$\begin{bmatrix} J_1 \\ J_2 \end{bmatrix} = -\begin{bmatrix} D_{11} & D_{12} \\ D_{21} & D_{22} \end{bmatrix} \begin{bmatrix} \partial c_1 / \partial z \\ \partial c_2 / \partial z \end{bmatrix} \qquad (2.18)$$

where z is the transmembrane direction. The elements of the Fickian diffusion matrix are in general functions of adsorbate concentrations, c_1 and c_2.

2.3.3 MEASUREMENT OF DIFFUSIVITIES USING MOLECULAR DYNAMICS

To measure the diffusivities of the molecules, Molecular dynamics (MD) is the most widely used molecular simulation method. MD is a numerical method for solving the Newton's equations of motions for many-body systems in a discretized form, which are solved repeatedly over many time steps to create a trajectory[28,29]. In this thesis, for MD calculations of spherical molecules we used the Velocity-Verlet integration scheme.

$$\vec{r}(t + \Delta t) = \vec{r}(t) + \Delta t \cdot \vec{v}(t) + \frac{\Delta t^2 \cdot \vec{F}(t)}{2m} \qquad (2.19)$$

$$\vec{v}(t + \Delta t) = \vec{v}(t) + \frac{\Delta t \cdot (\vec{F}(t) + \vec{F}(t + \Delta t))}{2m} \qquad (2.20)$$

Here, $\vec{r}(t)$ is the position vector, $\vec{v}(t)$ is the velocity vector, $\vec{F}(t)$ is the force vector, m is mass, t is time, and Δt is the time step. These equations are solved by getting the updated position $\vec{r}(t+\Delta t)$ vectors for all molecules, then updating the forces $\vec{F}(t+\Delta t)$ at given positions to calculate the velocities $\vec{v}(t+\Delta t)$ of all molecules. The positions of the molecules at next time step are updated again from these velocities. The potential energy surface described above is used to calculate the force with the relation of $\vec{F} = -\nabla U_{Tot}$ for any given particle.

2.3.4 MEASUREMENT OF DIFFUSIVITIES USING KMC

Although MD is an powerful method for simulating molecular diffusion in nanoporous materials, this method is not appropriate to measure very slow diffusion. Accurate integration of the molecular equations of motion requires time steps short enough (~10^{-15} s) to resolve each molecule's movement. Consequently, MD is typically limited to diffusion rates significantly faster than ~10^{-8} cm^2/s[37,38]. Since many of the small pore zeolites such as DDR, which is considered as a good candidate for CO_2/CH_4 separation, shows very slow diffusion of CH_4 molecules, we need to use other methods to measure the diffusion of these species.

Kinetic Monte Carlo attempts to overcome this limitation by exploiting the fact that the long-time dynamics of this kind of system typically consists of diffusive jumps from state to state. Rather than following the trajectory through every vibrational period, these state-to-state transitions are treated directly. When KMC is combined with the Transition State Theory (TST), it can reach vastly longer time scales, and in principle, give an accurate description of the dynamical properties of a system[9,38-48]. In this section, we introduce the TST-KMC methods we will use later to calculate the transport diffusivities of CH_4 in zeolites.

TST is based on the assumption that diffusive behavior can be described as a hopping process on a lattice, where particles hop randomly from lattice point to lattice point. This assumption works under the condition that the lattice points are separated by sufficiently high free-energy barriers for the diffusion that a hop is a rare event, and two subsequent hops can be considered uncorrelated. We define a reaction coordinate q, which indicates the progress of the diffusion event from minimum energy site A to minimum energy site B, as the Cartesian coordinate along the axis parallel to the line connecting the center of site A to site B. The location of the dividing barrier (i.e., the transition state) is denoted by q^*. In applying transition state theory (TST) to this situation, the transition rate for escape from state i to state j is taken to be the equilibrium flux through a dividing surface separating the two states. Because this TST rate is an equilibrium property of the system, we can also calculate k_{ij} without ever looking at dynamical trajectories. For a thermal ensemble, k_{ij} is simply proportional to the Boltzmann probability $P(q^*)$ of being at the dividing surface q^* relative to the probability of being anywhere. That is, the transition rate k_{ij} from state i to state j is[9,49]

$$k_{ij} = \kappa \times \left(2\pi m\beta\right)^{-1/2} P\left(q^*\right) \tag{2.21}$$

$$P\left(q^*\right) = \frac{\mathrm{e}^{-\beta F(q^*)}}{\int_{V_A} \mathrm{e}^{-\beta F(q)}\, dq} \tag{2.22}$$

Here, $\beta = 1/\left(k_B T\right)$, k_B is the Boltzmann constant, T is the temperature, m is the mass involved in the reaction coordinate, and $F(q)$ is the system's free energy as a function of q. TST assumes that the averaged velocity, $\left(2\pi m\beta\right)^{-1/2}$, of a particle at the top of the barrier follows a Maxwell-Bolzmann distribution. V_A defines the volume of site A.

The transmission coefficient, κ, in Eq. (2.21) defines the probability that the particle (system) ends up in site B (state j) once a trajectory reaches the dividing surface. This transmission coefficient corrects for recrossing events; i.e., it corrects for trajectories

which cross the dividing surface from *A* but fail to end up in *B*. From the definition, at infinite dilute loading, the transmission coefficient $\kappa \cong 1$. If transition state surface is known, the transmission coefficient can be calculated from a series of short MD simulations, this is known as the dynamically corrected-TST method[44,50].

Once all values of k_{ij} are calculated from TST, then we know the local hopping rates of guest molecules from specific sites to sites in our lattice model. The diffusivities of guest molecules can then be calculated from KMC simulations. To describe the diffusion of the molecules in zeolites, all adsorbate molecules are distributed initially into the all lattice sites of the simulation volume. For each KMC step, for a randomly chosen molecule, hops in lattice sites are attempted with the probability of $k_{ij} / k_{\max}$. After every attempted hop, time is incremented by $\Delta t = 1/ Nk_{\max}$, where *N* is the total number of guest molecules in the simulation volume. KMC simulations of this kind generate trajectories of the diffusing molecules, and these trajectories can be used to define the diffusion properties with the same formalism that we introduced above for MD simulations.

REFERENCES

(1) Skoulidas, A. I.; Sholl, D. S. *J. Phys. Chem. B* **2005**, *109*, 15760.
(2) Skoulidas, A. I.; Sholl, D. S. *J. Phys. Chem. A* **2003**, *107*, 10132.
(3) Skoulidas, A. I.; Sholl, D. S. *J. Phys. Chem. B* **2002**, *106*, 5058.
(4) Skoulidas, A. I.; Sholl, D. S. *J. Phys. Chem. B* **2001**, *105*, 3151.
(5) Dubbeldam, D.; Calero, S.; Vlugt, T. J. H.; Krishna, R.; Massen, T. L. M.; Smit, B. *Phys. Rev. Lett.* **2004**, *93*, 088302.
(6) Dubbeldam, D.; Calero, S.; Vlugt, T. J. H.; Krishna, R.; Massen, T. L. M.; Smit, B. *J. Phys. Chem. B* **2004**, *108*, 12301.
(7) Dubbeldam, D.; Calero, S.; Maesen, T. L. M.; Smit, B. *Phys. Rev. Lett.* **2003**, *90*, 245901.
(8) Dubbeldam, D.; Beerdsen, E. *J. Chem. Phys.* **2005**, *122*, 224712.
(9) Beerdsen, E.; Smit, B.; Dubbeldam, D. *Phys. Rev. Lett.* **2004**, *93*, 248301.
(10) Beerdsen, E.; Dubbeldam, D.; Smit, B. *Phys. Rev. Lett.* **2006**, *96*, 044501.
(11) Paschek, D.; Krishna, R. *Phys. Chem. Chem. Phys.* **2001**, *3*, 3185.
(12) Krishna, R.; van Baten, J. M.; Garcia-Perez, E.; Calero, S. *Chem. Phys. Lett.* **2006**, *429*, 219.
(13) Krishna, R.; van Baten, J. M. *Chem. Eng. Sci.* **2008**, *63*, 3120.
(14) Krishna, R.; van Baten, J. M. *Micropor. Mesopor. Mater.* **2008**, *109*, 91.
(15) Krishna, R.; van Baten, J. M. *Sep. Purif. Technol.* **2008**, *61*, 414.
(16) Chen, H.; Sholl, D. S. *J. Am. Chem. Soc.* **2004**, *126*, 7778.
(17) Skoulidas, A. I.; Ackerman, D. M.; Johnson, J. K.; Sholl, D. S. *Phys. Rev. Lett.* **2002**, *89*, 185901.
(18) Keskin, S.; Sholl, D. S. *Energy Environ. Sci.* **2010**, *3*, 343.
(19) Keskin, S.; Sholl, D. S. *Langmuir* **2009**, *25*, 11786.
(20) Keskin, S.; Sholl, D. S. *J. Phys. Chem. C* **2007**, *111*, 14055.
(21) Keskin, S.; Liu, J.; Johnson, K.; Sholl, D. S. *Langmuir* **2008**, *24*, 8254.
(22) Keskin, S.; Liu, J.; Johnson, J. K.; Sholl, D. S. *Micropor. Mesopor. Mater.* **2009**, *125*, 101.
(23) Makrodimitris, K.; Papadopoulos, G. K.; Theodorou, D. N. *J. Phys. Chem.* **2001**, *105*, 777.
(24) Heuchel, M.; Snurr, R. Q.; Buss, E. *Langmuir* **1997**, *13*, 6795.
(25) Skoulidas, A. I.; Sholl, D. S.; Johnson, J. K. *J. Chem. Phys.* **2006**, *124*, 054708.
(26) Rahmati, M.; Modarress, H. *J. Mol. Struct.: THEOCHEM* **2009**, *901*, 110.
(27) Liu, B.; Smit, B.; Rey, F.; Valencia, S.; Calero, S. *J. Phys. Chem. C* **2008**, *112*, 2492.
(28) Frenkel, D.; Smit, B. *Understanding molecular simulation: From algorithms to applications*; Academic Press: London, 2002.
(29) Allen, M. P.; Tildesley, D. J. *Computer simulation of liquids*; Oxford Science Publications: New York, 1986.
(30) Maginn, E. J.; Bell, A. T.; Theodorou, D. N. *J. Phys. Chem.* **1993**, *97*, 4173.
(31) Mori, H. *Prog. Theor. Phys.* **1965**, *33*, 423.

(32) Karger, J.; Ruthven, D. M. *Diffusion in zeolites and other microporous solids*; Wiley&Sons: New York, 1992.
(33) Keil, F. J.; Krishna, R.; Coppens, M. O. *Rev. Chem. Eng.* **2000**, *16*, 71.
(34) Theodorou, D. N.; Snurr, R. Q.; Bell, A. T. *Molecular Dynamics and diffusion in microporous materials* New York, 1996; Vol. 7.
(35) Skoulidas, A. I.; Sholl, D. S.; Krishna, R. *Langmuir* **2003**, *19*, 7977.
(36) Krishna, R.; van den Broeke, L. J. P. *CHem. Eng. J.* **195**, *57*, 155.
(37) Frenkel, D.; Smit, B. *Understanding Molecular Simulation : From Algorithms to Applications*; 2 ed.; Academic Press: San Diego, 2002.
(38) Keil, F. J.; Krishna, R.; Coppens, M. O. *Rev. Chem. Eng.* **2000**, *16*, 71.
(39) Fichthorn, K. A.; Weinberg, W. H. *J. Chem. Phys.* **1991**, *95*, 1090.
(40) Beerdsen, E.; Dubbeldam, D.; Smit, B. *Phys. Rev. Lett.* **2005**, *95*, 164505.
(41) Beerdsen, E.; Dubbeldam, D.; Smit, B. *J. Phys. Chem. B.* **2006**, *110*, 22754.
(42) Dubbeldam, D.; Smit, B. *J. Phys. Chem. B.* **2003**, *107*, 12138.
(43) Dubbeldam, D.; Beerdsen, E.; Vlugt, T. J. H.; Smit, B. *J. Chem. Phys.* **2005**, *122*, 224712.
(44) Tunca, C.; Ford, D. M. *J. Phys. Chem. B.* **2002**, *106*, 10982.
(45) Tunca, C.; Ford, D. M. *J. Chem. Phys.* **2004**, *120*, 10763.
(46) Sholl, D. S. *Langmuir* **2006**, *22*, 3707.
(47) Coppens, M.-O.; Bell, A. T.; Chakraborty, A. K. *Chemical Engineering Science* **1999**, *54*, 3455.
(48) Iyengar, V.; Coppens, M.-O. *Chemical Engineering Science* **2004**, *59*, 4747.
(49) Tunca, C.; Ford, D. M. *J. Chem. Phys.* **1999**, *111*, 2751.
(50) Dubbeldam, D.; Calero, S.; Maesen, T. L. M.; Smit, B. *Phys. Rev. Lett.* **2003**, *90*, 245901.

CHAPTER 3

H_2/CH_4 SEPARATION USING PORE MODIFIED SILICALITES*

Zeolite membranes are robust materials that are well suited to be used in harsh conditions, but they are not typically selective for hydrogen. Modification of pore mouth of zeolite membranes is known as one possible way to achieve high hydrogen selectivity. The key issue for this kind of material here is to retain hydrogen selectivity without significantly reducing the hydrogen flux. In this chapter we examine the effect of the pore mouth modification of silicalite on H_2/CH_4 separation using atomic-scale simulations.

3.1 H_2 SEPARATION USING PORE MODIFIED ZEOLITES

Conventional fuel sources are rapidly being depleted. Hydrogen is one attractive new energy source since once it is produced it can be used with little negative environmental effect. The most practical methods for obtaining large quantities of H_2 use hydrocarbon sources from which H_2 can be produced by steam reforming or by partial oxidation with oxygen. A common characteristic of these methods is that other gases are also produced, so separating H_2 efficiently is important for both economic and environmental reasons.[1] Inorganic membranes have the potential to play an important role in these separations if membranes with suitable permselectivities and durability can be developed.[2,3]

As a candidate for membrane-based separation of H_2, we will consider silicalite, the all-silica analog of ZSM-5(structure code MFI, space group *Pnma*). This structure has a three-dimensional porous network with typical pore size of ~5.5 Å.[4] Among all efforts

---

* The results described in this chapter have been published in Sang Eun Jee, Alan J. H. McGaughey, David S. Sholl, *Molecular Simulation*(2009), 35,70-78.

to fabricate zeolite membranes, methods for making membranes from silicalite are the most fully developed.[5-8]

A characteristic of silicalite that is common to essentially all zeolites is that its pores are too large to block the adsorption of small gas molecules mixed with H_2, so a separation cannot be achieved based on simple molecular sieving. Moreover, H_2 adsorption in silicalite is weaker than CO_2 or CH_4, two typical gases present during H_2 production. Experiments that have been performed with silicalite membranes using gas mixtures including H_2 have not yielded results with selectivities that would be desirable in H_2 separations.[9-14] The physical phenomena that make silicalite unselective for H_2 in these mixtures are also present for essentially all zeolites, so the limitations of this material cannot be solved simply by using another zeolite framework.

One avenue that may allow the properties of zeolite membranes to be improved for H_2 separations is to chemically modify the external surfaces of membranes. This strategy has been explored in two experimental studies using silicalite membranes.[15,16] and one using surface modified hybrid membranes.[17] In these experiments, methyl diethoxy silane was attached to the surfaces of ZSM-5 membranes as a modifier with the aim of reducing the width of the pores at the membrane surface. Ideally, this modifying layer could enhance the selectivity of the membrane for H_2 by reducing the effective pore size for molecules entering the membrane but still allow rapid transport of adsorbed molecules through the membrane. In the experiments by Hong et al., the selectivity of the membrane increased from 1.6 to 33 for the H_2/CH_4. Unfortunately, this improvement in selectivity was coupled with a large reduction in net H_2 flux.[15] An interesting question generated from these experiments is whether there is a regime where surface

modifications of zeolite membranes can be made to improve the selectivity of the membrane for a small species such as H_2 without a large decrease in the H_2 flux.

In this chapter, we examine the effect of pore modification on H_2 and CH_4 transport through silicalite via molecular simulations. To model modified membranes, a modifying layer is constructed near the surface by adding individual Si and O atoms to an initially crystalline sample. The net flux of H_2 and CH_4 is then calculated for the modified silicalite membrane as well as an unmodified crystal. While Molecular Dynamics (MD) techniques have been developed to simulate transport through the zeolite membranes, most of them are based on the assumption that intracrystalline diffusion determines the transport rate.[18-20] To describe pore-mouth modified zeolite membranes, however, the increased surface resistance associated with the modifying layer is a key factor. It is therefore vital that we use a calculation method that accounts for the impact of surface resistances during the operation of the membrane. To do this, we apply the Local Equilibrium Flux method (LEFM)[21,22], a method that can calculate surface resistances rapidly from an atomically-detailed model of a membrane material by describing the local fluxes that exist at the gas-membrane interface.

3.2 SURFACE CONSTRUCTION

3.2.1 PORE MODIFICATION WITH SIMULATION

To describe gas permeation through a modified zeolite membrane using molecular simulations, the atomic-scale configuration of the modified zeolite structure must be defined. In this section, we describe how a thin layer that mimics amorphous silica was added to the external surfaces of crystalline silicalite. The intention of this procedure was not to precisely model a specific experimental procedure, since detailed structural

information about the modifying layers from the limited number of experimental studies that have been performed is not available.

The diffusion of molecules through silicalite crystals is anisotropic because of the anisotropy of silicalite's pores. Sinusoidal channels go along the crystallographic *x*-orientation, straight channels go along the *y*-orientation, and although no pores exist along the *z*-orientation, net diffusion in the *z*-orientation can occur via diffusion in the *x* and *y*-orientation.[23,24] Since the *y*-orientation of silicalite provides the fastest intracrystalline diffusion for unmodified membranes,[25] modifying layers were created on the surface of 2×2 unit cells in xz plane.

For simplicity in making modified zeolite structures, we modified surface structures by directly adding individual Si and O atoms. Construction of the modified layer consists of two procedures. First, physically plausible positions are found via geometric criteria and then energetically stable position is found via relaxation of the structures. At the end, we finish the modification procedure by removing unnecessary dangling atoms which does not exist in experimental situation.

Firstly, to find the reasonable position for insertion, an atom is inserted at a random position near the surface. The inserted atoms are randomly chosen from Si and O with a Si:O ratio of 1:2. Each time an atom is inserted, a list of neighbor atoms is made to calculate bond lengths, bond angles and coordination numbers, with the latter defined as the number of bonds present within a specified range of bond lengths shown in Table 3.1.[26] The criteria for each of these quantities was adapted from extensive simulations of amorphous silica zeolites by Mukhopadhyay *et al.* [26,27] and simulations of internal grain boundaries in silicalite by Newsome and Sholl.[28] If all the criteria are satisfied for the

inserted atom, then this atom is accepted. For example, if an inserted O atom forms bonds with Si atoms with bond lengths between 1.42 and 1.82 Å, Si-O-Si bond angles between 90^o and 180^o, O-Si-O bond angles between 80^o and 140^o, has a coordination number between 1 and 3, and has all O-O distances > 2.21 Å, then the insertion of this O atom is accepted. If one (or more) of those criteria is not satisfied, then the trial position is rejected and the inserted atom is moved to a nearby position by a random walk. If no acceptable position can be found within 50 steps of the random walk, the atom is removed and a new insertion is begun. Atoms are inserted to randomly chosen positions within ±5 Å from the surface, which was defined as the position of the topmost atoms of the zeolite including any atoms in the modifying layer that have already been deposited.

The coordination number criteria for insertion on surface of silicalite are slightly different from those used previously to describe internal grain boundaries.[28] In the latter case, the allowable coordination numbers for Si were 3 to 5. When modifying the zeolite's surface, we allowed Si atoms to be inserted with coordination numbers from 1 to 5, to allow both the creation of new atoms on the external surface and bulk-like atoms. The valid coordination numbers for O atoms were defined to be the same as earlier work on grain boundary.[28]

Secondly, once an atom is inserted as described above, a quenching procedure was used to relax the atomic positions. In this procedure, the potential energy, U_{ij}, of Si and O atoms was defined using the BKS (van Beest-Kramer-van Santen) interatomic potential for silica.[29-31] This potential, with the additional Lennard-Jones 24-6 terms suggested by Guissani and Guillot[32] for amorphous silica, has the form

$$U_{ij} = \frac{q_i q_j}{r_{ij}} + A_{ij} \exp(-b_{ij} r_{ij}) - \frac{c_{ij}}{r_{ij}^{6}} + 4\varepsilon_{ij}[(\frac{\sigma_{ij}}{r_{ij}})^{24} - (\frac{\sigma_{ij}}{r_{ij}})^{6}] \qquad (3.1)$$

Here, the subscripts *i* and *j* refer to Si and O atoms, *q* is the charge of an atom, *A*, *b*, *c* are parameters and *r* is an interatomic distance. The first term contains the long range electrostatic interaction between the effective charges and second and third terms represent covalent bonding interaction and short range repulsion between oxygen atoms. Parameters have been derived to stabilize the tetrahedral structures of amorphous silica. The parameters for the BKS potential are shown in Table 3.2.[29,30,32] The electrostatic interactions were handled using the Wolf method with an α value of 0.345 $Å^{-1}$.[33]. The potential cutoff was 12 Å.

During our MD simulations using this potential, temperature was controlled using the Nosé-Hoover thermostat and the equations of motion were integrated with the Verlet leapfrog algorithm with 0.905 fs time step. A temperature quench was performed by removing kinetic energy at the rate of 7.3×10^{15} K/s from 200 K until the kinetic energy vanishes. The structure that results from this procedure defines a local minimum on the potential energy surface. For computational efficiency, only the inserted atom and its neighbors were relaxed. We typically inserted multiple atoms before MD was used to relax the positions of these atoms.

The procedure defined above leaves a small number of highly undercoordinated atoms near the upper boundary of the modifying layer. The final stage of defining a modified layer was to examine the atomic density *d* in the layer in slices 1 Å thick normal to the zeolite's initial surface. The atom density in these slices abruptly drops from a

roughly constant value inside the layer to zero outside the layer. In the region where this density drop occurs, we removed any Si atoms with coordination numbers of 1 or 2.

Si-O bond length [Å]	1.62 ± 0.20
O-O length[Å]	>2.21
Si-Si length[Å]	>2.79
Si-O-Si bond angle [deg]	135 ± 45
O-Si-O bond angle [deg]	110 ± 30
Coordination number of O	1-3
Coordination number of Si	1-5

Table 3.1: Criteria for inserting atoms as defined in text[26,27].

q_{Si}: 2.4 [e] q_O: -1.2 [e]	O-O	Si-O	Si-Si
A [eV]	1388.7730	18003.7572	-
B [$Å^{-1}$]	2.76	4.87318	-
C [eV $Å^6$]	175	133.5381	-
ε [kJ/mol]	0.04613	1.0834	1.2768E3
σ [Å]	2.2	1.3	0.4

Table 3.2: Parameters for the BKS potential [29,30,32].

3.2.2 PORE MODIFIED STRUCTURES

Figure 3.1 shows side views of modified silicalite with different degrees of modification. Although insertion attempts were made for positions within ±5 Å of the zeolite's surface, the great majority of inserted atoms lie on top of the surface rather than inside the zeolite pores. Figure 3.2 shows top views of unmodified and modified silicalite. After modification, the size of pores was reduced. It is reasonable to expect that this may reduce the flux of molecules into the pores when the crystal is used as a membrane.

One way to characterize the modifying layers in our simulated structures is to calculate the free volume in the layers available for diffusion of adsorbed molecules. Free volumes were measured by inserting spherical probes into the region of interest. To

measure the available free volume accessible by CH_4 (H_2), a spherical probe of radius 1.9 Å (1.445 Å) was used. The radius of Si and O atoms were assigned as the van der Waals radii of r_{Si}=2.10 Å and r_O=1.52 Å. The position for a probe sphere was considered as the part of the free volume if no overlaps existed between the probe sphere and the Si and O atoms, and the free volume was defined by the fraction of feasible locations for probe spheres after > 10^8 of trial insertions.

We calculated the ratio of free volume per total volume in a region 2 Å thick in the *y*-direction located 1.5~3.5 Å above the initial surface of the crystalline silicalite. Figure 3.3 shows the free volume of six modified silicalite membranes as a function of the two dimensional density of atoms in the modifying layers, *d*. Each membrane is numbered as 1 to 6. Since the probe sphere used for H_2 is smaller than for CH_4, the free volume is higher for H_2 in all cases. The free volume for each probe decreases steadily as more material is added to the modifying layer. For the membrane with the most Si and O atoms in the modifying layer, membrane 6, the free volume ratio for the CH_4 probe is reduced to 0.008, which is big reduction when comparing to 0.086 in crystalline silicalite. In addition, the difference in free volume between crystalline silicalite and the modifying layer for this membrane for the H_2 probe is less severe; these values reduced from 0.19 to 0.035, which differ by a factor of 5.

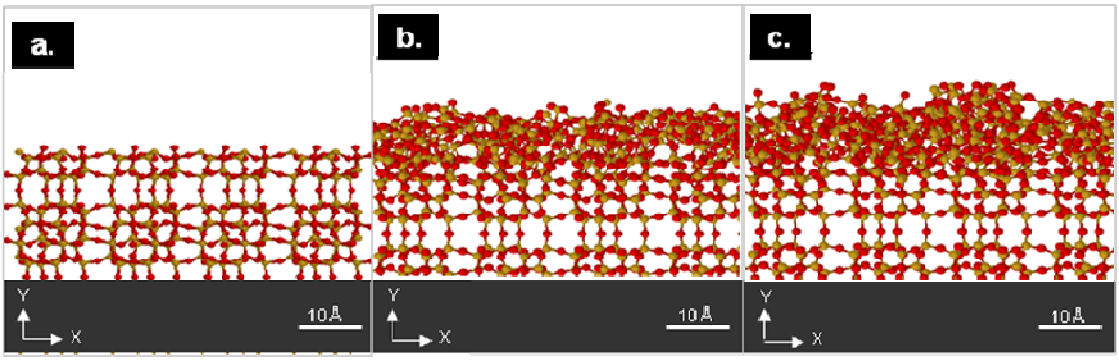

Figure 3.1: Side views of (a) unmodified silicalite and (b)-(c) surface modified silicalite with various degree of modification. As modification proceeds, the thickness of modifying layer increases.

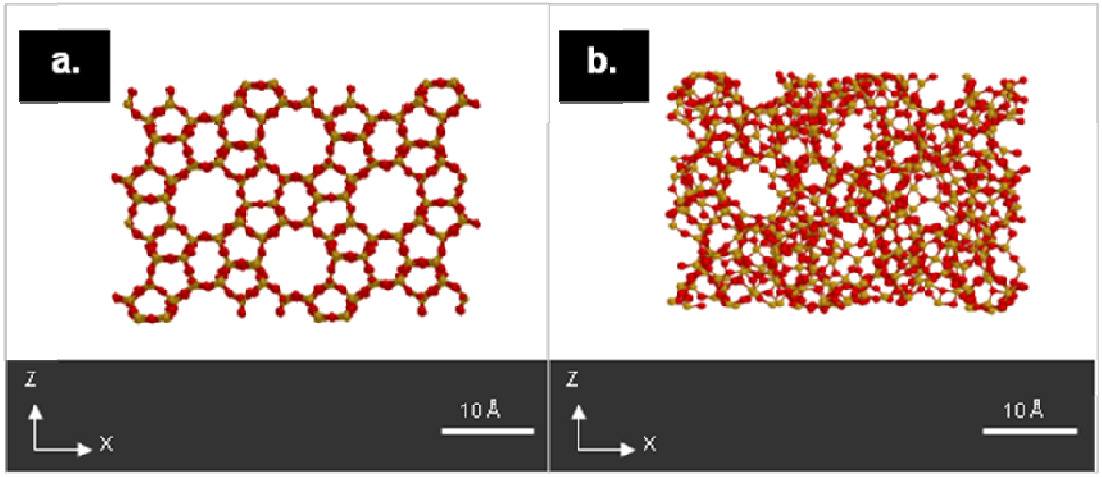

Figure 3.2: Top views of (a) unmodified silicalite and (b) surface modified silicalite

3.3 MEASUREMENT OF NET FLUX

3.3.1 LOCAL EQUILIBRIUM MOLECULAR DYNAMICS

Molecules pass through a zeolite membrane in three steps. Molecules must adsorb to the crystal's external surface, then they diffuse through the crystal's pores and finally molecules desorb from the downstream surface of the zeolite. In most models for molecular transport through zeolite, surface effects are assumed to be far smaller than

intracrystalline resistances. In this case, the steady-state flux of a single species permeating through a membrane can be calculated from [18,25,34]

$$J_{ideal} = \frac{1}{L}\int_{c_{permeate}}^{c_{feed}} D_t(c')dc' \quad (3.2)$$

Here, c_{feed} ($c_{permeate}$) is the adsorbed concentration at the feed (permeate) side of the membrane, L is the membrane thickness, and D_t is the transport diffusion coefficient of the adsorbed species. This diffusion coefficient, which is dependent on the concentration of the adsorbing species, can be calculated using equilibrium molecular dynamics.[25,34,35] In the absence of surface resistances, the concentration of the adsorbates is defined by the equilibrium adsorption isotherm via the gas phase pressure on the feed and permeate side, P_{feed} and P_{perm}, respectively.

In the case of surface modified zeolites, surface resistances are key factors in the performance of the material. One widely used simulation technique to measure flux in the presence of surface resistances is Dual Control Volume Grand Canonical Molecular Dynamics (DCV GCMD). This is a conceptually simple method in which the net flux, J, of molecules passing through a membrane is directly computed under nonequilibrium conditions. Unfortunately, this method is very computationally intensive and can only be applied to crystals much smaller than those relevant to current experiments.[21,28,36] The Local Equilibrium Flux Method (LEFM) offers a way to estimate surface resistances without directly observing J.[21] The LEFM has been compared to DCV GCMD simulations of gas permeation through unmodified silicalite membranes by Newsome and Sholl.[21,22] Although the LEFM is not exact, it was shown to accurately estimate the size of surface resistances in a way that can be used to examine much wider ranges of operating conditions than is possible using DCV GCMD. Importantly for our purposes,

the surface resistances associated with unmodified *y*-oriented silicalite membranes were shown to be small for all conditions we examine below. The LEFM has also been applied to estimate the role of surface resistances in carbon nanotube membranes.[37] In carbon nanotube membranes, surface resistances may be more important than for unmodified zeolites because of the extremely low resistance to mass transport that exists inside the membrane's pores.[38-40]

The aim of the LEFM is to characterize the net membrane flux in terms of the local fluxes that exist under equilibrium conditions. If j_+ (j_-) is the one way flux from left to right (right to left) at any plane through the membrane, the net flux J is $J = j_+ - j_-$. If the system is at equilibrium, then $j_{eq} = j_+ = j_-$ and $J = 0$. The equilibrium flux, j_{eq} can be measured by counting molecules crossing an interface using equilibrium MD simulations. The LEFM assumes the net steady state flux can be estimated by the difference of the one way equilibrium fluxes at different effective pressures.[21] The total feed side flux is

$$J_{feed} \cong j_{eq}(P_{feed}) - j_{eq}(P_{ads}) \qquad (3.3)$$

Here, P_{feed} is the actual gas phase pressure outside the membrane, while P_{ads} is an effective pressure in the membrane boundary layer. By writing $P_{ads} = P_{feed} - \delta P$, we can rewrite Eq. (3.3) as

$$J_{feed} \cong j_{eq}(P_{feed}) - j_{eq}(P_{feed} - \delta P) = \delta P\left(\frac{dj_{eq}}{dP}\bigg|_{P_{feed}}\right) \qquad (3.4)$$

Therefore, we can calculate the net flux on the feed side if we measure the local equilibrium flux at various pressures. In the case of interest to us where the surface resistance from a modifying layer appears only on the feed side, the intracrystalline flux can be calculated from

$$J_{\text{intra}} = \frac{1}{L}\int_{c_{permeate}}^{c_{ads}} D_t(c')dc' \qquad (3.5)$$

In this case, c_{ads} is the adsorbate concentration that corresponds to the effective pressure $P_{ads.}$ At steady state, the feed flux and intracrystalline flux obtained from Eqs. (3.4) and (3.5) must be the same. The net flux can be calculated by adjusting P_{ads} iteratively.

It is often convenient to describe net mass transfer through a membrane in terms of resistances associated with the different processes involved. Using this approach, the resistances to transport due to the feed side, intracrystalline region, and permeate side can be defined as R_{ads}, R_{intra}, and R_{des}.[36] If surface resistances on both the feed and the permeate side are negligible, then R_{ads} and R_{des} may be disregarded. The net flux associated with this idealized situation is related to R_{intra} by

$$J_{ideal} = \frac{\Delta c}{R_{\text{intra}}} \qquad (3.6)$$

where Δc is the concentration change in adsorbed concentration from feed to permeate side and $R_{\text{intra}} = L / \overline{D}_t$. The flux in this expression is the same as the flux defined in Eq. (3.2). For the surface-modified membranes, we want to consider the situation where R_{des} is negligible but R_{ads} is not. The net flux through the membrane can then be expressed in terms of resistances to mass transport as

$$J = \frac{\Delta c}{R_{ads} + R_{\text{intra}}} \qquad (3.7)$$

In this expression, the flux is the net flux defined iteratively using Eq. (3.4) and (3.5). From Eq. (3.6) and (3.7), it is convenient to define the ratio of adsorption resistance to the intracrystalline resistance by

$$\frac{R_{ads}}{R_{\text{intra}}} = \frac{J_{ideal}}{J} - 1 \qquad (3.8)$$

3.3.2 EQUILIBRIUM SIMULATION OF H_2/CH_4 FLUX

In our calculation CH_4 and H_2 molecules were treated as rigid spherical molecules and only dispersive interactions were considered to describe the potential energy surface. A Lennard-Jones (LJ) pair-wise potential was used to calculate adsorbate-adsorbate interaction and adsorbate-zeolite interaction.

$$U_{ij} = 4\varepsilon_{ij}[(\frac{\sigma_{ij}}{r_{ij}})^{12} - (\frac{\sigma_{ij}}{r_{ij}})^{6}] \qquad (3.9)$$

We used interaction parameters for CH_4 and H_2 from the literature.[41] These parameters are shown in Table 3.3. In many calculations for the adsorption in homogeneous zeolites, only the framework O atoms in the zeolite are considered to calculate the host-guest potential energy since Si atoms are shielded from the guest molecules.[41,42] In our calculations, however, we also considered the effect of the Si atoms on the total potential because Si atoms near the external surface can be exposed to the guest molecules. Interactions between Si atoms and guest molecules were described by a purely repulsive LJ-12 potential, that is, the first term of the Eq. (3.9). The parameters for this potential were chosen as $\varepsilon_{Si\text{-}Guest}$=200 K, σ = 1.5 Å to create a repulsive force near the Si atoms but not to affect adsorption in a homogeneous silicalite.

	CH_4 - O	H_2 - O	CH_4 - CH_4	H_2 - H_2
ε [K]	133.3	51.233	147.9	34.02
σ [Å]	3.21	2.62	3.73	2.96

Table 3.3: Parameters for LJ potential [41]

Two assumptions were made in performing our calculations. First, the structure of the zeolite was assumed to be rigid. This assumption leads to a great reduction in the computational effort, since the potential energy surface defined by the zeolite can be

pretabulated.[41,42] It is possible that local vibrations in the modifying layer could play a larger role in the transport of highly hindered molecules than in transport of the same molecules inside the zeolite pores. Inclusion of these vibrational degrees of freedom would be a useful topic to pursue in future extensions of this work. Second, the interactions of guest molecules with undercoordinated zeolite atoms on the surface of the membrane were treated with the same interaction potentials as fully coordinated zeolite atoms in the bulk material. In reality, it is likely that these undercoordinated atoms are terminated with hydroxyl or similar species.[43,44] By neglecting any differences in interaction potentials that might arise from these effects, our calculations are consistent with previous calculations for unmodified zeolite surfaces.[21,36]

To calculate the intracrystalline flux of CH_4 and H_2 in Eq. (3.5), we need the transport diffusivity, D_t , and adsorption isotherms in bulk silicalite. For CH_4, we used previously calculated data.[21,24] The values for H_2 were calculated using EMD (Equilibrium Molecular Dynamics) and GCMC (Grand Canonical Monte Carlo) simulation.[21,24,45] For all the simulations the cutoff distance for the interactions was set to 13 Å. For GCMC simulation to measure the adsorption isotherm, we used 2×10^7 Monte Carlo moves for equilibration, followed by 1×10^7 Monte Carlo moves for data collection. In our MD calculations, systems were initialized with 1.5×10^5 steps of canonical Monte Carlo moves and equilibrated by MD. Trajectories were measured for 10 ns with 1 fs time step with 30 trajectories.

The local equilibrium flux j_{eq} in Eq. (3.4) was measured with various pressures using EMD (Equilibrium Molecular Dynamics) with an Andersen thermostat.[45] The length of the gas region was 40 Å in the *y*-direction. Like previous MD simulations, the system was initialized by canonical Monte Carlo moves and equilibrated by MD.[21]

Approximately 42 to 160 molecules were located in the total system, and simulations were performed for 20 ns. From the forward and backward movement of molecules along the *y* direction, the local flux was calculated across various planes oriented perpendicular to the crystallographic *y*-orientation of the zeolite. The minimum local flux observed from this collection of planes was used for our LEFM calculations since this is the relevant flux for determining the net flux on the feed side. This minimum flux was observed to occur in the region of the modifying layer above the initial surface of crystalline silicalite that was characterized in terms of free volume in Fig. 3.3.

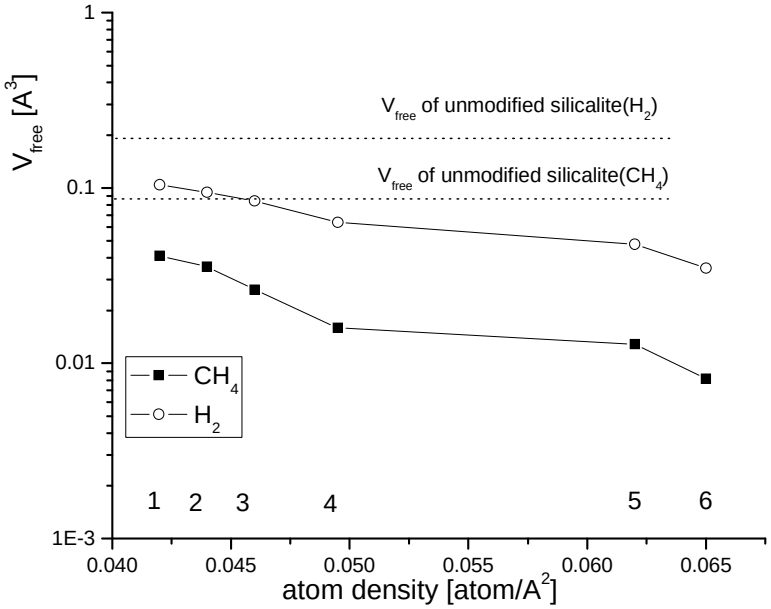

Figure 3.3: Free volume calculated in a 2 Å slice in the modifying layer on the modified silicalite membranes used in our calculations, shown as a function of the two dimensional density of atoms in the modifying layers, *d*. Dashed lines indicate the free volume of unmodified silicalite.

3.3.3 H_2/CH_4 FLUX MEASUREMENT

Using the methods described above, we examined the single-component flux of CH_4 and H_2 through silicalite membranes with various degrees of surface modification. We will discuss our results using the numbering system assigned to our simulated membranes in Fig. 3.4. Figure 3.4 shows the net flux of CH_4 calculated with the LEFM as a function of membrane length, L, with P_{feed} = 10 bar and P_{perm} = 0.3 bar. It can be seen from Eq. (7) that if the surface resistance is negligible, then a plot of log J versus log L is linear. This situation accurately describes the results in Fig. 3.4 for membranes 1-3. This supports our earlier statement that the surface resistances of the unmodified membrane could be neglected in our description of the permeate side of the membrane. For larger degrees of modification, the curves in Fig. 3.4 deviate strongly from linearity, indicating that the surface resistance becomes an important effect. These results are consistent with the free volume results shown in Fig. 3.3. For membranes 4 and 5, the calculated fluxes are not very different, and the free volume accessible to CH_4 in these two membranes is similar. For membrane 6, CH_4 could no longer permeate through the membrane, so the surface modification had blocked the pores to CH_4 molecules on MD time scales.

Figure 3.5 shows results similar to those in Fig. 3.4 for the permeation of H_2 with P_{feed} = 10 bar and P_{perm} = 0.3 bar. For surface modifications for membranes 1-5, the H_2 flux is negligibly affected by the modifying layer. For membrane 6 the H_2 flux was significantly reduced by the modifying layer. For a membrane with L = 1 μm under these conditions, the H_2 flux was reduced by 72% compared to the unmodified silicalite membrane. Crucially, however, CH_4 was blocked by this modifying layer.

The ratios of adsorption resistance to intracrystalline resistances for CH_4 and H_2 are shown for a variety of operating conditions for membrane 4 in Fig. 3.6. Figure 3.6 includes results with P_{feed} = 1, 10, and 20 bar. In this figure, circles are the results for membranes with a transmembrane pressure drop equal to the feed pressure, while crosses are for membranes where the pressure drop is only 1% of the feed pressure. For a given feed pressure, these two pressure drops span the full range of possible pressure drops. R_{ads}/R_{intra} is large when L is small because R_{intra} is proportional to L (see Eq. (3.2) and (3.6)), while R_{ads} is only weakly dependent on L. The most important observation from Fig. 3.6 is that for a broad range of operating conditions the surface resistance due to the modifying layer is much larger for CH_4 than for H_2. The magnitude of the surface resistance is more sensitive to the operating conditions for CH_4 than for H_2. While this is in part simply due to the much larger resistances that exist for CH_4, this sensitivity also stems from the fact that the range of pressures included in Fig. 3.6 spans a larger range of adsorbate concentrations for CH_4 than for H_2 because of the stronger adsorption of CH_4.

Figure 3.7 summarizes the ideal selectivity, that is, the ratio of single-component fluxes, of the membranes we have considered as the density of the modifying layer is increased. For membranes 1-3, the ideal selectivity is essentially that of the unmodified membrane, which significantly favors permeation of CH_4 under all operating conditions. As the thickness and density of the modifying layer increases, the ideal selectivity increases somewhat for membranes 4 and 5. In this range, the membrane is only selective for H_2 if the membrane thickness is less than 500 nm. Fabricating zeolite membranes with this thickness is currently a challenge.[46,47] For membrane 6, however, the ideal selectivity becomes infinity because CH_4 is excluded from the membrane. This

modifying layer is selective for H_2 because of a simple molecular sieving mechanism. When both species can permeate through the membrane, the selectivity of the membrane when exposed to a mixed gas feed can differ from the ideal selectivity.[48] This complication does not arise, however, if one species is excluded by molecular sieving. Figure 3.8 shows the selectivity and H_2 flux for membranes 4-6 when P_{feed} = 20 bar and P_{perrm} = 0 bar. For the unmodified membrane, the ideal selectivity is smaller than 1 because CH_4 is more favored by this membrane. For membrane 4 ideal selectivity decreases to 1 at L = 270 nm. The ideal selectivity of the membranes increased when degree of modification increased. For membrane 5, the ideal selectivity decreases to 1 at L = 400nm. While the ideal selectivity of membranes 4 and 5 are larger than that of the unmodified membranes, we can observe that the H_2 flux with those membranes is decreased slightly from the flux of the unmodified membranes. For these two modified membranes, the reduction of CH_4 flux is far more significant than the H_2 flux. That is, the modified pore mouths can effectively block CH_4 only while they still allow transport of most H_2 molecules. The most useful membrane, however, would be one in which CH_4 was excluded from the membrane, such as membrane 6. With this membrane, the ideal selectivity is infinity. H_2 can still diffuse through this membrane with 72 % of the flux through unmodified membrane when L=1000 nm. It is likely that membranes with thicker modifying layer could also exclude H_2 molecules. To date, however, we have not performed simulation for membranes with modifying layers thicker than the one already obtained.

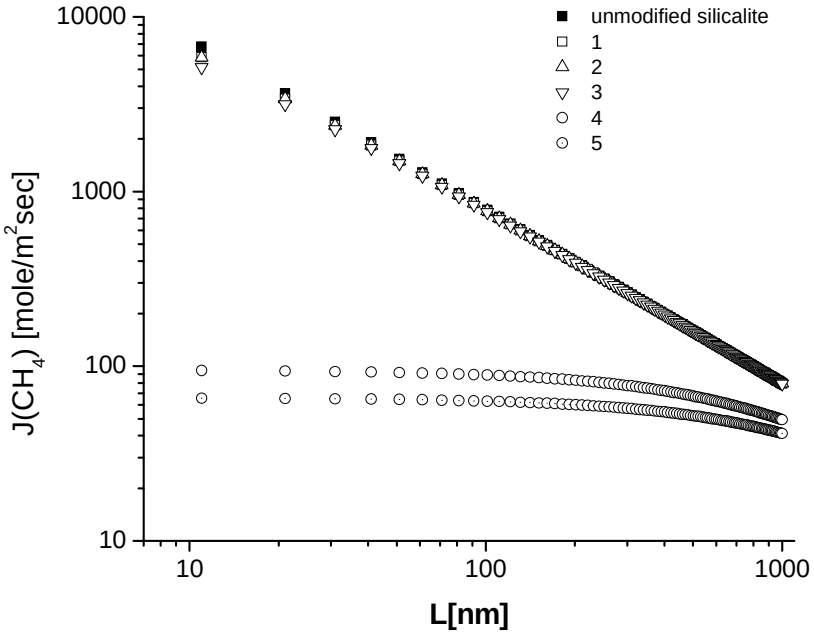

Figure 3.4: Net flux of CH_4 through surface modified silicalite. In every case, P_{feed}=10 bar and P_{perm}=0.3 bar.

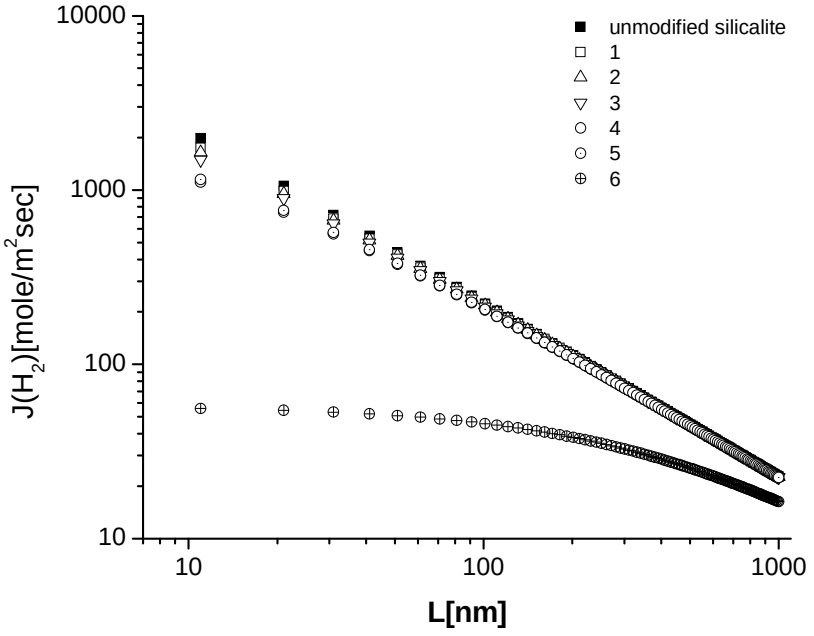

Figure 3.5: Net flux of H_2 through surface modified silicalite. In every case, P_{feed}=10 bar and P_{perm}=0.3 bar.

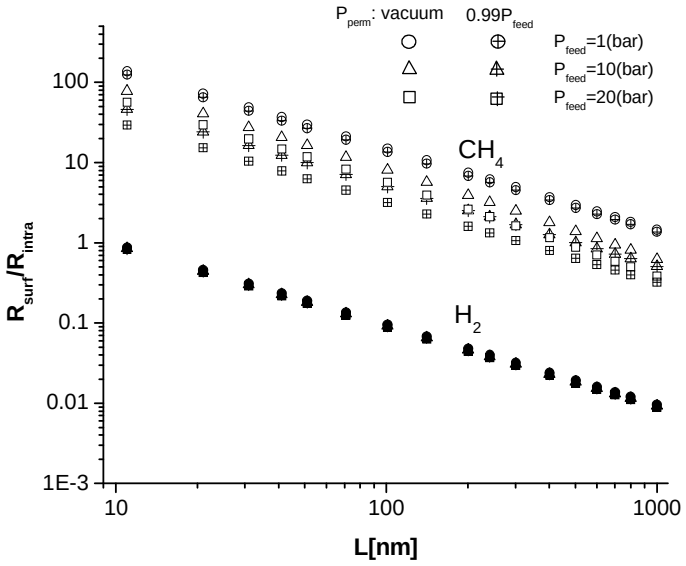

Figure 3.6: Surface resistance ratios as a function of membrane length, *L,* for surface-modified membrane 4. Results are shown for three values of P_{feed} and two values of P_{perm}. Open symbols represent CH_4 data, while closed symbols show H_2 data.

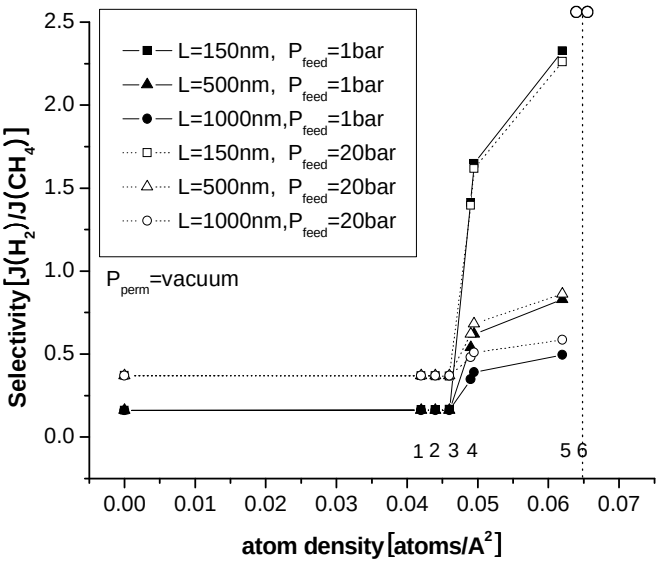

Figure 3.7: Ideal selectivity of H_2 relative to CH_4 as a function of the two dimensional density of the modifying layers. Results are shown for two values of P_{feed} and three membrane thicknesses. In every case, P_{perm} was assumed to be a vacuum. Selectivity is infinity at membrane 6 since CH_4 is blocked.

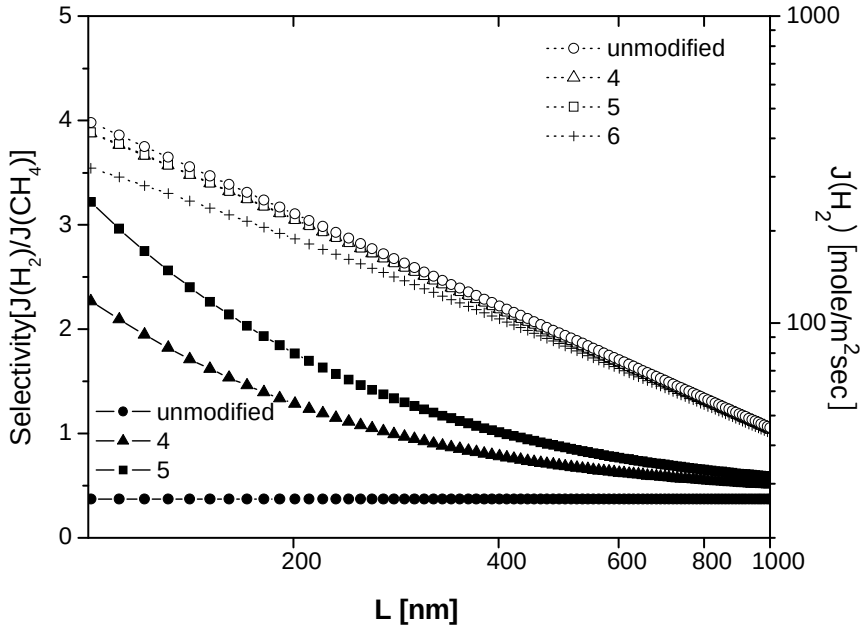

Figure 3.8: Ideal selectivity (filled symbols) and H_2 flux (open symbols) with an unmodified membrane and three modified membranes with various atom densities. Solid lines represent selectivity and dashed lines show flux.

3. 4 CONCLUSIONS

Our results indicate that it is possible, at least in principle, to make modifications to zeolites such as silicalite to make membranes that can selectively transport H_2 from H_2/CH_4 mixtures without a catastrophic drop in the membrane's H_2 flux. These membranes take advantage of a situation where increased surface resistances for CH_4 transport make it possible to separate CH_4 from H_2 with high selectivity. The general concept of making a local modification in the surface structure of a zeolite membrane may be useful in other separations in addition to the H_2/CH_4 separation we have considered here.

Although our simulations give some insight into the feasibility of this approach, several practical issues exist that would need to be carefully understood in order to use

this idea experimentally. If the density of the modifying layer is too high, the porous layers could become completely blocked, stopping permeation of both H_2 and CH_4. It is not clear what level of control in the surface modification would be necessary to create layers that block CH_4 without blocking all molecular transport. Another complication in real zeolite membranes is that net transport through polycrystalline films involves contributions from both zeolitic and non-zeolitic pores. High quality zeolite membranes are assumed to be dominated by transport through zeolitic pores, but non-zeolitic pores are always present and are typically thought to reduce separation selectivity.[49,50] It is conceivable that efforts to modify zeolite surfaces could also block or reduce access to non-zeolitic pores, although our simulations provide no direct information on this possibility. The simulation methods we have introduced here may be of use in understanding what impact modifying layers could have on non-zeolitic pores in polycrystalline films.

REFERENCES

(1) Department of Energy, U. S. *Fuel cell handbook 7th edition*; EG&G Technical Services, Inc., 2004.
(2) Ockwig, N. W.; Nenoff, T. M. *Chem. Rev.* **2007**, *107*, 4078.
(3) Kamakoti, P.; Morreale, B. D.; Ciocco, M. V.; Howard, B. H.; Killmeyer, R. P.; Cugini, A.; Sholl., D. S. *Science* **2005**, *307*, 569.
(4) Olson, D. H.; Kokotailo, G. T.; Lawton, S. L.; Meier, W. M. *J. Phys. Chem.* **1981**, *85*, 2238.
(5) Yu, M.; Amundsen, T. J.; Hong, M.; Falconer, J. L. *J. Membr. Sci.* **2007**, *298*, 182.
(6) Motuzas, J.; Julbe, A.; Noble, R. D. *Microporous Mesoporous Mater.* **2006**, *92*, 259.
(7) Julbe, A.; Motuzas, J.; Arruebo, M.; Noble, R. D.; Beresnevicius, J. *Stud. Surf. Sci. Catal.* **2005**, *158*, 129.
(8) Motuzas, J.; Julbe, A.; Noble, R. D.; Guizard, C.; Beresnevicius, Z. J.; Cot, D. *Microporous Mesoporous Mater.* **2005**, *80*, 73.
(9) Lai, R.; Gavalas, G. R. *Microporous Mesoporous Mater.* **2000**, *38*, 239.
(10) Lovallo, M. C.; Tsapatsis, M. *AIChE. J.* **1996**, *42*, 3020.
(11) Dong, W.; Long, Y. *Microporous Mesoporous Mater.* **2004**, *76*, 9.
(12) Aoki, K.; Kusakabe, K.; Morooka, S. *J. Membr. Sci.* **1998**, *141*, 197.
(13) Guan, G. Q.; Tanaka, T.; Kusakabe, K.; Sotowa, K. I.; Morooka, S. *J. Membr. Sci.* **2003**, *214*, 191.
(14) Poshusta, J. C.; Tuan, V. A.; Pape, E. A.; Noble, R. D.; Falconer, J. L. *Ind. Eng. Chem. Res.* **1998**, *37*, 3924.
(15) Hong, M.; Falconer, J. L.; Noble, R. D. *Ind. Eng. Chem. Res.* **2005**, *44*, 4035.
(16) Masuda, T.; Fukumoto, N.; Kitamura, M.; Mukai, S. R. *Microporous Mesoporous Mater.* **2001**, *48*, 239.
(17) Gopalakrishnan, S.; Yoshino, Y.; Nomura, M.; Nair, B. N.; Nakao, S. *J.Membr.Sci.* **2007**, *297*, 5.
(18) Skoulidas, A. I.; Sholl, D. S. *J. Phys. Chem. B* **2002**, *106*, 5058.
(19) Sholl, D. S. *Ind. Eng. Chem. Res.* **2000**, *39*, 3737.
(20) Bowen, T. C.; Falconer, J. L.; Noble, R. D.; Skoulidas, A. I.; Sholl, D. S. *Ind. Eng. Chem. Res.* **2002**, *41*, 1641.
(21) Newsome, D. A.; Sholl, D. S. *J. Phys. Chem. B* **2005**, *109*, 7237.
(22) Newsome, D. A.; Sholl, D. S. *Microporous Mesoporous Mater.* **2008**, *107*, 286.
(23) Skoulidas, A. I.; Sholl, D. S. *J. Phys. Chem. B* **2001**, *105*, 3151.
(24) Skoulidas, A. I.; Sholl, D. S. *J. Phys. Chem. A* **2003**, *107*, 10132.
(25) Sholl, D. S. *Acc. Chem. Res.* **2006**, *39*, 403.
(26) Mukhopadhyay, A. B.; Oligschleger, C.; Dolg, M. *Phys. Rev. B* **2003**, *67*, 014106.
(27) Mukhopadhyay, A. B.; Oligschleger, C.; Dolg, M. *J. Phys. Chem. B* **2004**, *108*, 16085.
(28) Newsome, D. A.; Sholl, D. S. *J. Phys. Chem. B* **2006**, *110*, 22681.

(29) van Beest, B. W. H.; Kramer, G. J.; van Santen, R. A. *Phys. Rev. Lett.* **1990**, *64*, 1955.
(30) Kramer, G. J.; Farragher, N. P.; van Beest, B. W. H.; van Santen, R. A. *Phys. Rev. B* **1991**, *43*, 5068.
(31) McGaughey, A. J. H.; Kaviany, M. *Int. J. Heat Mass Transfer* **2004**, *47*, 1799.
(32) Guissani, Y.; Guillot, B. *J. Chem. Phys.* **1996**, *104*, 7633.
(33) Wolf, D.; Keblinski, P.; Phillpot, S. R.; Eggebrecht, J. *J. Chem. Phys.* **1999**, *110*, 8254.
(34) Maginn, E. J.; Bell, A. T.; Theodorou, D. N. *J. Phys. Chem.* **1993**, *97*, 4173.
(35) Mori, H. *Prog. Theor. Phys.* **1965**, *33*, 423.
(36) Ahunbay, M. G.; Elliott, R. J.; Talu, O. *J. Phys. Chem.B.* **2005**, *109*, 923.
(37) Newsome, D. A.; Sholl, D. S. *Nano Lett.* **2006**, *6*, 2150.
(38) Chen, H.; Sholl, D. S. *J. Am. Chem. Soc.* **2004**, *126*, 7778.
(39) Skoulidas, A. I.; Ackerman, D. M.; Johnson, J. K.; Sholl, D. S. *Phys. Rev. Lett.* **2002**, *89*, 185901.
(40) Holt, J. K.; Park, H. G.; Wang, Y. M.; Stadermann, M.; Artyukhin, A. B.; Grigoropoulos, C. P.; Noy, A.; Bakajin, O. *Science* **2006**, *312*, 1034.
(41) Dubbeldam, D.; Calero, S.; Vlugt, T. J. H.; Krishna, R.; Massen, T. L. M.; Smit, B. *Phys. Rev. Lett.* **2004**, *93*, 088302.
(42) Heuchel, M.; Snurr, R. Q.; Buss, E. *Langmuir* **1997**, *13*, 6795.
(43) Han, J. W.; James, J. N.; Sholl, D. S. *Submitted to Surf. Sci.* **2008**.
(44) Goumans, T. P. M.; Wander, A.; Brown, W. A.; Catlow, C. R. A. *PCCP* **2007**, *9*, 2146.
(45) Frenkel, D.; Smit, B. *Understanding molecular simulation: From algorithms to applications*; Academic Press: London, 2002.
(46) Wang, Z.; Hedlund, J.; Sterte, J. *Microporous Mesoporous Mater.* **2002**, *52*, 191.
(47) Hedlund, J.; Sterte, J.; Anthonis, M.; Bons, A. J.; Carstensen, B.; Corcoran, N.; Cox, D.; Deckman, H.; De Gijst, W.; de Moor, P. P.; Lai, F.; McHenry, J.; Mortier, W.; Reinoso, J. *Microporous Mesoporous Mater.* **2002**, *52*, 179.
(48) Keskin, S.; Sholl, D. S. *J. Phys. Chem. C* **2007**, *111*, 14055.
(49) Poshusta, J. C.; Noble, R. D.; Falconer, J. L. *J. Membr. Sci.* **1999**, *160*, 115.
(50) Bowen, T. C.; Noble, R. D.; Falconer, J. L. *J. Membr. Sci.* **2004**, *245*, 1.

CHAPTER 4

CO_2/CH_4 SEPARATION USING DDR ZEOLITES*

The silica zeolite DDR is a strong candidate for separations of CO_2/CH_4 because of the narrow windows that control molecular transport inside the material's pores. To examine CO_2/CH_4 separation via molecular simulation, however, two issues remain unresolved: Forcefield parameterization and diffusivity calculation. In this chapter, we will introduce a new forcefield for this system that for the first time gives results that are consistent with all available experimental measurements and examine the mixture adsorption and single component diffusion properties which is essential for the mixture flux calculation.

4.1. CO_2/CH_4 SEPARATION USING DDR

Separation of CO_2 from CH_4 is an important problem because of the large volumes of natural gas that are known to contain high levels of CO_2.(1,2) Development of robust materials to achieve this gas separation in an energy efficient manner would have a significant impact on the possibility of using these resources in a manner that mitigates CO_2 emissions. Using small pore zeolites as separation membranes is an attractive approach to this challenge. A number of studies have focused on membranes made from SAPO-34, an aluminophosphate material with 8-membered rings (8MR).(3,4) Several pure silica zeolites also have pores defined by 8MR. Among these, the silica zeolite DDR ($Si_{120}O_{240}$) is especially attractive. The 8MR windows are 0.36×0.44 nm in size, similar in size to CH_4 but larger than CO_2.(5) This, in addition to the hydrophilic

---

* The results described in this chapter have been published in Sang Eun Jee, David S. Sholl, , *Journal of American Chemical Society* (2009), 131, 7896-7904

character of DDR, has led several groups to consider the use of DDR as a membrane for CO_2-related gas separations (6-11).

Despite the work that has been reported with DDR membranes, some important issues remain unresolved. To design a process using a zeolite membrane, it is essential to understand how mixtures of the relevant species adsorb and diffuse through the zeolite. Characterizing mixture diffusion in zeolites via experiments is a challenging task, and molecular simulations have become an important tool in providing detailed physical understanding of how diffusion in adsorbed mixtures occurs.(9,10,12-18) Molecular simulations have been reported to accurately describe the experimentally observed single component adsorption of CH_4 and CO_2 in DDR, and these simulations have highlighted features of the mixture adsorption of these species that are quite unusual compared to other zeolites and nanoporous materials.(9,10) As we will show below, the forcefields that were used in this previous work give inaccurate predictions of single component diffusion rates when compared to experimental measurements.(9,10) This means that previous efforts to characterize molecular diffusion in DDR via molecular simulations cannot reliably describe the properties of diffusing mixtures.

In chapter 4 and 5, therefore, we will describe a series of molecular simulations that provide the most accurate description of CO_2/CH_4 mixture transport in DDR to date. Throughout the calculation of DDR, we consider this adsorbed mixture at room temperature. The implications of our results for other temperatures are discussed in conclusion. Our results highlight some unusual properties of this material that greatly enhance its ability as a membrane for this gas separation. These calculations required a novel combination of simulation methods that will also be useful in studies of other small pore zeolites. In this chapter, firstly, we introduce a new forcefield that, for the first time, correctly describes the diffusion coefficients for single component CO_2 and CH_4 at low loading that have been reported experimentally. In developing this forcefield, we focused on the characteristics of the transition states that control molecular hopping between

adsorption sites in DDR. Previous forcefields have been based only on adsorption data,(19) meaning that they probe the energetic environment near preferred adsorption sites but include almost no information about transition states for diffusion. The experimentally observed diffusivities for CH_4 in DDR point to a complication that has not been addressed in previous treatments of this system, namely that this molecule diffuses so slowly that its diffusion cannot be successfully described using Molecular Dynamics (MD) simulations. To address this issue, we used a Transition State Theory (TST) approach discussed in chapter 2 to characterize the site-to-site hopping rates of CH_4 as a function of molecular loading in DDR. Subsequent Kinetic Monte Carlo (KMC) simulations using our TST-derived hopping rates provide information on the loading-dependent diffusivity of CH_4. CO_2 diffuses much more rapidly than CH_4, so it is possible to assess this diffusion using standard MD methods. With a new forcefield, we describe mixture adsorption properties at various conditions, which is necessary to calculate flux and selectivities. Single component diffusivities of CO_2 and CH_4 are also examined to understand the transport mechanism in DDR, suggesting insight of mixture transport properties.

Mixture diffusivities measurement is another significant factor in flux calculation. However, the difference in time scales between CH_4 diffusion and CO_2 diffusion in DDR raises technical challenges for accurately describing mixture diffusion with molecular simulations. We will show how these challenges can be overcome by developing new methods in chapter 5 and make a conclusion with the flux calculation.

4.2. TRANSPORT PROPERTIES MEASUREMENT

We used the DDR crystal structure measured experimentally by Gies et al.(5) The 19-hedra cages in DDR are the only cages relevant for molecular transport; the decahedral and dodecahedral cages are not accessible to diffusing molecules. Molecules

were not allowed to adsorb inside the smaller cages in our simulations. The structure of one of the 19-hedra cages that defines the accessible volume in DDR is shown in Fig. 4.1.

Our simulations treated the DDR crystal as being rigid. The molecule-DDR interaction energies were precomputed for a high resolution spatial grid and in subsequent simulations these energies were computed by high quality interpolation from the precomputed values. Periodic boundary conditions were used in all simulations. All calculations were performed at room temperature.

CH_4-CH_4 and CO_2-CO_2 interactions were treated using the potentials introduced by Goodbody *et al.*(20) and Makrodimitris *et al.*(21) without adjustment. The potentials are summarized in Table 1. All cross-species interactions were defined using Lorenz-Berthelot combining rules based on the interaction potentials listed in Table 1. All calculations used spherical cutoffs of radius 13 Å for Lennard-Jones potentials and 25 Å for the Coulombic contributions to CO_2-CO_2 interactions.

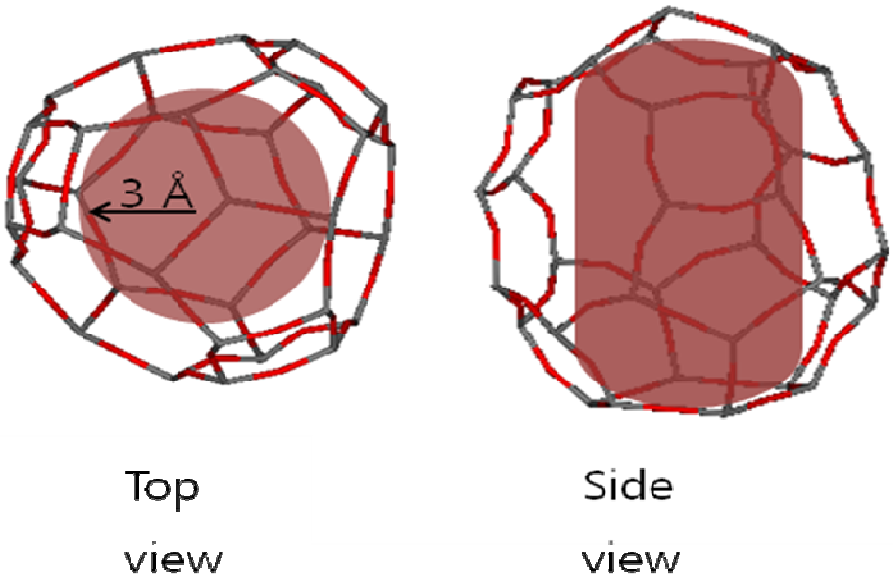

Figure 4.1: Top and side view of a single 19-hedra cage in DDR, with shaded regions indicating the a cylindrical volume with radius 3 Å associated with adsorption in this cage. In the top view, the three 8MR are visible to the right, the bottom left and top left.

.

Grand Canonical Monte Carlo (GCMC) was used to calculate adsorption isotherms in a simulation volume containing 6 DDR unit cells. These simulations involved a total of 5×10^7 moves for equilibration and up to 5×10^7 moves for data collection for each state point. All results below are reported in terms of fugacities. At the highest fugacities we simulated, the non-ideality of CO_2 would need to be included to convert fugacities to pressures.

As we will show below, single component diffusion of CH_4 in DDR gives diffusivities less than 10^{-7} cm^2/s in most cases, making simulation of this situation with MD challenging. We only applied MD to measure single component diffusion in cases where the resulting diffusivity was larger than 10^{-7} cm^2/s. This restriction allowed us to examine CO_2 diffusion at all loadings with MD, but only a small number of CH_4 loadings. MD simulations were performed using a simulation volume of 6-24 unit cells, depending on the adsorbate loading. In single component MD simulations, 2×10^7-4×10^7 GCMC steps were used to initialize each system with the desired number of molecules. We found that this procedure was important in order to correctly distribute molecules on DDR's inhomogeneous potential energy surface. Each simulation was further equilibrated with 1.5×10^7 canonical MC moves and 1.5×10^7 MD steps. Data was then collected from MD simulations 20 ns in duration using 1 fs timesteps. These MD simulations were used to measure both the self diffusivity, D_s, and the corrected diffusivity, D_0 by averaging over 30 independent trajectories for each adsorbate loading.(12,14,22)

As mentioned above, MD is not suitable for accurately simulating CH_4 diffusion in DDR because of its slow diffusion. Instead, we developed a transition state theory (TST) based lattice model that accurately describes the loading-dependent diffusion of CH_4 in DDR. Once this model is defined, Kinetic Monte Carlo (KMC) can be used to simulate diffusion. This approach is based on the methods of Tunca and Ford(23-26) and the subsequent work by Dubbledam and coworkers.(27,28) We define the hopping rate of

CH_4 molecules from a DDR cage containing *i* molecules into an adjacent cage containing j molecules as

$$k_{ij} = \kappa \sqrt{\frac{1}{2\beta\pi m}} \frac{\exp(-\beta F(q^*))}{\int dq \exp(-\beta F(q))} \qquad (4.1)$$

where, $\beta = (k_B T)^{-1}$, q is the reaction coordinate, q^* defines the dividing plane associated with the transition state, $F(q)$ is the system's free energy when the moving molecule is at q, and the integral is evaluated over the microstate defined by one DDR cage. We assume that the transmission coefficient, κ, is unity. At some loadings, it is possible to directly compare MD simulations with our TST/KMC results and we show below that these two methods are in good agreement, supporting the validity of this treatment. We find that the maximum loading of CH_4 in DDR is 5 molecules per cage, so 6×5 distinct hopping rates, k_{ij}, were computed with $1 \le i \le 5$ and $0 \le j \le 5$. Once these rates are known, KMC can be used to simulate net diffusion at any loading of interest.

To apply Eq. (1), we computed the free energy, $F(q)$, using a histogram sampling method.(24,25) We considered a dividing surface in the middle of an 8MR window as q^*. At the beginning of the simulation, molecules are inserted in each site at the loadings required for the transition rate of interest. 1×10^8 canonical MC moves per particle were then used to equilibrate system and 2×10^8 canonical moves were used to produce data. All degrees of freedom, that is, the positions of all adsorbed molecules at the loading of interest, were sampled in these simulations. Moves that would have transferred molecules past the dividing surface were rejected. After every MC step, particle positions are recorded, allowing the free energy to be computed using $\beta F(q) = -\ln < P(q) >$, where $P(q)$ is the probability that the molecule of interest lies at reaction coordinate q. No bias potential was applied during these calculations.

4.3. FORCEFIELD PARAMETERIZATION IN SMALL PORE ZEOLITES

Previous simulations of CH_4 and CO_2 adsorption in DDR(9,10) were based on adsorbate-zeolite potentials introduced by Dubbeldam *et al.*(19) and Makrodimitris *et al.*.(21) However, we have found these potentials do not reproduce recently reported experimental data by Hedin *et al.* and Chance *et al.*.(29,30) Figure 4.2(a) shows adsorption isotherms from GCMC simulations for CO_2 and CH_4 in DDR at 298 K using the forcefields cited above, as well as experimental data.(29,30) The uncertainties in the simulated data are smaller than the symbol sizes. Our adsorption isotherms are presented in terms of molecules per unit cell and fugacity. A loading of 1 molecule/unit cell corresponds to 2.22 (6.11) mg/g adsorption for CH_4 (CO_2). To allow a comparison with experimental data, the Peng-Robinson equation of state was used to estimate the fugacity associated with the experimentally reported pressures. It is clear from Fig. 4.2(a) that these interatomic potentials provide a reasonable description of CO_2 and CH_4 adsorption in DDR.

Figure 4.2(b) shows the computed self diffusion coefficients for CO_2 and CH_4 from simulations using the interatomic potentials defined above. These results for both species were computed using MD because the predicted diffusion coefficients are larger than 10^{-7} cm^2/s. These results are compared to experimental data for diffusion of each species at dilute loadings, which is also shown on the same figure.(29,30) In contrast to the adsorption isotherms, the predicted diffusion coefficients differ strongly from the experimental data. These simulations overpredict the CH_4 (CO_2) diffusivity at dilute loadings by about two orders (one order) of magnitude. It is useful to note that because the diffusion data in Fig. 4.2(b) comes from PFG-NMR experiments, it is clear that the slow diffusion that is observed is associated with the intrinsic pore topology of DDR, not with intracrystalline grain boundaries or other defects that might affect diffusion rates over large length scales.

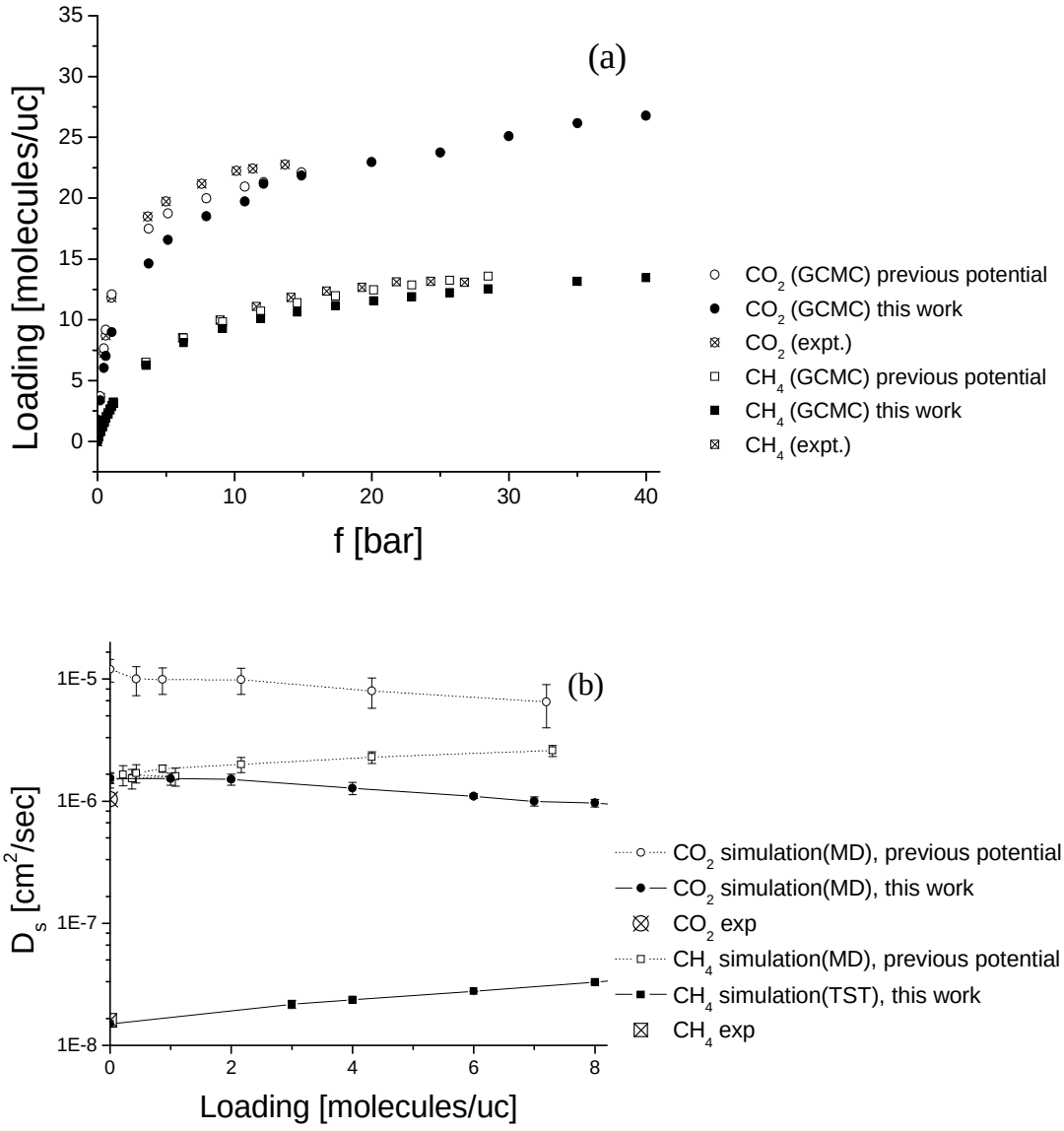

Figure 4.2: (a) Single component adsorption isotherms of CO_2 and CH_4 in DDR from GCMC simulations and experiments at 298 K. Open symbols show GCMC simulation results using a previous potential,(19) closed symbols show GCMC results using potentials from this work. Crossed symbols show experimental data.(29,30) (b) Single component self diffusivities of CO_2 and CH_4 in DDR from MD simulations at 298 K, using the same notation as (a).

Motivated by this observation, we have developed new forcefields that are more consistent with the experimental adsorption and diffusion data. To improve the treatment of diffusion for each species, we focused on the transition states for diffusion of each molecule. In DDR, CH_4 adsorbs inside the zeolite cages(9,10) and the transition states for CH_4 diffusion are the 8MR rings that separate adjacent cages. The energy of CH_4 in the 8MR is strongly influenced by the repulsive core of the CH_4-O potential. We examined CH_4-O potentials of the form

$$V(r)=\varepsilon \left(\frac{C_1}{(r/\sigma)^n}-\frac{C_2}{(r/\sigma)^6}\right) \qquad (4.2)$$

When $n=12$ and $C_1=C_2=4$, this is the standard LJ potential. For other values of n, we defined C_1 and C_2 so the minimum of the resulting potential lies at the same coordinate as the standard LJ potential and so that they have minimal differences in energy at the coordinates the define the inflection points of the two potentials. With these choices, the differences in adsorption energy between the two potentials are small in the vicinity of the energy minima that dominate adsorption. After examining a range of parameters, we found that the slow diffusion of CH_4 observed experimentally could best be reproduced by using $n=18$ instead of 12. The key feature of this approach is that the repulsive wall of the potential is considerably steeper than the standard Lennard-Jones potential. It was not possible to correctly describe CH_4 diffusion and adsorption using potentials that varied the well depth of the potential without also varying the steepness of the repulsive portion of the potential.

CH_4- CH_4	CH_4- O_{zeo}	C_{CO2}- C_{CO2}	O_{CO2}- O_{CO2}	O_{zeo}- O_{zeo}
n=12	n=18	n=12	n=12	n=18
C_1=4	C_1=4	C_1=4	C_1=4	C_1=4
C_2=4	C_2=3	C_2=4	C_2=4	C_2=3
ε / k_B=	ε / k_B=	ε / k_B=	ε / k_B=	ε / k_B=
147.9 [K]	160.9 [K]	28.129 [K]	80.507 [K]	76 [K]
σ=3.73 [Å]	σ=3.218 [Å]	σ=2.757 [Å]	σ=3.033 [Å]	σ=2.5 [Å]

Table 4.1: Interaction potential and forcefield parameters of CH_4, CO_2 in DDR structures are developed to reproduce experimental data.

The adsorption sites of CO_2 in DDR are very different from CH_4. The most energetically preferred sites for CO_2 adsorption lie inside the 8MR, with CO_2 adsorbing in the zeolite's cages only after the 8MR are occupied.(9,10) Diffusion of CO_2 in DDR is controlled by the transition state for hopping of CO_2 from an 8MR into an adjacent cage. Examination of this TS indicated that the TS energy is primarily controlled by the electrostatic interactions between CO_2 and the zeolite. As a result, the only avenue for significantly altering the energy of this TS while retaining the form of the interatomic potentials defined above was to increase the partial charges of O and Si. We chose to increase these charges to -1.5e and +3e, which are considerably larger than would typically be assigned in materials of this kind.(21,31-33) Using smaller charges significantly decreased the agreement between the diffusivities calculated with MD and the experimental data. Because increasing these charges increases adsorption of CO_2 in DDR, the LJ-parameters for interactions between atoms in CO_2 and the framework oxygens were also adjusted. An 18-6 LJ potential was used for these interactions because we found that this slightly increased the TS energy relative to the energy minimum in the 8MR. The effect of modifying the LJ potential in this way was relatively small compared

to the effect of the framework partial charges. By making these adjustments, our forcefield simultaneously reproduces the Henry's coefficient of adsorption and the dilute loading diffusivity at the same time.

Table 4.1 summarizes our new forcefield. With our potential, we calculated adsorption with GCMC and diffusion using MD (for CO_2) and TST-based KMC (for CH_4), giving the results shown in Fig. 4.2. By construction, these potentials reproduce the experimental adsorption isotherms and dilute loading diffusivities with reasonable (although not perfect) accuracy. We emphasize that this forcefield was derived by treating the zeolite framework as rigid, as were earlier forcefield in the literature. If a flexible framework was to be considered, a new forcefield for molecule-framework interactions would have to be developed in order for this approach to yield results consistent with the experimental data. The adsorption isotherms from the earlier potentials and our new potentials are similar, although the earlier CO_2 potential is in better agreement with the experimental isotherm over the full range of pressures for which data is available. In the remainder of the paper, we use the forcefield introduced above to examine adsorption and diffusion of CO_2/CH_4 mixtures in DDR at 300 K.

4.4. ADSORPTION PROPERTIES

As described above, CO_2 and CH_4 molecules prefer different adsorption sites in DDR.(9,10). Understanding the impact of these sites on adsorption of CO_2/CH_4 mixtures is important for understanding diffusion of these molecules, so in this section we highlight several aspects of CO_2/CH_4 adsorption. CO_2 adsorbs more strongly than CH_4 in single component as well as binary adsorption, as shown in Fig. 4.3 and Fig. 4.4, which show GCMC results for adsorption from an equimolar gas phase mixture. Figure 4.5 shows GCMC results for mixture adsorption over a range of bulk compositions at two

representative fugacities. The adsorption selectivities for CO_2 relative to CH_4 are 2~9 under these conditions.

To characterize where molecules adsorbed in DDR, we divided adsorption into volumes associated with 8MR windows and DDR cages for CO_2 and CH_4. The main cages of DDR are similar to spheres with radius 4 Å. We partitioned the pore volume by defining molecules with their center of mass located 3 Å or closer to the center of a cage as lying in a cage and all other molecules as being situated in a window. This partitioning differs slightly from the method used previously by Krishna,(9) but we feel it describes the geometry of the pore volume in a somewhat more natural way. Figure 4.6 shows single component adsorption isotherm in terms of the adsorbed amounts in the two regions. No CH_4 was found to adsorb in DDR's windows, so only total CH_4 loadings are shown in Fig. 4.6. CO_2 prefers the windows at low total loadings and then occupies cages as the pressure is increased.(9,10) Figure 4.7 shows the adsorbed CO_2 molecules per window as a function of total adsorbed amount of CO_2 in both single component and binary mixtures. It is clear that the CO_2 adsorption in DDR windows is almost independent of the CH_4 loading. This shows that CO_2 adsorption and CH_4 adsorption is competitive only in the cages.

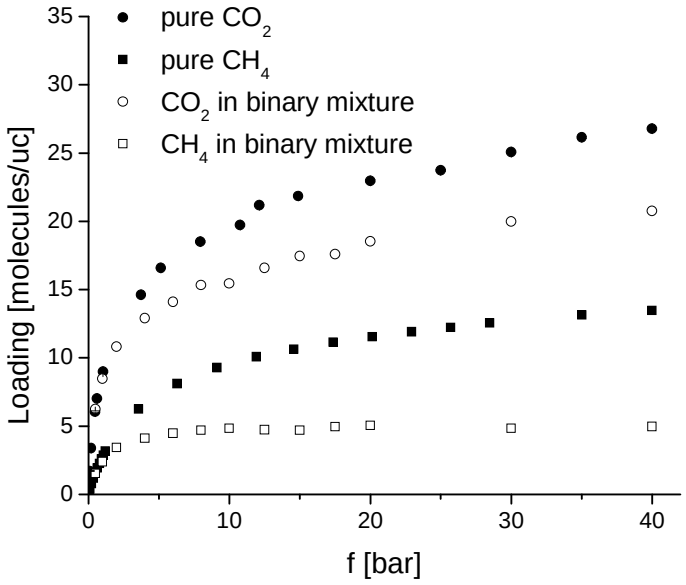

Figure 4.3: Single component (filled symbols) and binary adsorption (open symbols) isotherms of CO_2 and CH_4 in DDR from GCMC simulations. The binary adsorption isotherm is for an equimolar bulk phase. Circles and rectangles represent CO_2 and CH_4.

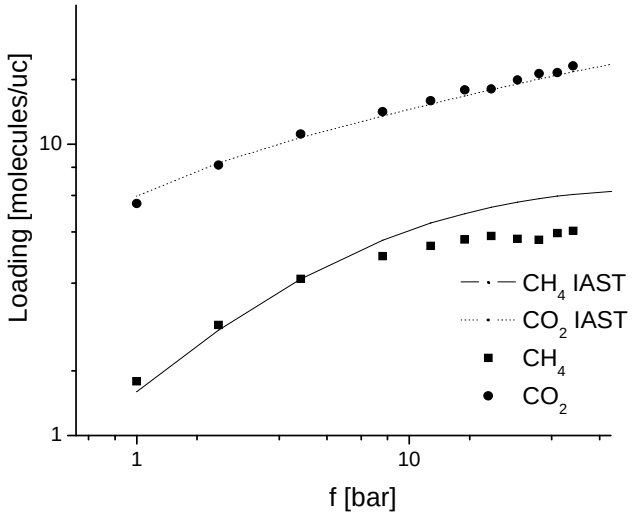

Figure 4.4: Binary adsorption isotherm data from GCMC (symbols) and modified IAST (curves) for adsorption from an equimolar bulk CO_2/CH_4 mixture.

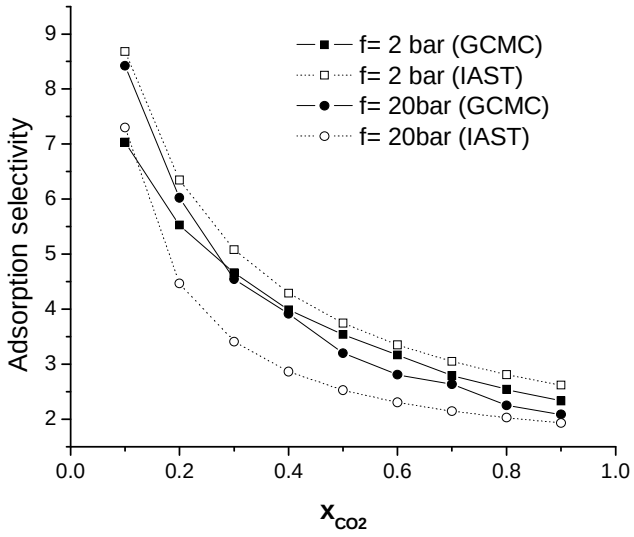

Figure 4.5: Adsorption selectivity from GCMC (filled symbols) and modified IAST (open symbols) are shown as a function of mole fraction of CO_2 in the bulk phase. Squares (circles) shows results from a bulk phase fugacity of 2 (20) bar.

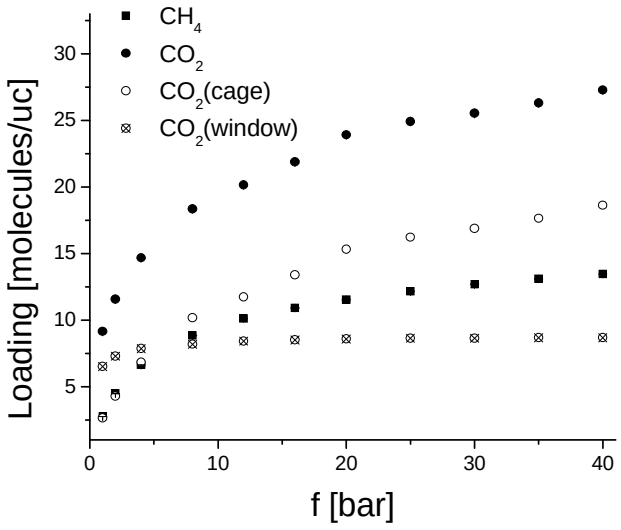

Figure 4.6: Single component adsorption isotherm of CH_4 and CO_2 in DDR from GCMC with the contributions from the DDR cages and windows shown separately for CO_2.

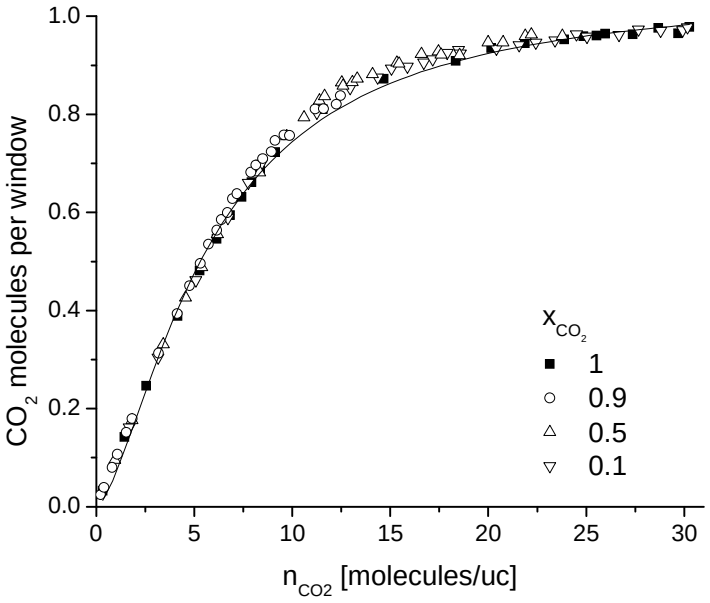

Figure 4.7: The number of CO_2 molecules per 8MR window as a function of total CO_2 loading in DDR for single-component adsorption (filled squares) and mixture adsorption with CH_4 (open symbols) with the indicated bulk phase mole fractions. The solid line was fitted to the single component data.

The results above provide useful insight into predicting mixture adsorption isotherms in DDR using Ideal Adsorbed Solution Theory (IAST). IAST is a well-known method to predict mixture isotherms from single-component data,(34) but applying conventional IAST to CH_4/CO_2 mixtures in DDR overestimates (underestimates) the adsorbed amount of CO_2 (CH_4).(8-10) Figures 4.6 and 4.7 suggest that a simple modification of IAST can be used to describe mixture adsorption in this system. Specifically, we used IAST to describe the adsorption of mixtures of CH_4 and CO_2 in the cages of DDR, but then predicted the total adsorbed amount of CO_2 by adding the adsorbed CO_2 in the 8MR windows directly from our single-component data. Figure 4.4 shows that our modified IAST method works accurately for equimolar bulk mixtures,

although the amount of CH_4 adsorption is overpredicted at the highest fugacities we examined. Figure 4.5 shows that this method also captures the trends in adsorption selectivity seen in our GCMC calculations as the composition of the bulk phase is varied. This application of IAST does not predict the mixture isotherms at high loadings with quantitative accuracy, but its performance is considerably better than the results of conventional IAST for this adsorbed mixture.(34)

4.5. SINGLE COMPONENT DIFFUSION PROPERTIES

Figure 4.8 shows single-component self and corrected diffusivities, D_s and D_0, respectively, as a function of loading for CO_2 and CH_4 in DDR at 298 K from calculations using the new forcefields we described above. Here, the CO_2 results were computed using MD while the CH_4 results were computed using TST-based KMC. The individual hopping rates determined from TST for CH_4 are shown in Fig. 4.9. From Fig. 4.8, three observations can be made. First, CO_2 diffuses 1-2 orders of magnitude faster than CH_4 in DDR at all loadings. This is an important observation for practical use of DDR as a membrane to separate CO_2/CH_4 mixtures, because it means that both adsorption and diffusion in this material favor transport of CO_2. Second, $D_0 \approx D_s$ for both species. That is, collective motions of the diffusing molecules are minimal,(14) a situation that is not unusual in cage type zeolites.(27,28,35,36) Finally, the CO_2 diffusion coefficients decrease as a function of loading while CH_4 diffusion initially increases as a function of loading and then decreases.

The qualitative trends in the loading-dependent diffusion coefficients of CH_4 and CO_2 can be understood in terms of the adsorption sites preferred by each species. For CH_4, diffusion is dominated by the large energy barrier that exists for molecules hopping through the 8MR windows between cages. As the CH_4 loading increases, adsorbate-

adsorbate interactions between additional CH_4 molecules in the initial and final cages in this process reduce the net energy barrier, causing an increase in the overall diffusivity. This tendency is reversed as the CH_4 loading become very high and steric hindrance effects reduce the possibility of CH_4 molecules hopping from cage to cage. This behavior has been seen in the diffusion in a variety of nanoporous materials with cages separated by sizeable energy barriers.(9,27,35,37-41)

Unlike CH_4, the diffusivity of CO_2 decreases monotonically as the loading is increased. This occurs because adsorbed CO_2 molecules preferentially occupy the 8MR windows and, while in these positions, block hopping by other CO_2 molecules. The fact that the preferred site for CO_2 can accommodate only one molecule makes this situation quite different from the behavior of CH_4, where multiple molecules can coexist in the preferred adsorption sites.

In measuring CH_4 diffusion in DDR, we used TST-based KMC methods since MD cannot measure slow diffusion in the range of 10^{-8} cm^2/s, as discussed above. One outcome from our calculations is that for a small range of CH_4 loadings, the diffusivities predicted via this TST-based KMC method are larger than 10^{-7} cm^2/s. We therefore performed MD simulations to examine CH_4 diffusion at these loadings (14-18 molecules/unit cell). The results from these MD calculations are shown in Fig. 4.8. The close agreement between these MD results and our TST-based KMC calculations provides strong support for the validity of the latter approach.

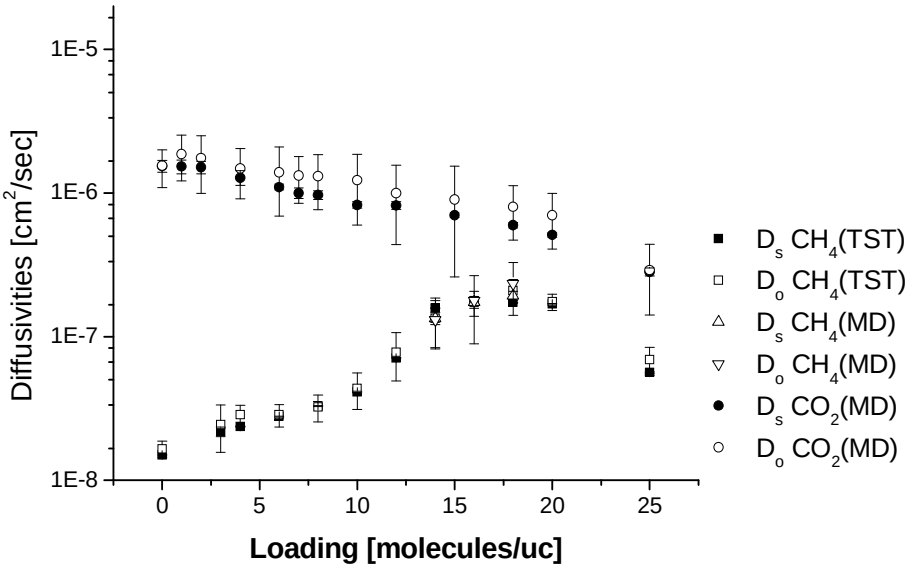

Figure 4.8: Calculated single component diffusivities of CH_4 and CO_2 in DDR. All CO_2 results are from MD simulations. CH_4 results are shown at all loadings from TST-based KMC simulations and over a limited range of loadings from MD simulations.

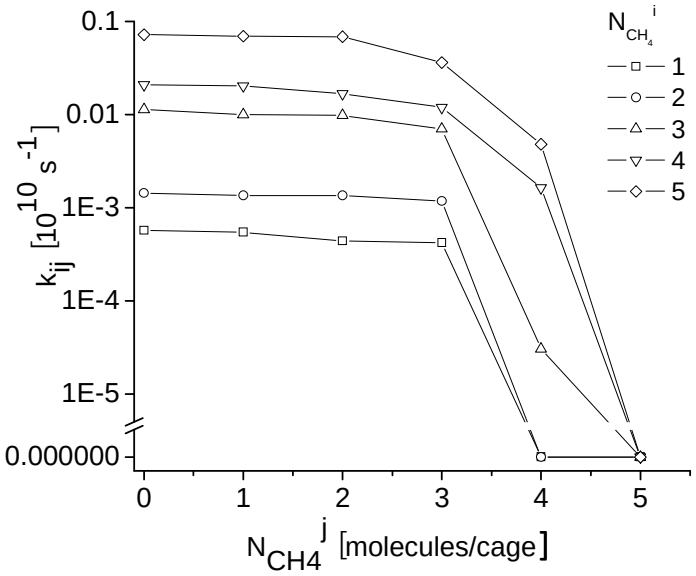

Figure 4.9: Hopping rate k_{ij} from i cage to j cage as calculated from TST shown as the number of the CH_4 molecules in the target cage, N_{CH4}^{j}. N_{CH4}^{i} is the number of the CH_4 molecules in the cage from which the hopping CH_4 molecule departs.

4.6. CONCLUSIONS

The development of materials that can efficiently separate CO_2 from other gases has the potential to allow large-scale mitigation of CO_2 emissions. The efficient separation of CO_2 and CH_4 is challenging because of the similar size of these two molecules. This specific separation has great practical significance because of the large volumes of CO_2-contaminated natural gas that are known worldwide.

We have shown that the adsorption properties and single component diffusion properties of CO_2 and CH_4 in the silica zeolite DDR have potentially useful properties that make this material attractive as a membrane for CO_2/CH_4 separations.

Our results required a methodological advance that were crucial for an accurate description of DDR and will also be relevant for modeling of other small pore zeolites. We have introduced new forcefields to simulate these adsorbed species that for the first time correctly capture the experimentally observed adsorption and dilute loading diffusion data. Previous molecular simulations of DDR used forcefields that greatly overpredicted the diffusion rates of both molecular species, so they could not give reliable information on the performance of DDR as a membrane. Once the diffusion of CH_4 is described accurately in DDR, it is clear that MD is not suitable for characterizing this slowly diffusing species. We introduced a transition state theory-based approach that rigorously describes the loading dependent diffusion of CH_4 as a single adsorbed component.

Mixture adsorption isotherms have been measured with new forcefields and we confirmed the well known results: CO_2 adsorbs preferentially in DDR relative to CH_4 and CO_2 adsorbs the window and cage sites of DDR while CH_4 adsorbs only in the cage(10,39). CO_2 molecules saturate window sites at first both in single component and mixture adsorption and CO_2 molecules per window is not affected by CH_4 molecules, suggesting the prohibition of the mobility of CH_4 in diffusion procedure. We will discuss about the effect of window saturation on the mixture component diffusivities at chapter 5.

Modified IAST method showed more accurate results than conventional IAST by considering competitions of two species only in the cages.

Single component diffusivities with new forcefields showed that CO_2 molecules diffuse faster than CH_4 one to two orders of magnitude. However, usually diffusion in mixtures is expected to occur via what can be thought of reversion to the mean: the existence of a slowly diffusing species slows down more rapidly diffusing molecules and vice versa. We will examine mixture diffusivities and discuss interactions at chapter 5 and conclude with permeability calculation based on adsorption and diffusion.

REFERENCES

(1) RW Baker: Membrane technology and applications, McGraw-Hill, New York, 2000.

(2) RW Baker: Future directions of membrane gas separation technology. Ind. Eng. Chem. Res. 41 (2002) 1393-411.

(3) SG Li, JL Falconer, RD Noble: SAPO-34 membranes for CO_2/CH_4 separation. J. Membr. Sci. 241 (2004) 121-35.

(4) SG Li, JL Falconer, RD Noble: Improved SAPO-34 membranes for CO_2/CH_4 separations. Adv. Mater. 18 (2006) 2601-03.

(5) H Gies: Studies on clathrasils .9. crystal-structure of deca-dodecasil 3R, the missing link between zeolites and clathrasils. Z. Kristallogr. 175 (1986) 93-104.

(6) W Zhu, F Kapteijn, JA Moulijn, MC den Exter: Shape selectivity in adsorption on the all-silica DD3R. Langmuir 16 (2000) 3322-29.

(7) W Zhu, F Kapteijn, JA Moulijn, JC Jansen: Selective adsorption of unsaturated linear C-4 molecules on the all-silica DD3R. Phys. Chem. Chem. Phys. 8 (2000) 1773-2779.

(8) H Chen, DS Sholl: Examining the accuracy of ideal adsorbed solution theory without curve-fitting using transition matrix Monte Carlo simulations. Langmuir 23 (2007) 6431-37.

(9) R Krishna, JM van Baten: Influence of segregated adsorption on mixture diffusion in DDR zeolite. Chem. Phys. Lett. 446 (2007) 344-49.

(10) R Krishna, JM van Baten: Segregation effects in adsorption of CO_2-containing mixtures and their consequences for separation selectivities in cage-type zeolites. Sep. Purif. Technol. 61 (2008) 414-23.

(11) T Tomita, K Nakayama, H Sakai: Gas separation characteristics of DDR type zeolite membrane. Micropor. Mesopor. Mater. 68 (2004) 71-75.

(12) DS Sholl: Understanding macroscopic diffusion of adsorbed molecules in crystalline nanoporous materials via atomistic simulations. Acc. Chem. Res. 39 (2006) 403-11.

(13) AI Skoulidas, DS Sholl: Direct tests of the darken approximation for molecular diffusion in zeolites using equilibrium molecular dynamics. J. Phys. Chem. B 105 (2001) 3151-54.

(14) AI Skoulidas, DS Sholl: Transport diffusivities of CH_4, CF_4, He, Ne, Ar, Xe, and SF_6 in silicalite from atomistic simulations. J. Phys. Chem. B 106 (2002) 5058-67.

(15) R Krishna, D Paschek: Self-diffusivities in multicomponent mixtures in zeolites. Phys. Chem. Chem. Phys. 4 (2002) 1891-98.

(16) R Krishna, JM van Baten: Describing binary mixture diffusion in carbon nanotubes with the Maxwell-Stefan equations. An investigation using molecular dynamics simulations. Ind. Eng. Chem. Res. 45 (2006) 2084-93.

(17) R Krishna, JM van Baten, E Garcia-Perez, S Calero: Diffusion of CH_4 and CO_2 in MFI, CHA and DDR zeolites. Chem. Phys. Lett. 429 (2006) 219-24.

(18) D Paschek, R Krishna: Kinetic monte carlo simulations of tranport diffusivities of binary mixtures in zeolites. Phys. Chem. Chem. Phys. 3 (2001) 3185-91.

(19) D Dubbeldam, S Calero, TJH Vlugt, R Krishna, TLM Massen, B Smit: United atom force field for alkanes in nanoporous materials. J. Phys. Chem. B 108 (2004) 12301-13.

(20) SJ Goodbody, K Watanabe, D MacGowan, JPRB Walton, N Quirke: Molecular simulation of methane and butane in silicalite. J. Chem. Soc. Faraday Trans. 87 (1991) 1951-58.
(21) K Makrodimitris, GK Papadopoulos, DN Theodorou: Prediction of permeation properties of CO_2 and N_2 through silicalite via molecular simulations. J. Phys. Chem. 105 (2001) 777-88.
(22) EJ Maginn, AT Bell, DN Theodorou: Transport diffusivity of methane in silicalite from equilibrium and nonequilibrium simulations. J. Phys. Chem. 97 (1993) 4173-81.
(23) DM Ford, ED Glandt: Molecular simulation study of the surface-barrier effect - dilute gas limit. J. Phys. Chem. 99 (1995) 11543-49.
(24) C Tunca, DM Ford: A hierarchical approach to the molecular modeling of diffusion and adsorption at nonzero loading in microporous materials. Chem. Eng. Sci. 58 (2003) 3373-83.
(25) C Tunca, DM Ford: Coarse-grained nonequilibrium approach to the molecular modeling of permeation through microporous membranes. J. Chem. Phys. 120 (2004) 10763-67.
(26) C Tunca, DM Ford: A transition-state theory approach to adsorbate dynamics at arbitrary loadings. J. Chem. Phys. 111 (1999) 2751-60.
(27) D Dubbeldam, E Beerdsen: Molecular simulation of loading-dependent diffusion in nanoporous materials using extended dynamically corrected transition state theory. J. Chem. Phys. 122 (2005) 224712.
(28) D Dubbeldam, S Calero, TLM Maesen, B Smit: Incommensurate diffusion in confined systems Phys. Rev. Lett. 90 (2003) 245901.
(29) RR Chance, CO_2/CH_4 separation: Molecular transport in microporous inorganic membranes, 229th ACS National Meeting, San Diego, CA, United States, 2005.
(30) N Hedin, GJ DeMartin, WJ Roth, KG Strohmaier: PFG NMR self-diffusion of small hydrocarbons in high silica DDR, CHA and LTA structures. Micropor. Mesopor. Mater. 109 (2008) 327.
(31) GJ Kramer, NP Farragher, BWH van Beest, RA van Santen: Interatomic force-fields for silicas, aluminophosphates, and zeolites - derivation based on ab initio calculations. Phys. Rev. B 43 (1991) 5068-80.
(32) BWH van Beest, GJ Kramer, RA van Santen: Force-fields for silicas and alumninophosphates based on ab initio calculations. Phys. Rev. Lett. 64 (1990) 1955-58.
(33) AI Skoulidas, DS Sholl, JK Johnson: Adsorption and diffusion of carbon dioxide and nitrogen through single-walled carbon nanotube membranes. J. Chem. Phys. 124 (2006) 054708.
(34) A.L.Myers, JM Prausnitz: Thermodynamics of mixed-gas adsorption. AIChE. J. 11 (1965) 121-27.
(35) E Beerdsen, D Dubbeldam, B Smit: Understanding diffusion in nanoporous materials. Phys. Rev. Lett. 96 (2006) 044501.
(36) D Selassie, D Davis, J Dahlin, E Feise, G Haman, DS Sholl, D Kohen: Atomistic Simulations of CO_2 and N_2 Diffusion in Silica Zeolites: The Impact of Pore Size and Shape. J. Phys. Chem. C 112 (2008) 16521-31.

(37) AI Skoulidas, DS Sholl: Self-Diffusion and transport diffusion of light gases in metal-organic framework materials assessed using molecular dynamics simulations. J. Phys. Chem. B 109 (2005) 15760-68.
(38) AI Skoulidas, DS Sholl: Molecular dynamics simulations of self-diffusivities, corrected diffusivities, and transport diffusivities of light gases in four silica zeolites to assess influences of pore shape and connectivity. J. Phys. Chem. A 107 (2003) 10132-41.
(39) R Krishna, JM van Baten: Insights into diffusion of gases in zeolites gained from molecular dynamics simulations. Micropor. Mesopor. Mater. 109 (2008) 91-108.
(40) R Krishna, JM van Baten: Onsager coefficients for binary mixture diffusion in nanopores. Chem. Eng. Sci. 63 (2008) 3120-40.
(41) E Beerdsen, B Smit, D Dubbeldam: Molecular simulation of loading dependent slow diffusion in confined systems. Phys. Rev. Lett. 93 (2004) 248301.

CHAPTER 5

PERMEANCE OF CO_2/CH_4 MIXTURES IN DDR ZEOLITES

5.1. MIXTURE DIFFUSION PROPERTIES

In chapter 4, we examined the adsorption properties and single component diffusivities of CO_2 and CH_4 in DDR. As we discussed in chapter 2, to examine the selectivities and permeability for mixtures through a membrane, binary diffusivities and mixture adsorption properties are required. The combination of rapidly diffusing CO_2 and slowly diffusing CH_4 in DDR superficially makes this material extremely attractive for membrane-based separations, since this difference in diffusivities can enhance the adsorption-based selectivity of DDR for CO_2 relative to CH_4. Unfortunately, a general expectation for mixture diffusion in nanoporous materials is that the presence of a slower species will retard the diffusion of a more mobile species, and vice versa[1-4]. When this occurs, any beneficial effects that might be inferred from the differences in single component diffusivities tend to be diminished under practical conditions where transport of an adsorbed mixture occurs. For this reason, therefore, measurement of diffusivities in both species is important for separation selectivities

As we discussed above in chapter 4, one important challenge in measuring diffusion of CH_4 in DDR via computer simulation is it is too slow to measure using conventional MD. As a result, the development of specific tools to measure binary diffusivities in the mixture is required. This chapter shows how we used binary KMC to solve this challenge using two methods: TST-KMC and MD-KMC. To measure the self diffusivities to examine the effect from the other species during transport, self diffusivities of CH_4 were calculated using TST. Using this information, binary KMC was used to describe CH_4 diffusion in adsorbed mixtures. This approach is then extended to assess interactions of CO_2 and CH_4 molecules in binary diffusion. These methods give

useful information about DDR, but will also be useful for future studies of other small pore zeolites.

5.2. MIXTURE DIFFUSION USING MD AND TST-KMC

All of the results below examine CH_4/CO_2 mixtures in DDR at room temperature. For the reasons discussed above, it is not possible to directly characterize diffusion of both species using MD. We therefore used an approach in which CO_2 diffusion in an adsorbed mixture was directly characterized using MD while CH_4 diffusion in a mixture was described using an extension of our TST-based KMC approach that includes rapidly diffusing CO_2 molecules. Results from each of these calculations are discussed below.

5.2.1 SELF DIFFUSIVITIES OF CO_2 AND CH_4 IN DDR

Because of the relatively rapid diffusion of CO_2 in adsorbed mixtures, we used MD simulations to describe CO_2 self diffusion in CO_2/CH_4 mixtures. For MD simulations of this kind, the system was initialized by 2×10^7~ 4×10^7 GCMC steps to get an appropriate distribution of the adsorbed molecules, followed by 1.5×10^7 canonical MC moves and 1.5×10^7 steps of MD for equilibration. Subsequently, MD data was collected for 20 ns with a 1 fs time step. At each loading, five independent trajectories were used to measure the self diffusion of CO_2. Because CO_2 adsorbs preferentially relative to CH_4 in DDR, we only examined adsorbed loadings with CO_2 mole fractions varying from 0.9 to 0.5. At a pressure of 2 (20) bar, for example, a bulk phase composition that is 10% CO_2 and 90% CH_4 is in equilibrium with an adsorbed phase that is 43.8 % (48.3 %) CO_2.

The CO_2 self diffusivities observed in these MD simulations are shown in Fig. 5.1. The most important observation from these results is that the diffusion of CO_2 is not greatly affected by CH_4 at most physically relevant mixture compositions. For loadings of 10 CO_2 molecules/unit cell or less, the CO_2 diffusivity is only reduced significantly when the adsorbed phase is 50% CH_4; a situation that requires a gas phase with >90%

CH_4. This is a very unusual result; it is typical in the diffusive transport of gas mixtures to find that the diffusivity of the more mobile species is reduced by the presence of a slower species.[1,2,4] This unusual (and potentially useful) outcome occurs because of the different adsorption sites and diffusion mechanisms of the two species.

To include CO_2 in our TST-based KMC simulation of CH_4 diffusion, we assumed that CO_2 can be treated as being at equilibrium in our lattice model because CO_2 diffuses much more quickly than CH_4. This assumption was strongly supported by direct examination of MD trajectories from adsorbed mixtures. We therefore treated the population of CO_2 in the 8MR windows using the solid curve shown in Fig. 4.7 for all adsorbed mixtures. When a CO_2 molecule was present in an 8MR, the hopping rate for CH_4 through that window was assumed to be zero. At every step in our KMC simulation, the population of each 8MR window was assigned randomly.

We also assumed that the quantities of CO_2 in the windows appearing in the Fig. 4.7 were only dependent on the molecules in the cages. This means that the TST-based calculations we discussed in chapter 4 can be extended to describe CH_4 hopping rates as a function of the number of CH_4 and CO_2 molecules in each cage. We applied the histogram methods defined previously to calculate the hopping rate of CH_4 molecules from cage *i* to cage *j* in terms of the numbers of molecules in each cage, $k_{ij} = k_{ij}(n_{\mathrm{CH_4},i}, n_{\mathrm{CH_4},j}, n_{\mathrm{CO_2},i}, n_{\mathrm{CO_2},j})$. Calculations of this kind were performed for 0-4 CO_2 molecules per cage and 0-2 CH_4 molecules, a range that allows us to describe almost all possible adsorbed loadings. For each rate calculation, 10^8 canonical MC moves per particle were used to equilibrate the system and 2×10^8 canonical moves per particle were used to produce data. The hopping rates for CH_4 calculated using this approach are shown in Fig. 5.2.

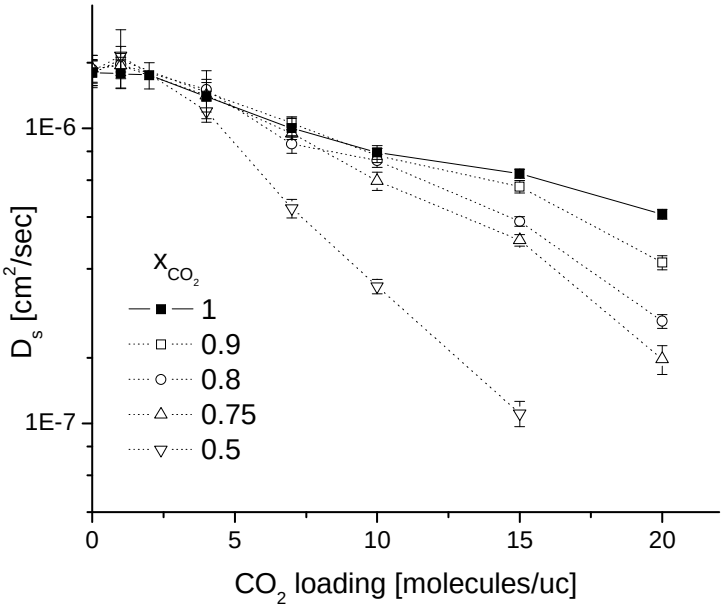

Figure 5.1: Self diffusivities of CO_2 in CO_2/CH_4 mixtures in DDR as a function of CO_2 loading at various compositions of the adsorbed mixture. The results for $x_{co_2} = 1$ correspond to single component diffusion of CO_2.

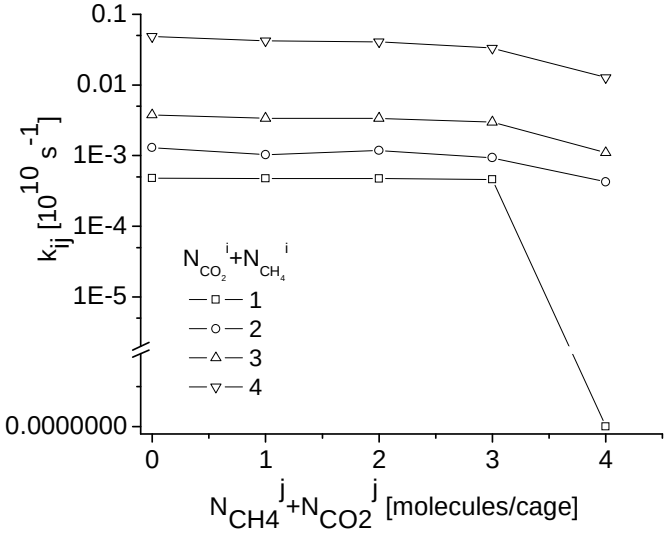

Figure 5.2: Similar to Fig.4.9, but for hopping of CH_4 in adsorbed CH_4/CO_2 mixtures. The horizontal axis and legend show the total number of molecules in the final cage and initial cage for the hopping CH_4 molecule, respectively.

Using our TST-based KMC model, we examined CH_4 self diffusion at a range of mixture loadings. At each loading, the system was equilibrated for $>1.5\times10^5$ KMC steps per particle and data were produced from 5×10^5 steps per particle. Figure 5.3 shows the calculated CH_4 diffusivities in adsorbed CH_4/CO_2 mixtures. The response of CH_4 to CO_2 is quite different from the effect of CH_4 on CO_2 because the presence of adsorbed CO_2 reduces the diffusivity of CH_4. At low loadings, the diffusivity of CH_4 in mixtures is reduced to ~40-80% of the values for single component CH_4. Larger decreases are seen at higher loadings.

It is useful to discuss the diffusion of CH_4 in the presence of adsorbed CO_2 in terms of two competing effects. First, the presence of adsorbed CO_2 tends to block the 8MR windows in DDR and hinders CH_4 diffusion. The diffusivity obtained from a KMC simulation that included these effects but no other CO_2 effects is shown in Fig. 5.3(b). As expected, this effect reduces the diffusivity of CH_4 at all loadings. The presence of CO_2 also has an effect on the cage-to-cage hopping rates for CH_4 molecules. Similar to what is seen for single component adsorbed CH_4, the presence of CO_2 molecules in cages acts to reduce the net energy barrier for hopping of CH_4 molecules. This effect is quantified in Fig. 5.3(b) by results from a KMC simulation that included the effects of CO_2 in our TST-based rate calculations but did not include window blocking effects. It is evident from this figure that this effect increases the diffusivity of CH_4. The overall influence of CO_2 on the diffusion of CH_4 occurs through a combination of these two effects, leading to the net outcome shown in Fig. 5.3(a).

A useful way to further illustrate the unusual properties of molecular diffusion in DDR is to compare our observations with the results of a correlation that have been developed to predict mixture properties from single-component data. A particularly successful correlation for the self diffusion of molecular mixtures in zeolites and other nanopores was introduced by Krishna and Paschek.[2]

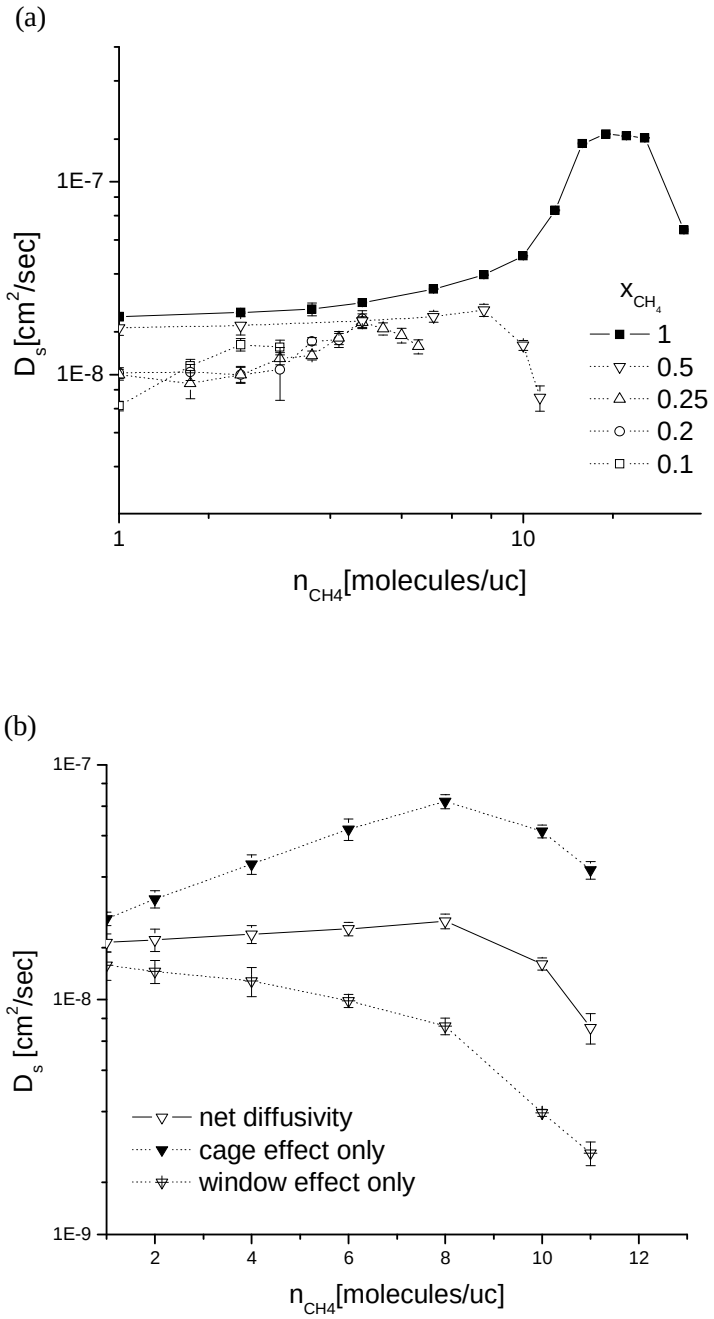

Figure 5.3: CH_4 diffusion data from CH_4/CO_2 mixtures in DDR, showing (a) self-diffusivities of CH_4 loading at various mixture compositions, and (b) the self diffusion of CH_4 in an equimolar adsorbed mixture ($x_{CH_4} = 0.5$) showing the separate effects from cage occupation by CO_2 and window blocking by CO_2.

In the mixture, two diffusion coefficients can define the correlation effects, the self-exchange coefficient, D_{corr}^{ii}, and binary-exchange coefficient, D_{corr}^{ij}. Once the single-component self and corrected diffusivities are known, the self-exchange coefficients are defined via

$$D_s^{\ i}(\theta) = \frac{1}{\frac{1}{D_o^{\ i}(\theta)} + \frac{\theta_i}{D_{corr}^{ii}}} \qquad (5.1)$$

Here, θ_i is fractional loading of species *i* in binary mixture with species *j*. $D_s^{\ i}$ is the self diffusivity and $D_o^{\ i}$ is the pure component corrected diffusivity of species *i*. The binary-exchange coefficients, D_{corr}^{ij}, reflecting correlation effects between different species in a mixture, are then estimated using

$$q_{sat}^{j} D_{corr}^{ij}(\theta) = [q_{sat}^{j} D_{corr}^{ii}(\theta)]^{\theta_i/(\theta_i+\theta_j)} [q_{sat}^{i} D_{corr}^{jj}(\theta)]^{\theta_j/(\theta_i+\theta_j)} \qquad (5.2)$$

Here, $q_{sat}^{\ i}$ is saturation loading for species *i*. Finally, the binary self diffusivities in the mixture are predicted using

$$D_s^{\ i} = \frac{1}{\frac{1}{D_o^{\ i}} + \frac{\theta_{\ i}}{D_{corr}^{ii}} + \frac{\theta_{\ j}}{D_{corr}^{ij}}} \qquad (5.3)$$

This correlation has given relatively good predictions in a variety of nanoporous materials, including the silica zeolites ITQ-7, FAU, AFI and MFI,[1,2,5-8] carbon nanotubes[9] and CuBTC.[10] Using an earlier forcefield for CO_2 and CH_4 in DDR, Krishna *et al*. showed this correlation did not accurately capture the mixture diffusivities seen in mixture MD simulations in DDR.[11,12] Because our new forcefield predicts molecular diffusion coefficients that are considerably slower than those from the earlier MD calculations (in accord with experimental observation, as discussed above), it is useful to revisit the ability of Krishna and Paschek's correlation for describing CO_2/CH_4 mixture diffusion in DDR.

The accuracy of Krishna and Paschek's correlation for describing CH_4/CO_2 mixtures at $x_{CO_2} = 0.9$ in DDR is shown in Fig. 5.4. The ratios of the predicted diffusivities to the measured diffusivities are shown as a function of total loading. For both species, the ratio is far from 1, indicating deviation of the predicted values from simulation data. The deviation was particularly large at higher total loadings for CO_2 and at lower total loadings for CH_4. Similar tendencies were observed at all other compositions we examined (data not shown). In light of the diffusion mechanisms that exist in DDR, it is not surprising that this correlation gives inaccurate results, since the correlation is based on the heuristic idea that the adsorbing molecules are well mixed.

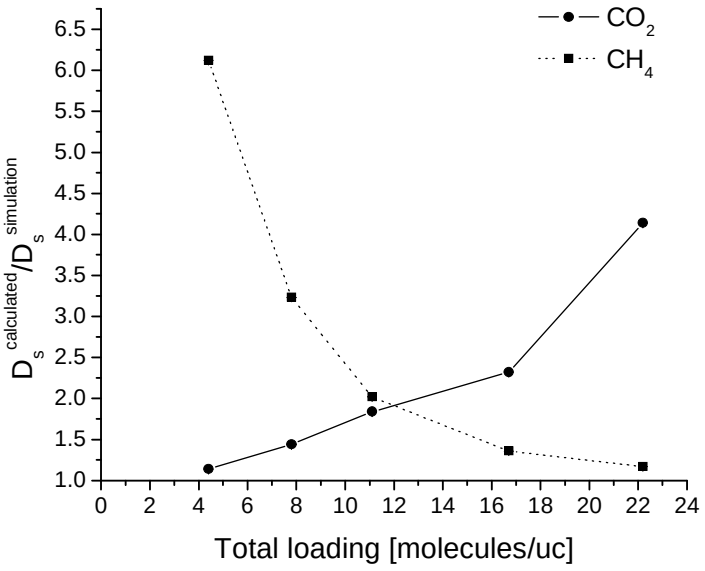

Figure 5.4: The ratio of the predicted mixture self diffusivities from Krishna and Paschek's formulation to the simulation data from our work at $x_{CO_2} = 0.9$ as a function of total loading. Circles and rectangles denote CO_2 and CH_4, respectively.

5.3 MIXTURE DIFFUSION USNG BINARY MD-KMC

In the previous section we used different methods for measuring the self diffusion of CO_2 and CH_4 in DDR. Since MD is not suitable for characterizing the slowly diffusing CH_4, a transition state theory based approach that rigorously describes the loading dependent diffusion of CH_4 was used. However, to estimate the permeance and the selectivities of mixtures permeating through DDR, a description of self diffusion is not sufficient. Instead, information on the binary Fickian diffusion coefficients, or equivalently, the mixture's Onsager coefficients, is required [3]. To make this possible, we need developed a new approach to describe simultaneous transport of the two species in DDR to measure their Onsager coefficients.

5.3.1 DIRECT MEASUREMENT OF k_{ij} USING MD

Binary KMC using a lattice model of molecular diffusion would be a good method to describe binary mixture diffusion if the hopping rates for each molecular species can be defined in an appropriate way. The main quantity used to define a model of this kind is the matrix of transition rates, k_{ij}, defined as the hopping rates from well defined lattice sites to neighboring sites as a function of the occupation of nearby sites. When TST is applied, the transition rates for escape from state *i* to state *j* are taken to be the equilibrium flux through a dividing surface separating the two states. This approach worked well for CH_4 diffusion in DDR, as described in the previous chapter. Because the dividing surfaces associated with hopping of CO_2 in this material are more complex than for CH_4, however, achieving accurate results using this idea for CO_2 was more difficult. To avoid this complication, we took advantage of the observation that CO_2 diffusion is fast enough to be observed with MD, and derived values of the hopping rates for CO_2 directly from MD trajectories.

Figure 5.5 shows a representative trajectory of one CO_2 molecule in DDR during an MD simulation. The preferred sites for CO_2 in DDR are window and center of the

DDR cages. The large circles in Fig. 5.5 indicate individual cages, and the center of each cage is represented by a solid symbol. The 8MR windows that connect adjacent cages lie at the intersection of the large circles in Fig. 5.5. It is clear from the figure that the trajectory of the CO_2 molecule can be described as hops between window and cage sites. Molecules were considered to be within the window site when they were within planes located 1 Å from the plane of the window. The molecules in other location are regarded to present in the cage. The transition rates k_{ij} were measured from the number of observed hopping rates during MD trajectories similar to those shown in this figure.

We defined the transition rate for a single molecule hopping from cage A to one of the neighboring window as $k_{\text{cage to window}}(N_A)$ where N_A is the number of total molecules in the cage A. Similarly, the hopping rate from a window to cage A is written as $k_{\text{window to cage}}(N_A, N_B)$, where N_A and N_B are the number of total molecules in the cage A and cage B, where cage B is the other cage accessible from the window. The maximum number of CO_2 molecule per cage (window) was set to 3 (1) based on results from our binary adsorption calculation. To interpret our MD trajectories, the effective N_A and N_B were taken to be the instantaneous configuration when a hop is observed. To allow for the possibility of "bounce back" trajectories, hopping was recorded only when the molecule stays in the new site for more than 18 ps. This numerical value was chosen after visual inspection of a number of representative trajectories. For MD simulations of this kind, the system was initialized by 2×10^7~ 4×10^7 GCMC steps to get an appropriate distribution of the adsorbed molecules, followed by 1.5×10^7 canonical MC moves and 1.5×10^7 steps of MD for equilibration. Each k_{ij} was collected from MD for n_{CO2}=1~20 molecules with x_{CO2}=0.3, 0.5, 0.7, 1 at 298 K.

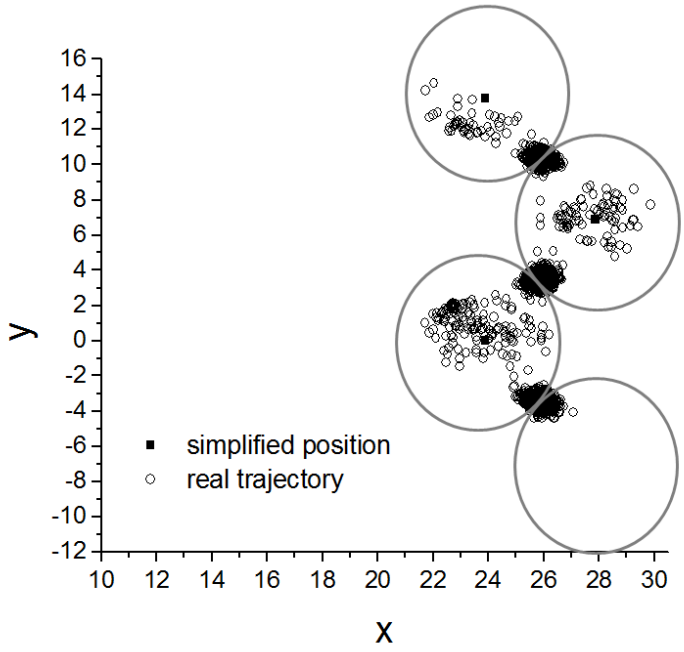

Figure 5.5: Trajectory of one CO_2 molecule in DDR measured by MD. The x and y axes show the molecule's position in DDR in Å.

Figure 5.6(a) shows the calculated transition rates of CO_2 from a cage to a neighboring window as a function of total number of molecules in the cage, N_i. The transition rate is an increasing function of N_i. We verified that these rates are not sensitive to the loadings of the other window sites that are neighbors of the same cage. Figure 5.6(b) shows the transition rates of a hop of CO_2 from a window site to the center of cage *j*. These rates are not only a function N_j but also strongly affected by N_i, the number of particles in the cage which is on the opposite side of the window into which the CO_2 molecule is hopping. The transition rates from cage to window sites are larger than those for hopping from a window to a cage, indicating the rate determining steps for CO_2 diffusion are window to cage hops. This is consistent with the observation that window sites are energetically more favorable for CO_2 adsorption.

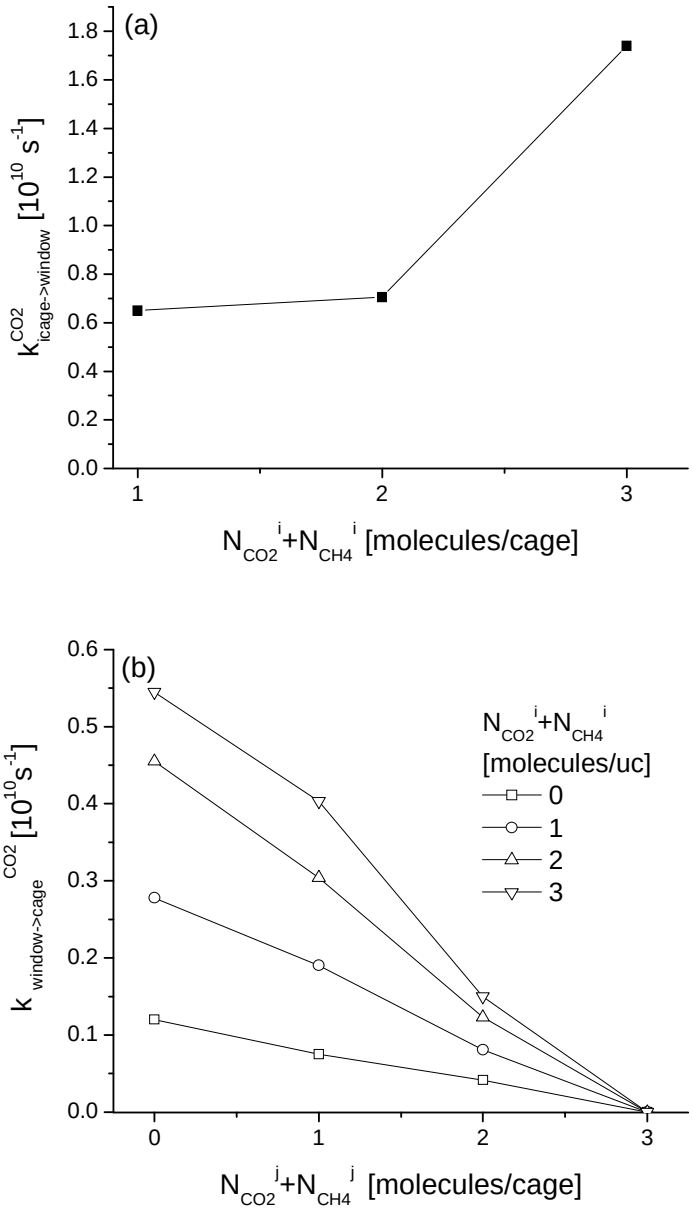

Figure 5.6: Measured values of k_{ij} for CO_2 in an adsorbed mixture in DDR. (a) Hopping rates of CO_2 from cage to the window and (b) hopping rates of CO_2 from window to cage.

5.3.2 BINARY KMC MEASUREMENT AND FLUX CALCULATION

The model summarized above defines the local hopping rates of CO_2 molecules and CH_4 molecules in a lattice model that includes both diffusing species in a consistent manner. The dynamics of molecules in this adsorbed mixture can now be simulated using KMC. Once a lattice model like this is available, the methods required to measure the Onsager coefficients associated with binary diffusion or mixture self diffusion are well developed [4,13].

To use KMC calculate the diffusivities of CO_2 and CH_4 in DDR, CO_2 is initially distributed among the window and cages sites based on the GCMC calculation shown in Fig 4.7 and CH_4 molecules are randomly distributed among cage sites. In making a single KMC step, an adsorbate molecule is selected randomly from all adsorbate molecules in the simulation volume and a move direction from current site is selected randomly from the three (two) directions available for a cage (window) site. Our KMC algorithm requires knowledge of the fastest transition rate; this was set by inspection to ($k^{CO_2}{}_{\text{cage to window},N=3} = k_{\max}$). Hops that move a CO_2 molecule from a cage site to a window site are accepted with probability k_{ij}/k_{max}, while hops that move a CO_2 molecule from the window to a cage site are accepted with probability $2k_{ij}/3k_{max}$, where k_{ij} is the specified transition rate. The factor of 2/3 in this acceptance probability arises from the different number of hopping directions of the attempted hop. Hops that move a CH_4 molecule from a cage to cage site are accepted with probability k_{ij}/k_{max} only when the interconnecting window is vacant. After every attempted hop, time is incremented by $\Delta t = 1/3Nk_{\max}$, where N is the total number of guest molecules in the simulation volume. This algorithm rigorously describes a realization of the dynamics of the adsorbing molecules with the set

of individual hopping rates used as input to the simulation. Unlike most previous implementations on binary KMC for molecular diffusion in zeolites, the hopping rates in our calculations were directly determined from an atomic-scale description of the diffusing species.

To measure the diffusivity of guest molecules at various loadings in our lattice model, the lattice size was varied from 90 to 21600 cages and the total number of guest molecules was varied from 100 to 200, depending on the overall loading. After molecules were initially distributed as described above, a large number of KMC steps (typically > 500000 MC steps per particle) were then used to equilibrate the system. After equilibration, a further 500000 MC steps per particle were performed while collecting data on the trajectory of each molecule. Each simulation of this kind corresponds to a trajectory of length ~1.3×10^{-6} s. Direct simulation of this system with MD requires time steps of ~1 fs, so each KMC trajectory corresponds to a situation that would require more than 10^9 MD steps.

First, we compared the self diffusivities from the binary KMC simulations with our earlier results. Figure 5.7(a) compares the calculated self diffusivities of CO_2 calculated directly from MD with the outcome of our binary lattice model at a range of adsorbed compositions and loadings. In this case, the MD results should be viewed as giving the "correct" values of the self diffusivities, since no assumptions had to be imposed to extract these quantities from the MD data. The good agreement between the outcomes from the binary lattice model and the MD data is strong evidence that the binary lattice model accurately describes CO_2 diffusion in this adsorbed mixture. It is not possible to make such an unambiguous comparison for the self diffusion of CH_4, since MD cannot be used to directly calculate this quantity. It is interesting, however, to compare the self diffusivities of CH_4 calculated with our binary KMC method with our

earlier KMC calculations that assumed CO_2 moved infinitely quickly relative to CH_4. This comparison is shown in Fig. 5.7(b).

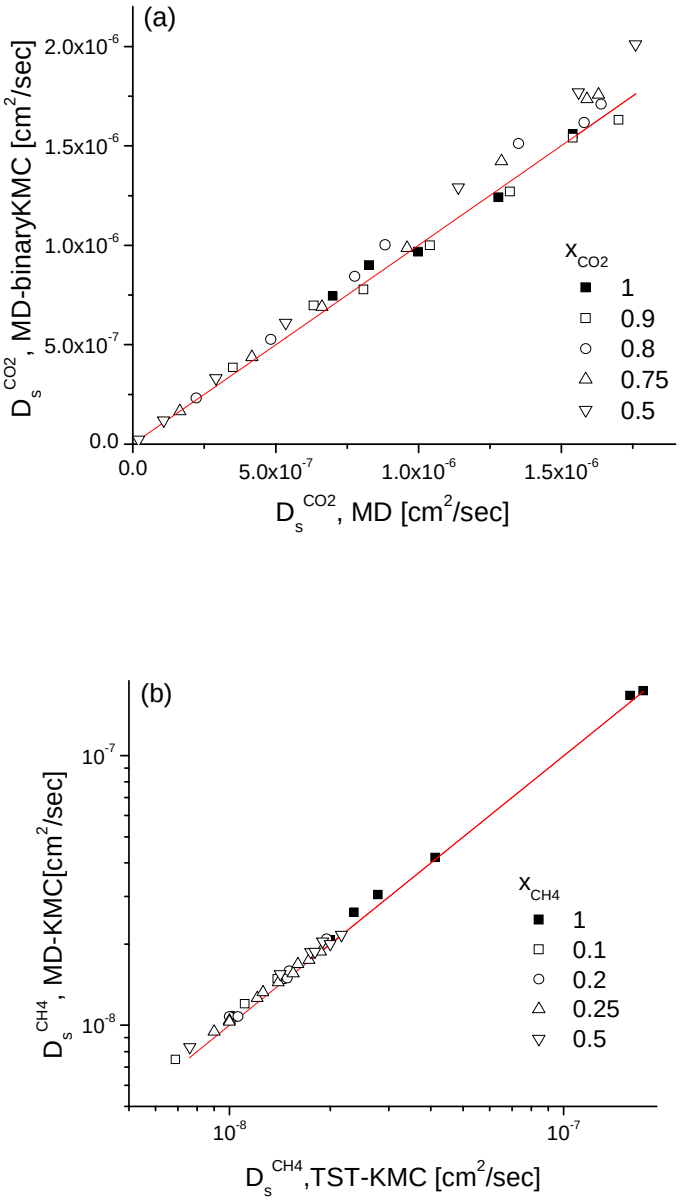

Figure 5.7: Comparison of D_s computed using the binary lattice model with data from (a) MD for $CO_2$and (b) the simplified lattice model for CH_4 in CO_2/CH_4 mixtures over the entire range of interesting adsorbed compositions and adsorbed loadings.

The good agreement between the two KMC calculations indicates that the assumption made in our earlier calculations that the movement of CH_4 could be decoupled from the more rapid movement of CO_2 was reasonable.

To make it possible to describe the flux of mixtures permeating through a membrane, we used our binary KMC simulations to calculate the Onsager coefficients of a variety of adsorbed mixtures. The technical details of this calculation were explained in chapter 2. 20 independent trajectories were used to accumulate data for each adsorbed composition and loading of interest. Fig 5.8 shows the computed Onsager coefficients as a function of loading for 80:20 adsorbed compositions. Because of the adsorption selectivity of DDR for CO_2, this adsorbed composition corresponds to a gas phase that is approximately equimolar. Here and below, species 1 (2) denotes CO_2 (CH_4).

As we observed before in Fig 5.3, CO_2 is more mobile in DDR than CH_4. This observation can also be made from Fig. 5.8, where $L_{11} \gg L_{22}$ at all loadings. The off-diagonal Onsager coefficients, L_{12}, are even smaller. In a number of our KMC calculations, the off-diagonal Onsager coefficients were found to be negative; these values are indicated by solid symbols in Fig. 5.8. We suspect that the off-diagonal Onsager coefficients are positive at all loadings and that the observation of negative values comes from the statistical uncertainty associated with these calculations. In any event, the off diagonal components are very small compared to the diagonal components. This suggests that we can accurately approximate the off-diagonal Onsager coefficients as zero. We take this approach below when calculating the binary Fickian diffusivities.

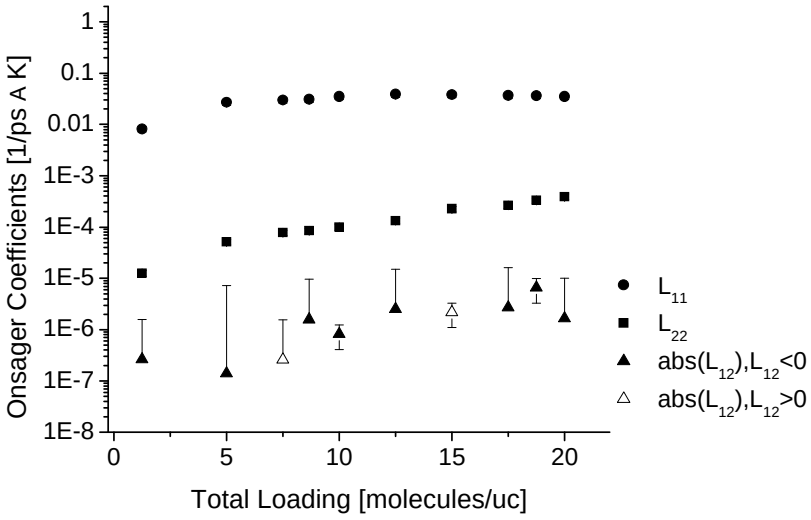

Figure 5.8: Measured values of L_{11}, L_{12}, L_{22} from binary KMC simulations of CO_2/CH_4 mixtures with an adsorbed composition of 80:20.

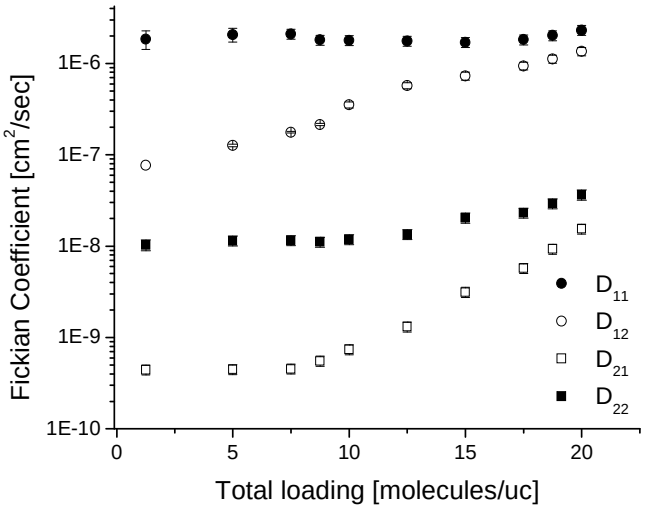

Figure 5.9: The binary Fickian diffusivities, D_{11}, D_{12}, D_{21}, and D_{22} of CO_2/CH_4 mixtures at adsorbed phase compositions of 80:20 compositions computed from binary KMC results as described in the text.

In the macroscopic model of the permeance we explicitly use the Fickian diffusivities calculated from the Onsager coefficients and adsorption isotherms with the use of equation (2.16) and (2.17). Fig 5.9 shows the Fickian diffusivities of CO_2/CH_4 mixtures at representative conditions. It is clear that $D_{11}>D_{22}$, showing that the diffusivity of CO_2 is faster than CH_4 in DDR structure. D_{11} and D_{22} show only a weak concentration dependence under the conditions examined in Fig. 5.9. One important observation here is D_{12} is relatively large, meaning that gradients in CO_2 concentration have a strong influence on transport CH_4 molecules. D_{21}, in contrast, is negligible, meaning that CO2 transport is only weakly influenced by gradients in the CH_4 concentration. Under the conditions shown in Fig. 5.9, D_{12} increases monotonically with the pore loadings at lower concentration and sharply increases at a total loading of ~9 molecules/uc. At this loading, almost all of the window sites are occupied by CO_2 molecules.

5.4 BINARY PERMEANCE PREDICTIONS

In this section we examine the permeance of CO_2/CH_4 mixtures through a defect-free DDR crystal at room temperature. Three important factors that affect the flux are the feed pressure, feed composition, and the transmembrane pressure drop. For simplicity, we assumed that the permeate is a vacuum and the feed has a 50:50 composition. All calculations were performed using a 1μm membrane thickness, although this choice only influences that overall flux, not the selectivity. The calculated mixture permeances for 50:50 bulk phase CO_2/CH_4 mixtures are shown in Fig. 5.10, along with the single component flux of CO_2 and CH_4 at the same conditions. One interesting observation here is that the CO_2 permeance in the mixture and the single component system are quite similar, while the CH_4 permeance in the mixture is greatly reduced in the mixture compared to the single component flux. That is, the mixture selectivity of this membrane

is far more favorable than the ideal selectivity. This is consistent with what we discussed in the diffusivity calculations: the CO_2 diffusivity is not reduced by the presence of CH_4 while the CH_4 diffusivity is strongly reduced by the presence of CO_2.

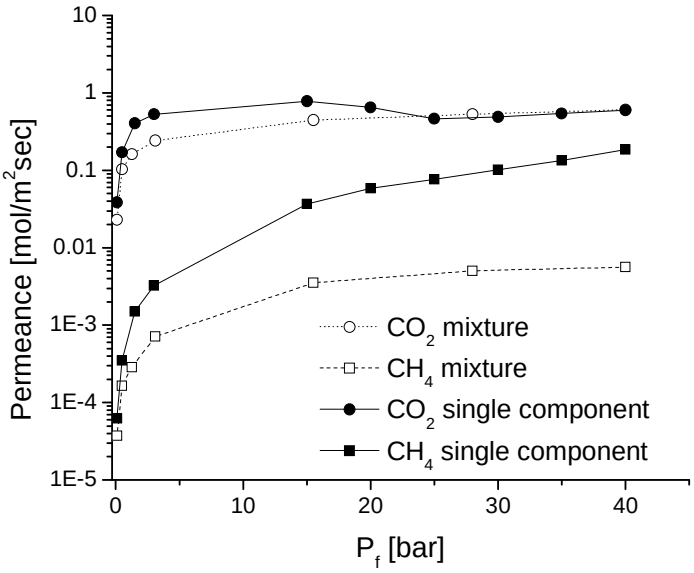

Figure 5.10: Calculated permeance of 50:50 bulk phase CO_2/CH_4 mixtures at 298 K and single component fluxes at the same condition. The permeate pressure is assumed to be a vacuum and the membrane thickness was taken to be 1μm.

Fig 5.11 shows mixture selectivities from our flux calculations as a function of feed pressure. The predicted membrane selectivity is 100-1000 over the entire range of pressures, indicating that DDR is a highly selective membrane material for this gas separation. Several experimental measurements are available from experiments where the permeate pressure is 1 bar; the observed mixture selectivities from these experiments at 301 K[15], 300 K[16], and 298 K[17] are also shown in Fig. 5.11. The agreement between the predicted and experimental data is very good. The predicted mixture selectivities are somewhat higher than the experimental observations. Because practical zeolite

membranes always allow some molecular transport through non-zeolitic pores, it seems reasonable to conclude that the observed behavior of a membrane with a high selectivity for a defect-free zeolite will typically be lowered to some extent by non-zeolitic pores.

The calculations shown in Fig. 5.11 involve fairly elaborate calculations involving the mixture diffusion coefficients. It is useful to compare these predictions with those made with less time consuming methods. In particular, we examined the simplified approach introduced recently by Keskin and Sholl[14] that was motivated by earlier suggestions by Krishna and coworkers. In this approach, the membrane's mixture selectivity is approximated by

$$S = \frac{(q_1 / q_2)}{(y_1 / y_2)} \frac{D_s^{\,1}(q_1, q_2)}{D_s^{\,2}(q_1, q_2)} \qquad (5.4)$$

where y_i is the mole fraction of the component *i* in the bulk phase and q_i is the adsorbed amount of species *i*. A central idea in this approximation is that the mixture self diffusivities are measured at binary adsorbed loading $q_{1,}\ q_2$ defined by the binary adsorption isotherm. As discussed by Keskin and Sholl, this approach is designed to be most applicable (that is, the least approximate) when the permeate side is a vacuum. The results of this approach are compared to our more detailed calculations in Fig. 5.11. The two calculation methods are not in exact agreement, which is not surprising given the approximate nature of Keskin and Sholl's method. Nevertheless, this approximate method clearly captures the overall trends in the true mixture selectivities, suggesting that this approximate approach could be useful in rapidly screening other materials.

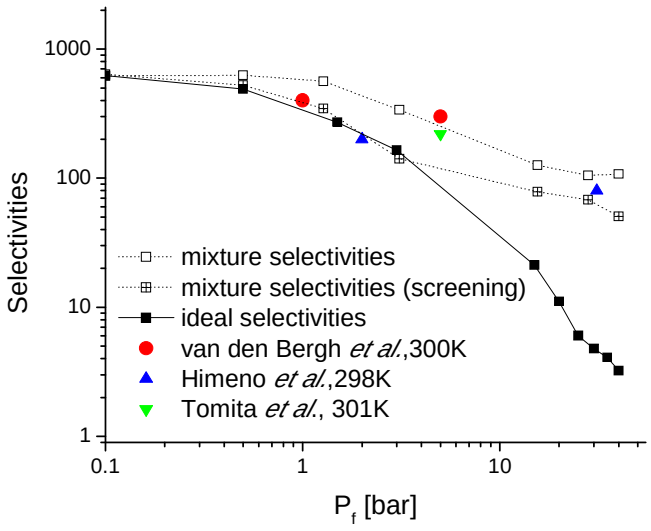

Figure 5.11: Mixture selectivities of 50:50 bulk phase CO_2/CH_4 mixtures at 298K from Onsager coefficient, estimated membrane selectivities using Eq. (5.4) and ideal selectivities. In all selectivity calculation and the experiments by van den Bergh *et al.* [17], P_{perm} is vacuum, so that pressure drop is equal to the P_f. In the experimental data by Himeno *et al.* [16] and Tomita *et al.*[15], P_{perm}=1 bar so that pressure drop of P_f-1 bar.

5.5 CONCLUSIONS

In chapter 5, we have examined the diffusion properties of DDR membranes for separation of CO_2/CH_4 and more importantly, calculated the permeability and selectivity of these membranes over a wide range of feed pressure. Since MD is not a suitable method for characterizing slowly diffusing CH_4 molecules, we introduced a binary KMC method to measure diffusivities. To describe the transition rates used for KMC, a transition state theory-based approach was used to examine the loading dependent diffusion of CH4 in the mixture and MD-based approach was used for CO_2.

It is well known that CO_2 adsorbs preferentially in DDR relative to CH_4. The typical expectation in nanoporous materials is that the more strongly adsorbing species will diffuse more slowly than more weakly adsorbing species. Moreover, diffusion in mixtures is expected to occur via what can be thought of reversion to the mean; the existence of a slowly diffusing species slows down more rapidly diffusing molecules and vice versa. These expectations mean that, in general, a nanoporous membrane will have lower selectivity than when the same material is used in an adsorption-based separation, and the selectivity of a membrane for a permeating mixture will be less pronounced than the selectivity that would be predicted from single component experiments. The key macroscopic observation from our calculations is these expectations are incorrect for CO_2/CH_4 diffusion in DDR. As was already known from experiments, single component CO_2 diffuses much more rapidly than CH_4 at dilute loadings. Our detailed calculations predict that in adsorbed mixtures of CO_2 and CH_4, the rapidly diffusing CO_2 is only slightly affected by the presence of CH_4, while the slowly diffusing CH_4 is strongly retarded by the presence of CO_2. This situation is very unusual, and it occurs because the

two molecules prefer different kinds of adsorption sites inside DDR. CO_2 molecules prefer to sit in the 8MR windows that separate DDR's cages, but these same windows are the transition states for hopping of CH_4 molecules from cage to cage.

CO_2/CH_4 selectivities of the equimolar mixtures are higher than 100 at the entire range of feed pressure, indicating that membranes made from DDR can be expected to have a significantly higher performance for separation. This selectivity prediction is consistent with the experimentally measured selectivities in the literature, confirming the estimation of the unique transport properties in DDR membrane.

The main factor to achieve high separation selectivities in DDR is its characteristic structures differing diffusivities of two species. It seems likely that this situation is not unique to DDR, so our methods should make it possible to search for other small pore zeolites with similarly attractive properties. In chapter 6, we will examine other small pore zeolites with the forcefields and tools we have developed for DDR.

REFERENCES

(1) Paschek, D.; Krishna, R. *Phys. Chem. Chem. Phys.* **2001**, *3*, 3185.
(2) Krishna, R.; Paschek, D. *Phys. Chem. Chem. Phys.* **2002**, *4*, 1891.
(3) Sholl, D. S. *Acc. Chem. Res.* **2006**, *39*, 403.
(4) Maceiras, D. B.; Sholl, D. S. *Langmuir* **2002**, *18*, 7393.
(5) Selassie, D.; Davis, D.; Dahlin, J.; Feise, E.; Haman, G.; Sholl, D. S.; Kohen, D. *J. Phys. Chem. C* **2008**, *112*, 16521.
(6) Skoulidas, A. I.; Sholl, D. S.; Krishna, R. *Langmuir* **2003**, *19*, 7977.
(7) Krishna, R.; van Baten, J. M. *Micropor. Mesopor. Mater.* **2008**, *109*, 91.
(8) Krishna, R.; van Baten, J. M. *Chem. Eng. Sci.* **2008**, *63*, 3120.
(9) Krishna, R.; van Baten, J. M. *Ind. Eng. Chem. Res.* **2006**, *45*, 2084.
(10) Keskin, S.; Liu, J.; Johnson, K.; Sholl, D. S. *Langmuir* **2008**, *24*, 8254.
(11) Krishna, R.; van Baten, J. M. *Chem. Phys. Lett.* **2007**, *446*, 344.
(12) Krishna, R.; van Baten, J. M. *Sep. Purif. Technol.* **2008**, *61*, 414.
(13) Sholl, D. S. *Langmuir* **2006**, *22*, 3707.
(14) Keskin, S.; Sholl, D. S. *Langmuir* **2009**, *25*, 11786.
(15) Tomita, T.; Nakayama, K.; Sakai, H. *Micropor. Mesopor. Mater.* **2004**, *68*, 71.
(16) Himeno, S.; Tomita, T.; Suzuki, K.; Nakayama, K.; Yajima, K.; Yoshida, S. *Ind. Eng. Chem. Res.* **2007**, *46*, 6989.
(17) van den Bergh, J.; Zhu, W.; Kapteijn, F.; Moulijn, J. A.; Yajima, K.; Nakayama, K.; Tomita, T.; Yoshida, S. *Res. Chem. Intermed.* **2008**, *34*, 467.

CHAPTER 6

SMALL PORE ZEOLITES WITH DIFFERENT TOPOLOGIES

As we discussed in the previous chapters, DDR is a good candidate as a separation membrane for CO_2/CH_4 separations. The most important factor for achieving high selectivities for this separation is the narrow 8MR windows that control molecular diffusion in DDR. According to this, we can expect that other small pore zeolites may have high separation ability for CO_2/CH_4 separation. In this chapter, we will examine the separation ability of 10 small pore silica zeolites.

6.1 SMALL PORE ZEOLITES FOR CO_2/CH_4 SEPARATION

The silica zeolite DDR is a strong candidate for CO_2/CH_4 separation because of the narrow 8MR window that control molecular transport inside the material's pores. Therefore, other zeolite structures with 8MR are expected to share this desirable property. In this chapter we consider 10 pure silica zeolites with small windows for CO_2/CH_4 separation. These materials are listed in Table 6.1. The structures of zeolites were defined using the atomic coordinates measured experimentally [1-11]. Among these materials, DDR, CHA, LTA and IHW have large cages that are interconnected with 8MR windows. STT also has large cages interconnected with 7MR and 9MR windows. ITE, ITW, MTF, SAS and RTE have 1D channel with 8MR. RWR has two independent channels without interconnection.

When CO_2 and CH_4 diffuse in the DDR, we observed that the diffusivities of CO_2 are only weakly affected by the presence of CH_4, while the slowly diffusing molecule CH_4 is retarded by the CO_2, leading very high separation selectivity. We anticipate that similar phenomena may occur in the other small pore zeolites, especially for cage type structures such as CHA, LTA, IHW and STT.

The aim of this chapter is to find good candidates for CO_2/CH_4 separation from the 10 structures in Table 6.1 based on an examination of molecular transport properties in these zeolites. We first screen candidates based on a model for membrane selectivity in more detail. Subsequently, transport properties of several selected candidates are examined in more detail to verify their separation selectivities at relevant conditions. Finally, we calculate the separation selectivities of selected materials and compare these properties to the performance of DDR. For all of the atomistic simulations in these small pore zeolites, we will use forcefield parameters of CO_2 and CH_4 derived for DDR in chapter 4.

Structure	8MR size [Å]	Chemical formula	Channels
DDR[1]	3.6×4.4	$Si_{120}O_{240}$	2D*
LTA[2]	4.1×4.1	$Si_{l92}O_{384}$	3D*
CHA[3]	3.8×3.8	$Si_{12}O_{24}$	3D*
IHW[4]	3.5×4.3	$Si_{112}O_{224}$	2D*
ITE[5]	3.8×4.3, 2.7×5.8	$Si_{64}O_{128}$	1D
ITW[6]	3.9×4.2, 2.4×5.4	$Si_{24}O_{48}$	1D
MTF[7]	3.6×3.9	$Si_{44}O_{88}$	1D
RWR[8]	2.8×5.0	$Si_{32}O_{64}$	2D
SAS[9]	4.2×4.2	$Si_{16}O_{32}$	1D
STT[10]	3.7×5.3, 2.4×3.7	$Si_{64}O_{128}$	2D*
RTE[11]	3.7×4.4	$Si_{24}O_{48}$	1D

Table 6.1: List of pure silica zeolites with 8MR pores Materials denoted * have channels that are interconnected forming cages.

6.2 DETAILS OF SCREENING CRITERIA

Calculating CO_2/CH_4 separation using detailed atomistic calculation for the entire small pore zeolites requires a good deal of effort. As discussed in the previous chapters for DDR. Therefore, rapid screening using a minimum number of calculations is extremely useful to find interesting materials efficiently. To approach this task, we estimated membrane selectivities using binary adsorption and diffusivity calculations at relevant conditions with methods described by Keskin and Sholl's method for screening MOFs[12]. In this method, the adsorption selectivities are calculated from

$$S_a = \frac{(q_1 / q_2)}{(y_1 / y_2)} \tag{6.1}$$

where y_i is the mole fraction of the component *i* in the bulk phase and q_i is the adsorbed amount of *i* species. Secondly, the self diffusivities of the adsorbed molecules are calculated at relevant adsorbed loadings q_i and the diffusion selectivities are defined as

$$S_D = \frac{D_s^{\,1}(q_1, q_2)}{D_s^{\,2}(q_1, q_2)} \tag{6.2}$$

where self diffusivities of the mixtures are measured using MD at adsorbed loadings q_1,q_2 for given condition. For the structures like DDR or IHW, CH_4 diffusivities are slower than 10^{-8}cm^2/sec, which is not measurable using MD. For these structures, we assumed $D_s^{CH4} = 10^{-8}$ cm^2/sec, which gives a lower bound on S_D when CH_4 is taken to be species 2. The membrane's mixture selectivity at a specified feed pressure and composition is then estimated using

$$S = S_a \cdot S_D = \frac{(q_1 / q_2)}{(y_1 / y_2)} \frac{D_s^{\,1}(q_1, q_2)}{D_s^{\,2}(q_1, q_2)} \tag{6.3}$$

In principle, the feed pressure, transmembrane pressure drop and compositions are all important factors to decide selectivities for the separation. For simplicity, we assumed a

50:50 bulk phase on the feed side of a membrane and a vacuum on the permeate side.

Binary adsorption selectivities were calculated at 0~45 bar as shown in Fig. 6.1. RWR and MTF have very high adsorption selectivities representing the dominance of CO_2 molecules. This is due to the narrow, one dimensional channel exclude the CH_4 adsorption even in the single component adsorption, so we can consider these materials are good candidates for all compositions due to their high selectivities at adsorption. Fig 6.2 shows the amount of CO_2 adsorbed in these two materials is smaller than the other zeolites. SAS also shows high adsorption selectivity. Therefore, we can suggest that MTF, RWR and SAS can be good candidates as separation membranes based on adsorption data alone. For CHA and ITE, the adsorption selectivities are higher than the remaining structures, but still there is considerable amount of CH_4 present during binary adsorption. Therefore, we need to consider diffusion selectivities for these materials.

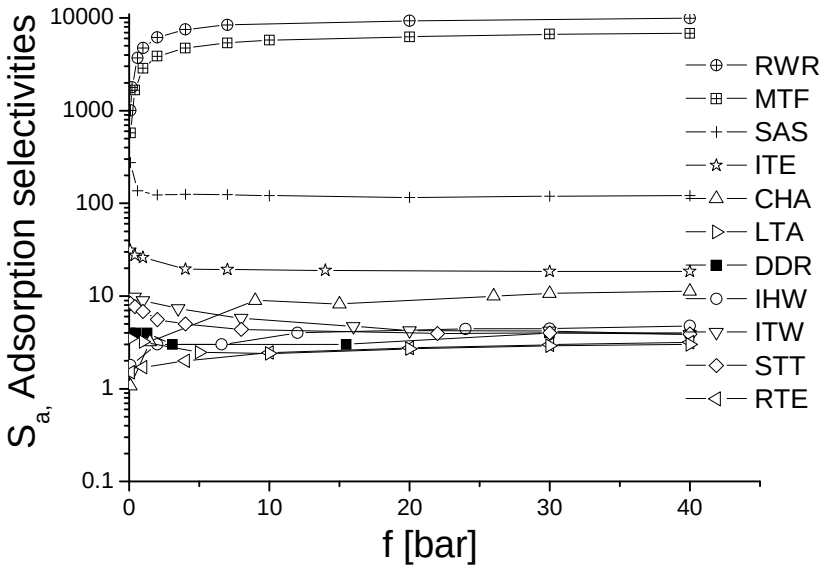

Fig 6.1: Room temperature Binary adsorption selectivities of CO_2 and CH_4 in 11 small pore zeolites at 0~45 bar with 50:50 bulk compositions.

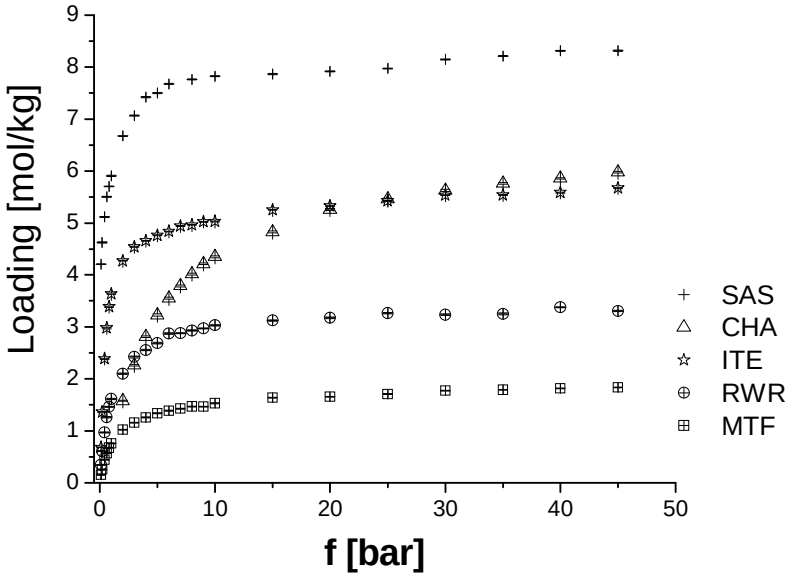

Fig 6.2: CO_2 adsorption amount in SAS, CHA, ITE, RWR and MTF at 0~45 bar with 50:50 bulk compositions.

Diffusion selectivities based on the self diffusivities at the given feed pressure are shown at Fig 6.3 for materials except MTF, RWR and SAS. The self diffusivities are calculated at the specific adsorbed loadings of CO_2 and CH_4 at given feed pressure. The self diffusivities of CH_4 in DDR were calculated from TST-KMC. The CH_4 diffusivities of IHW at entire range of the pressure and the CO_2 and CH_4 diffusivities of ITE at P_f <15 bar were assumed to be $10^{-8}cm^2/sec$ as discussed above. The diffusivities in the other structures were calculated using MD at relevant adsorbed loadings. As can be observed, the diffusion selectivities of IHW, DDR and CHA are high compared to other structures. The structures of IHW and CHA are very similar to DDR in that they have large cages interconnected with small 8MR windows. In DDR, cages are interconnected with three windows in 2D, while the cage of the CHA has six windows and the cage of IHW has four windows.

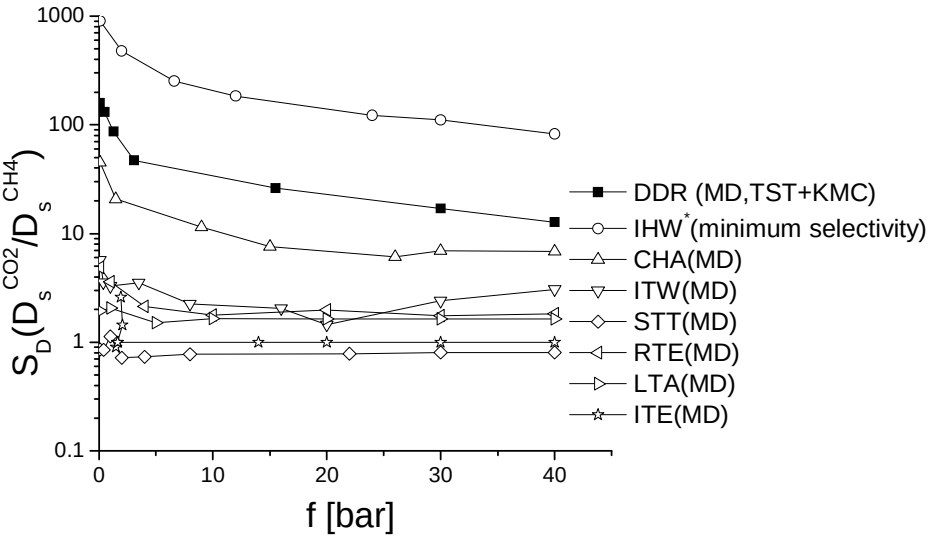

Fig 6.3: Binary diffusion selectivities of CO_2 and CH_4 in 11 small pore zeolites at 0~45 bar with 50:50 bulk compositions.

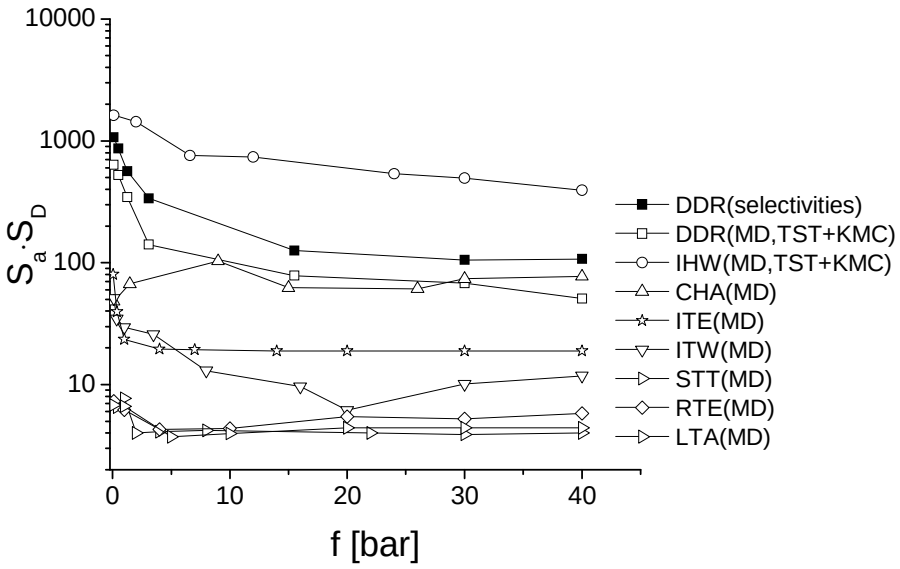

Fig 6.4: Estimated membrane selectivities using Eq. (6.3) at 0~45 bar with 50:50 bulk feed. For DDR, selectivities calculated from fickian diffusivities are also shown for comparison (filled squares).

The membrane selectivities estimated from equation (6.3) for 8 small pore zeolites are shown in Fig 6.4. The selectivities of CO_2/CH_4 from chapter 5 for DDR, shown as filled squares, can be compared with the selectivities using Eq. (6.3), shown as open squares. The approximate results based on Eq. (6.3) are in good agreement with the more detailed calculations, supporting the use of this approximate approach as a screening tool. The predicted selectivities of IHW and CHA are comparable with those of DDR. Therefore, from screening procedure, we can conclude that MTF, RWR, SAS, IHW and CHA may be good candidates as separation membranes. Below, we examine these materials in more detail.

6.3 TRANSPORT PROPERTIES OF SELECTIVE MATERIALS

6.3.1. TRANSPORT PROPERTIES OF SAS

As shown before, SAS has very high adsorption selectivities for 50:50 bulk compositions, allowing very few CH_4 molecules in the adsorbed mixture. To examine if this material is selective when for other bulk compositions, the adsorption selectivities for a range of compositions were calculated. As seen in Fig.6.5, selectivities are higher than 100 for all bulk phase compositions, indicating that CO_2 is strongly selected in adsorption in SAS.

In a membrane-based separation, permeation of CO_2 is also an important factor. Therefore, even though SAS gives high selectivities in adsorption, the diffusivities of CO_2 in the presence of CH_4 should be examined. Figure 6.6 shows that the self diffusivities of CO_2 in the mixture is not significantly decreased by the presence of CH_4, while giving self diffusivities of a 10^{-7}~10^{-6} cm^2/sec. We also verified that the single file diffusion does not occur in this structure[13,14]. These results strongly suggest that SAS is a good candidate membrane material for CO_2/CH_4 separations.

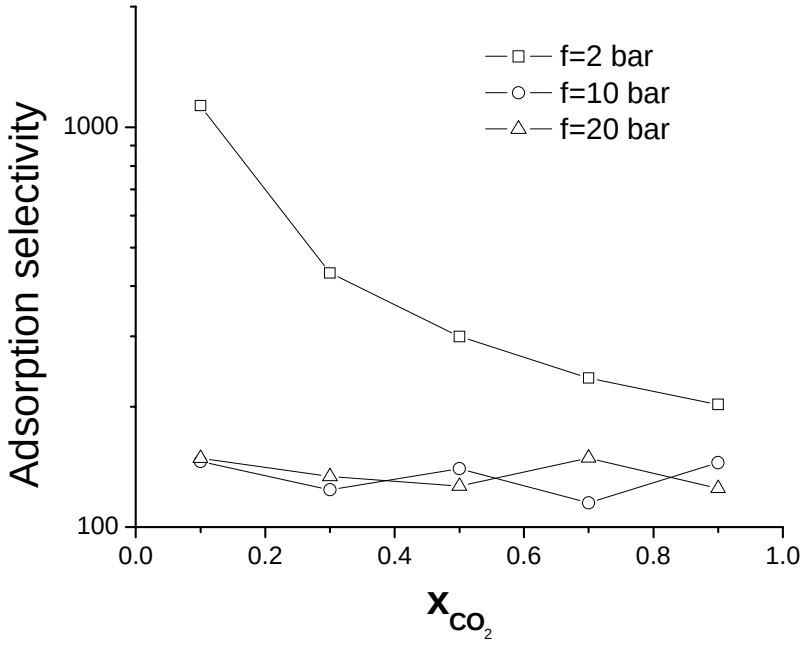

Fig 6.5: Room temperature binary adsorption selectivities of CO_2/CH_4 in SAS

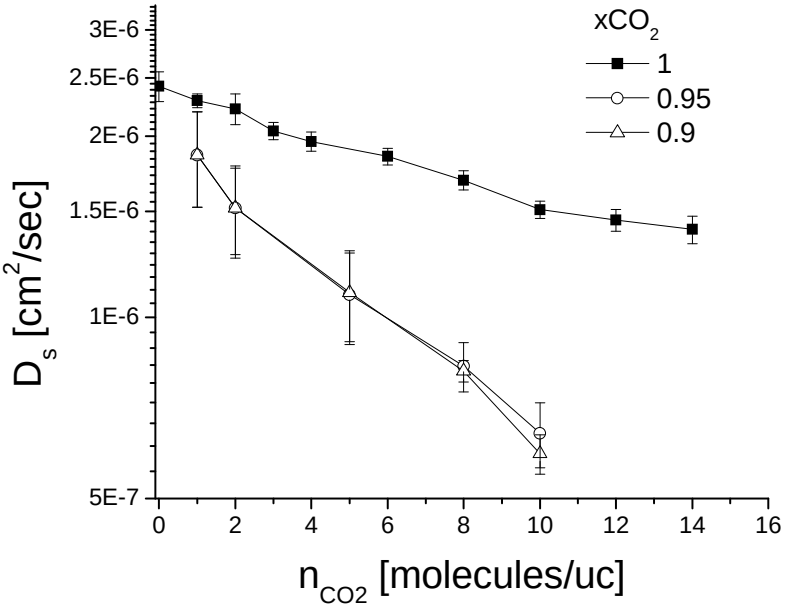

Fig 6.6: Room temperature single and binary component diffusivities of CO_2 computed with MD in SAS

6.3.2. TRANSPORT PROPERTIES OF CHA

The CHA has large cages which are interconnected with six 8MR windows (window size 0.38x0.38 nm) in 3 dimensions[3]. The shapes of the cage and its six windows are shown in Fig. 6.7. The cages are approximately spheroid shapes with the polar axis diameter of 0.11 nm and equatorial diameter of 0.8 nm. The calculated free energy profile between CH_4 and cage sites show that transition states exist in 8MR windows for CH_4 as it did in DDR. Although it has a similar structure to DDR, the slightly larger size 8MR windows in CHA might not cause as much difference in diffusion rates of CO_2 and CH_4 as in DDR. To examine the selectivities at all relevant conditions, the adsorption and diffusion properties were calculated for various compositions and pressures.

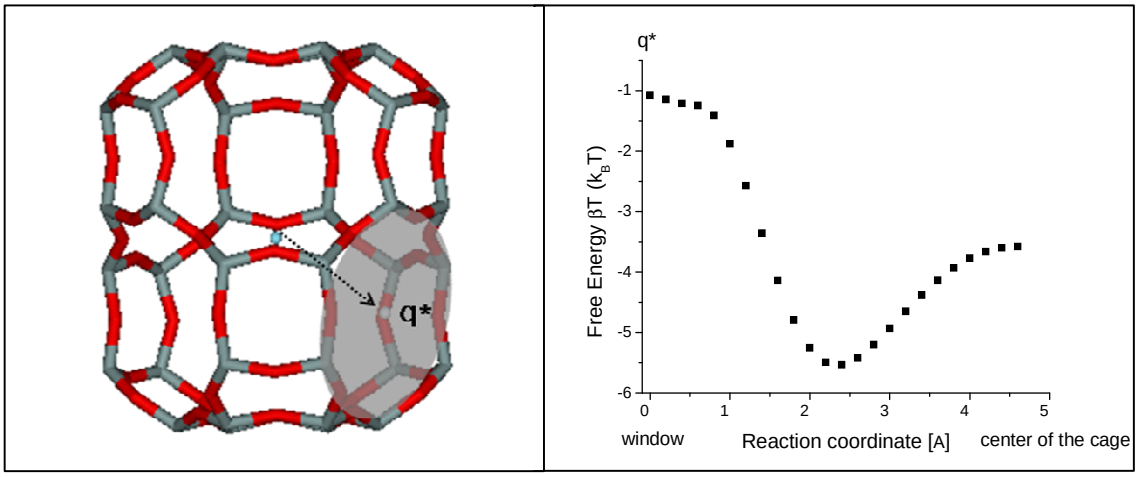

Figure 6.7: (left) View of cage of CHA and reaction coordinates for CH_4 molecule (right) The calculated free energy profile of CH_4 in CHA zeolite at infinite dilution at 298 K as a function of the reaction coordinate

Binary adsorption selectivities at various compositions are shown for a range of bulk compositions for three practically relevant fugacities in Fig. 6.8. The adsorption selectivities range over 3 to 12, showing higher selectivities than in DDR (Fig. 4.5) for

CO_2 rich bulk phase. We also examined the adsorbed amount of CO_2 and CH_4 in the cage and window sites separately to examine the segregation of the molecules at specific sites.

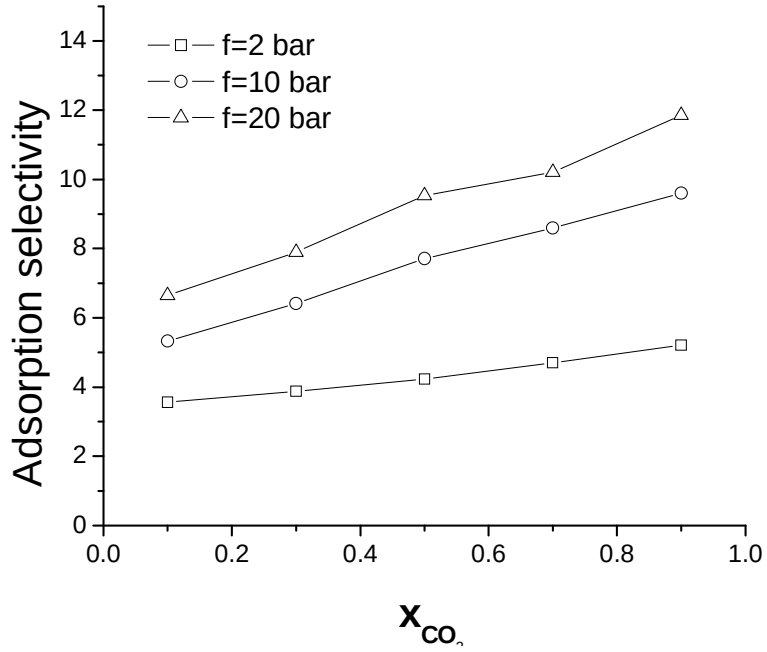

Fig 6.8: Binary adsorption selectivities of CO_2/CH_4 in CHA

Figure 6.9 shows the self diffusivities of CO_2 for adsorbed binary mixture. As shown, faster molecule CO_2 is slowed down by the CH_4 in CHA. For loadings of 10 CO_2 molecules/unit cell, the CO_2 diffusivity is reduced to <50% at adsorbed CO_2 composition is 0.9 when compared to the single component diffusivities. This decrease rate is larger than in DDR but still smaller than the interaction happening in other large pore zeolites. As shown in Fig. 6.10, CH_4 diffusivities are accelerated by the presence of CO_2, which is usual situation for the diffusion of the mixtures unlike in DDR. This is because it is difficult to block all of the six window sites per one cage in CHA, so CO_2 in the cage sites accelerated CH4 diffusion without blocking the pathways. Therefore, as a result, the selectivities of the diffusivities are expected to decrease significantly in the mixture than we expect from the single component data.

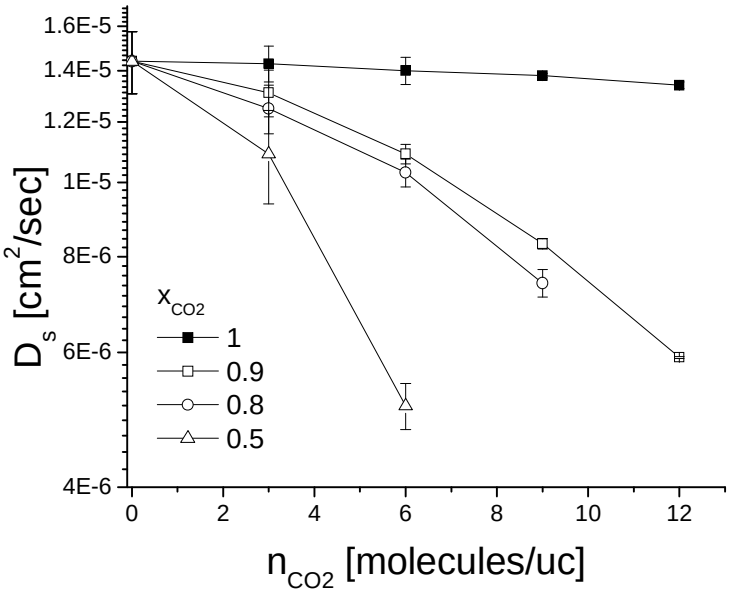

Fig 6.9: The self diffusivities of CO_2 in CHA for single component and binary mixtures for the entire compositions at bulk conditions

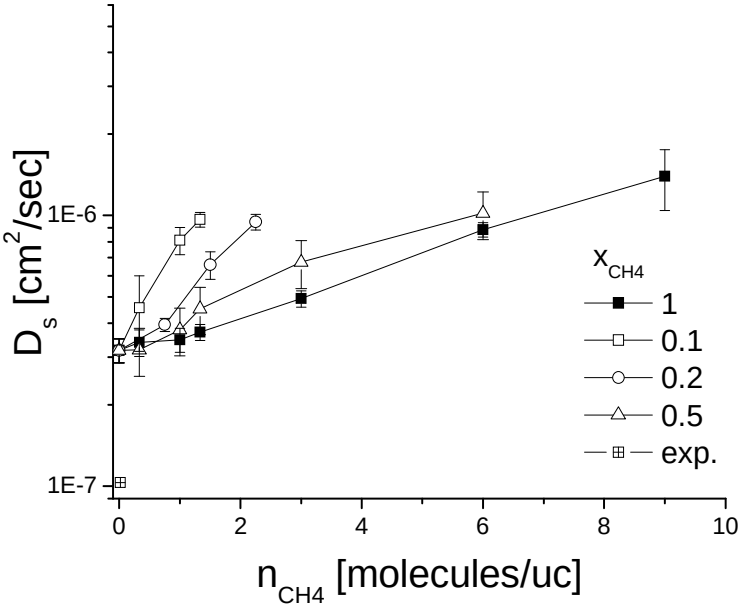

Fig 6.10: The self diffusivities of CH_4 in CHA for single component and binary mixtures for the entire compositions at bulk conditions

6.3.3. TRANSPORT PROPERTIES OF IHW

The structure of the all silica form of IHW (ITQ-32) was defined using atomic coordinates measured experimentally by Cantin[4]. IHW has a similar structure to DDR. One unit cell consists of large cages, leading to a material with relatively large micropore volume (0.17cm^3/g), interconnected with four 8MR oxygen windows (window size 0.35x0.43 nm) which are smaller than the window size of DDR (window size 0.36x0.44 nm). The cages are interconnected in the xz plane via four interconnecting windows while the cages are interconnected with three windows in the xy plane in DDR. The cages are approximately spheroid shapes with the polar axis diameter of 0.4 nm and equatorial diameter of 0.12 nm. Therefore, we could expect similar transport properties exist in IHW, which is favorable for CO_2/CH_4 separation.

Recent publications about IHW have started to provide data on gas adsorption. Palomino *et al.* experimentally measured the adsorption of propane and propene[15]. The adsorption isotherm of ethane, propane and nitrogen was investigated by Liu *et al.*[16] and Rahmati *et al.*[17]. To the best of our knowledge, there is not a reported study of CO_2/CH_4 separation by IHW to date. In this section, we use GCMC, MD and KMC simulations to study the CO_2/CH_4 single component and mixture adsorption and diffusion at relevant conditions to calculate membrane selectivities for IHW.

Figure 6.11 shows the calculated binary adsorption selectivities over a range of bulk compositions at three representative fugacities. The adsorption selectivities for CO_2 in IHW are 1.5~3.5, which are lower than those in DDR at low x_{CO2}. As we did for DDR, the adsorption associated with windows and cages was calculated to examine the segregation of CO_2/CH_4. When the center of the mass of the adsorbed molecules is located within 3.5 Å of the center of the window, they are defined as window sites and all other molecules are considered to be in the cage. Figure 6.12 shows the adsorbed molecules in equilibrium with equimolar CO_2/CH_4 bulk mixtures at these sites. CH_4 molecules only adsorb in the cage sites. CO_2 adsorbs in both sites but window sites aer

preferred. Figure 6.13 represents the CO_2 molecules per window as a function of total adsorbed amount of CO_2 in both single component and binary mixtures. As we observed in DDR, CO_2 adsorption in the window is almost independent of CH_4 loading, showing the competition between CO_2 and CH_4 molecules exist only in the cage. The binary adsorption shows that similar tendencies occur in IHW and DDR: CO_2 prefers window and cage sites while CH_4 only occupies cage sites. One difference between IHW and DDR is that IHW has larger cages, causing less CO_2 in the window sites. This might be important in CO_2/CH_4 diffusion since the presence of CO_2 in window sites is related with the blocking of CH_4 moves between cages.

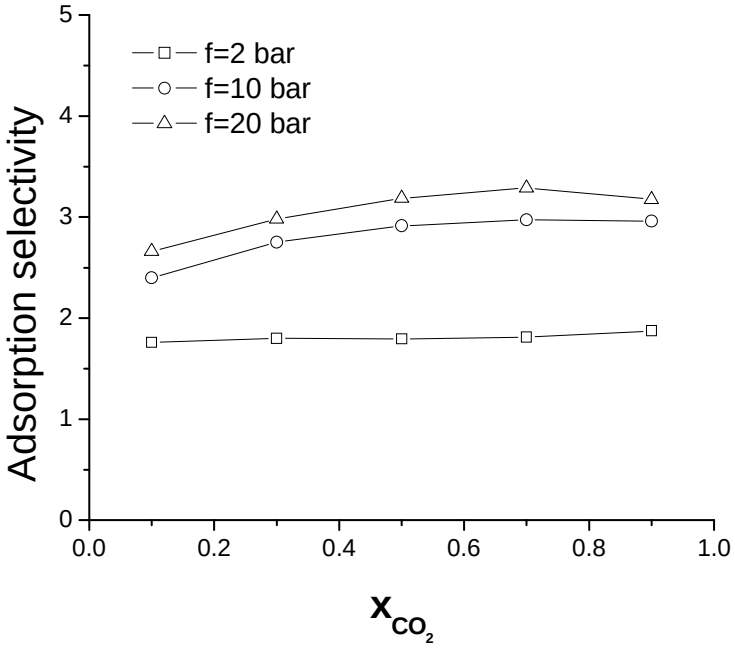

Figure 6.11: Room temperature binary adsorption selectivities of CO_2/CH_4 in IHW

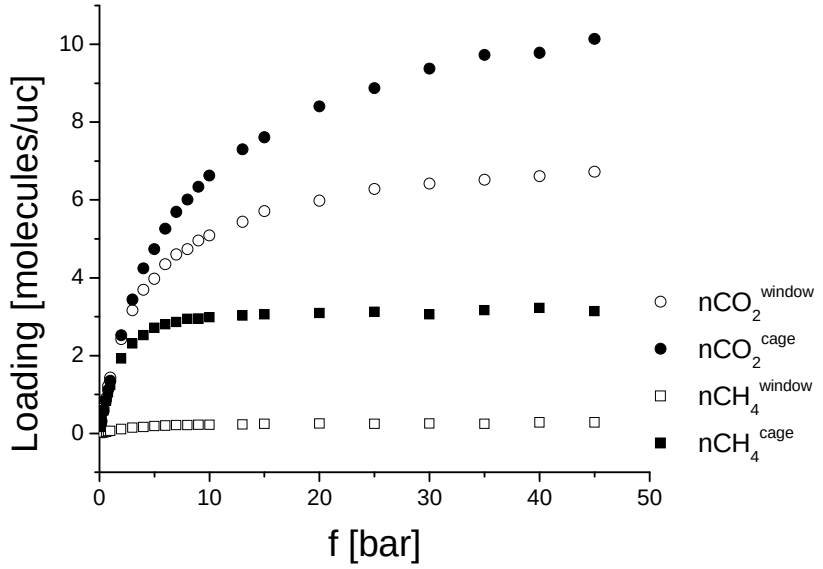

Fig 6.12: Binary component adsorption (open symbols) isotherms for equimolar bulk CO_2/CH_4 mixtures in IHW from GCMC simulations. Filled symbols show the adsorption in the cage while open symbols represent the adsorption in the windows.

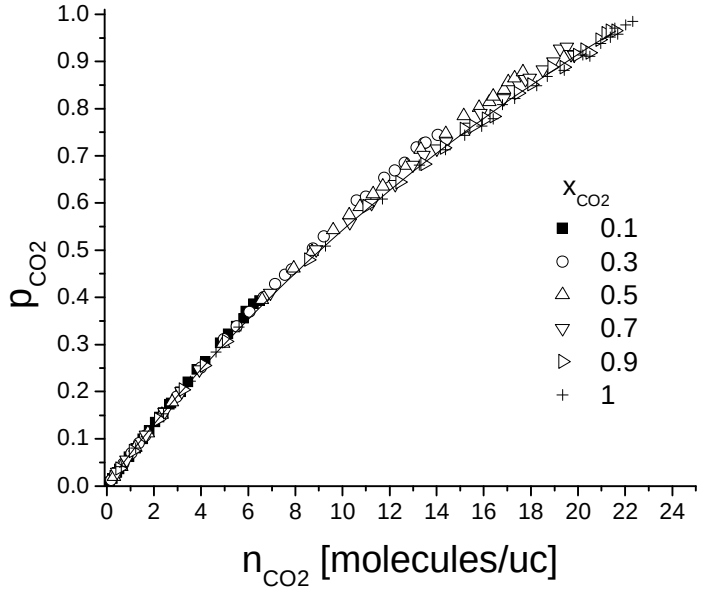

Figure 6.13: The probability that CO_2 molecules block the window sites as a function of CO_2 loading in IHW

As we discussed before in section 6.2, the diffusivity of CH_4 in IHW is slower than the measurable range accessible with MD. Therefore, we computed self diffusivities of CO_2 using MD and CH_4 using TST-KMC as we did for DDR in chapter 5. For MD simulations to measure CO_2 diffusion, the system was initialized by 1.5×10^7 canonical MC moves and 1.5×10^7 steps of MD for equilibration. The MD data was sampled for 20 ns with a 1 fs time step. CO_2 self diffusivities are shown as a function of the adsorbed CO_2 loadings for single component and mixtures in Fig. 6.14. For loadings of 7 CO_2 molecules/unit cell, the CO_2 diffusivity is reduced to <50% when compared to the single component diffusivities. The presence of CH_4 reduced CO_2 diffusion in IHW more than in DDR. However, considering CO_2 diffusivities are 2~3 orders of magnitude larger than CH_4 diffusivities, this decrease is likely to not be to be problematic for considering IHW as a membrane.

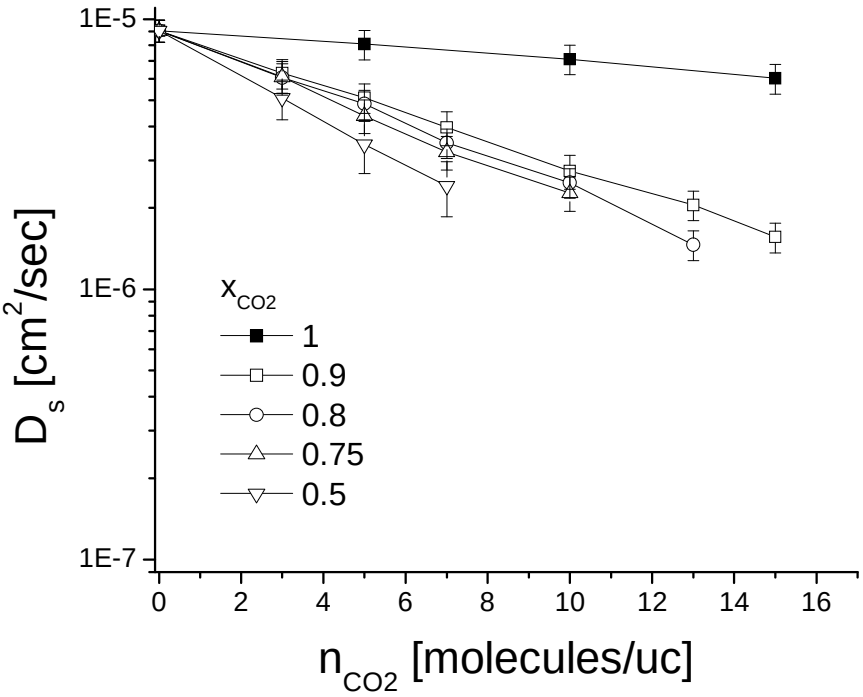

Fig 6.14: Self diffusivities of CO_2 shown as the adsorbed CO_2 loadings at single component and at various compositions of CH_4/CO_2 mixtures

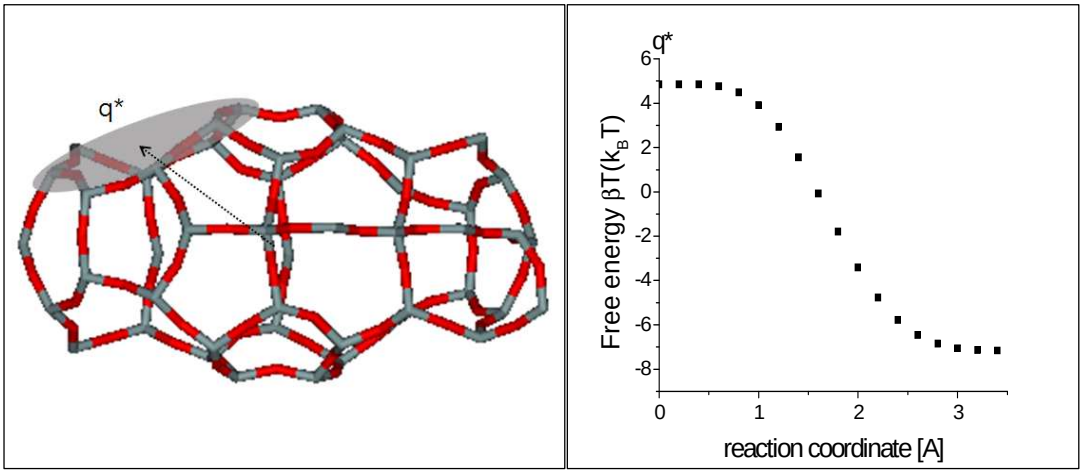

Figure 6.15: (left) View of cage of IHW and reaction coordinates for a CH_4 molecule. (right) The calculated free energy profile of CH_4 in IHW at infinite dilute loading at 298 K as a function of the reaction coordinate

To measure the CH_4 diffusivities in IHW, we used the TST-KMC method described in chapter 5 for CH_4 diffusion in DDR. To identify the transition state, we divided the volume of the cage and carefully determined the transition state for CH_4 molecules. Figure 6.15 shows the cage of IHW and the potential energy surface as a function of a reaction coordinate for a CH_4 molecule at infinite dilute loading. The dominant local energy minimum lies at the center of the cage and a line connecting the center of two adjacent cages defines a convenient reaction coordinate.

The transition rate for CH_4 molecule as a single component and in adsorbed mixtures was measured using Canonical Monte Carlo as described in chapter 2. Specifically, k_{ij} (N_i, N_j) was computed where N_i and N_j is the total number of molecules in adjacent cages *i* and *j*. For each rate calculation, 2×10^8 canonical MC moves per particle were used to equilibrate the system and 2×10^8 canonical moves per particle were used to produce data. Since we observed the maximum number of molecules per cage is <4 in adsorption, transition rates were calculated for N_i=1~3 and N_j=0~3. As seen in Fig.

6.16, the CH_4 hopping rates increase when the total number of molecules in cage *i* increases because of the decrease in energy barrier. The number of molecules in the cage *j* did not affect the transition states except when N_j is 3.

Using TST-based KMC, we examined CH_4 self diffusion at a range of mixture loadings. At each loading, the system was equilibrated for $>2.0\times10^5$ KMC steps per particle and data were produced from 8×10^5 steps per particle. Figure 6.17(a) shows the self diffusivities of CH_4 as a single component and for adsorbed with the mixtures at 0.1~0.5 x_{CH4} compositions. This choice of adsorbed phase composition cover a large range of bulk phase compositions because of IHW's adsorption selectivity. When CO_2 is present, the self diffusivities of CH_4 for the same adsorbed loadings increase compared to the single component diffusivities. This is different from what we observed from DDR, where CH_4 diffusivities are reduced by CO_2 molecules by blocking the windows, the transition state for CH_4 diffusion. We examined the effect from the the adsorbed CO_2 in the cage and window sites, which are two competing effects for CH_4 diffusion at x_{CH4}=0.25. This adsorbed phase compositions corresponds to approximately equimolar bulk mixtures. As can be seen from Fig. 6.17(b), the presence of CO_2 in the cage increased the diffusivities of CH_4 significantly, while the CO_2 in the window sites does not reduce the CH_4 diffusivities as much. As we showed above in Fig. 6.13, CO_2 adsorbs less into the window in IHW than in DDR. This causes the reduction of the window blocking effect by CO_2 molecules followed by the increase of diffusion rates of CH_4 by the presence of the CO_2.

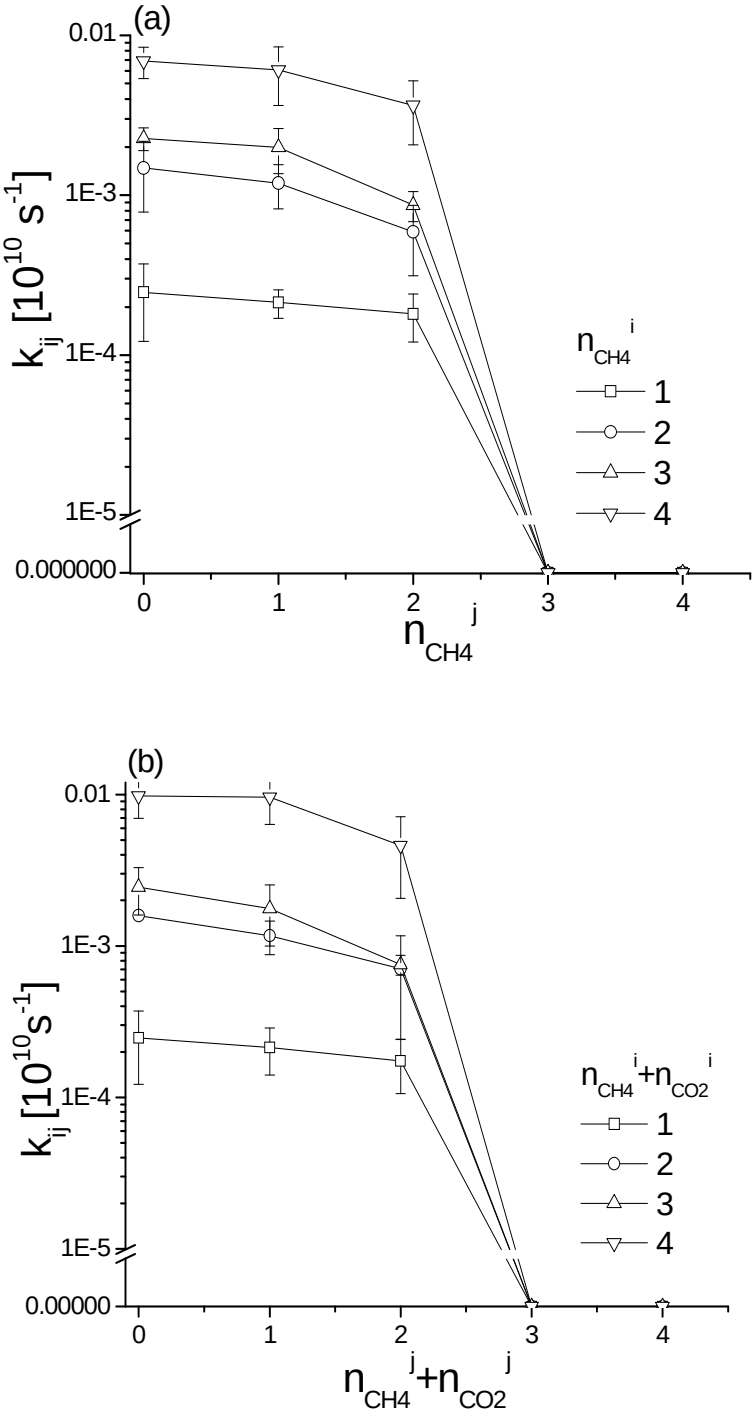

Figure 6.16: k_{ij} of CH_4 molecules cage *i* to cage *j* at single component (a) CH_4 and (b) in adsorbed CO_2/CH_4 mixtures

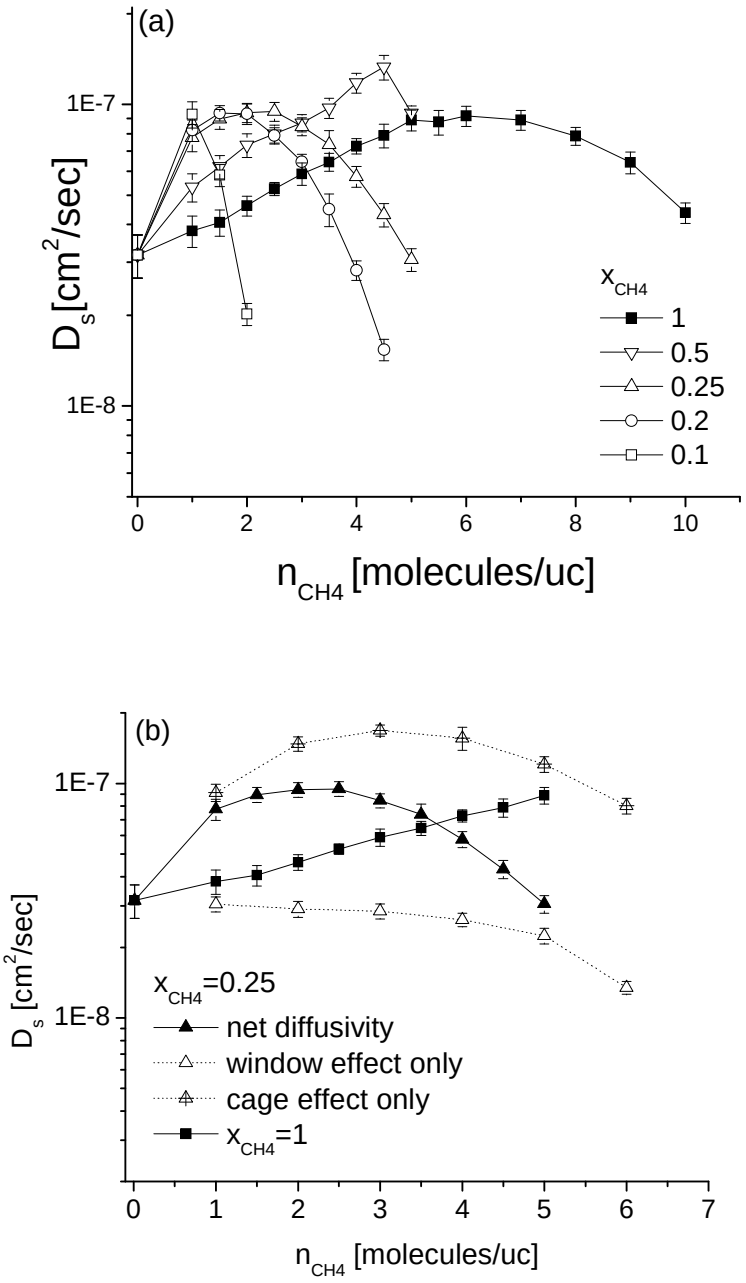

Figure 6.17: CH_4 diffusion data from CH_4/CO_2 mixtures in DDR, showing (a) self-diffusivities of CH_4 at various mixture compositions, and (b) the self diffusion of CH_4 in an approximately equimolar mixture at bulk conditions ($x_{CH_4} = 0.25$) showing the separate effects from cage occupation by CO_2 and window blocking by CO_2.

6.4 CONCLUSIONS

Our aim in this chapter was to examine separation ability of small pore zeolites that can be synthesized in pure silica form and find good candidates for CO_2/CH_4 separation. To screen the 10 possible structures efficiently, we initially calculated selectivities for binary adsorption and the self diffusivities using MD at loadings for 50:50 bulk compositions. Based on this screening, MTF, RWR, SAS, CHA and IHW were identified as potentially giving high selectivities for separation. The separation abilities of SAS, CHA, and IHW at various conditions were then measured using detailed calculation.

SAS has very high adsorption selectivities (>100) at all bulk compositions with considerable amount of CO_2 adsorption. The computed self diffusivities of CO_2 in this material are 10^{-6}~10^{-7} cm^2/sec. Therefore, SAS is a good candidate as a membrane for CO_2/CH_4 separation. The narrow, one dimensional pore of the MTF and RWR structures excluded the CH_4 adsorption, resulting very high selectivities at entire compositions. Although the adsorbed amount of CO_2 is smaller than in SAS structure, they could be considered as good candidates.

Adsorption isotherms and diffusivities for a large range of compositions in CHA and IHW were examined using detailed calculation. Although the structures of the CHA and IHW are similar, the detailed calculation results showed that slight differences in the structures, especially the 8MR size and the cage size, caused large differences in the diffusivities of the mixtures. In CHA, the faster molecule (CO_2) is retarded and the slower molecule (CH_4) is accelerated in the mixture as observed in mixture diffusion in large pore zeolites[18-22]. The 8MR window of IHW is even smaller than that of DDR, so only CO_2 is favored in the window sites. Thus, CO_2 diffusivities are not reduced by the presence of the CH_4 in IHW. However, the larger cage volume attracts the CO_2 molecules into the cage as well as window sites so, between the effect of the CO_2 in the cage and window, the effect from the cage sites is larger than for DDR. Because the small 8MR

windows leads to large differences in CO_2 and CH_4 diffusion rates, still the CO_2/CH_4 selectivity in diffusion might be large enough in IHW to make this material a good membrane.

The predicted membrane selectivities for the small pore zeolites we have considered for feeds with a 50:50 composition are shown in Fig.6.18 (a). The selectivities are calculated from the equation (6.3) using the calculation results in the previous section for CH_4 diffusion in IHW. For this feed composition, IHW, DDR and CHA showed high selectivities compared to other structures. More specifically, IHW gives the highest selectivities among these three zeolites while DDR and CHA selectivities are similar. Several experimental measurements are available from experiments for SAPO-34, analogous of the CHA in the literature though selectivities largely depend on the supports of the membrane[23-26]. The maximum experimental selectivities for CO_2/CH_4 separation are 180 for P_f=3bar[25], 171 P_f=2bar[26] while permeate pressure is 0.8 bar for equimolar mixtures, showing reasonable agreement with our predicted selectivities All three zeolites have selectivities that are high enough to make them excellent candidates as membranes. In Fig 6.18 (b) and (c) we show the calculated selectivities for 10:90 and 90:10 feed compositions for DDR, IHW and CHA. When the CO_2 composition is low in the feed, DDR shows highest selectivities at most pressures. CHA shows the highest selectivities at CO_2 rich feeds because of its high adsorption selectivities at this condition.

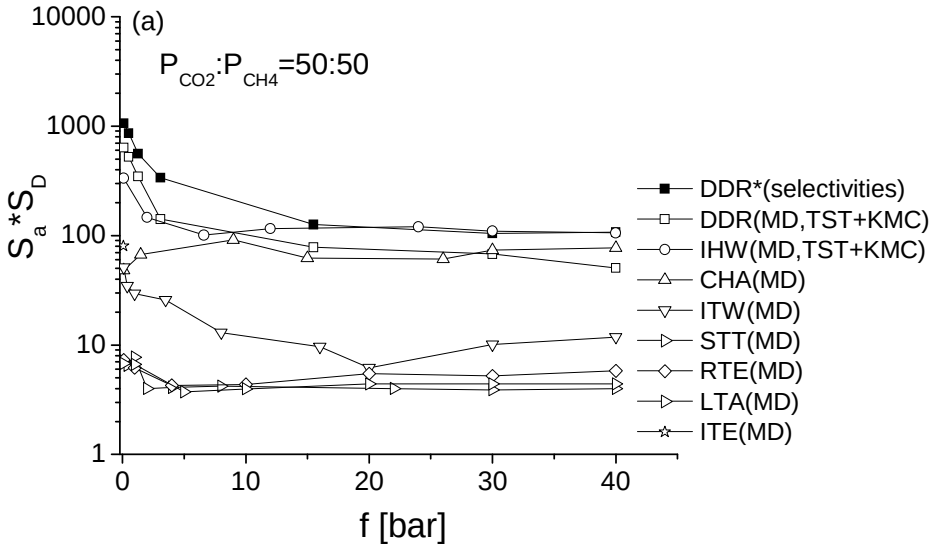
(a)
P_{CO2}:P_{CH4}=50:50
S_a*S_D
f [bar]
DDR*(selectivities)
DDR(MD,TST+KMC)
IHW(MD,TST+KMC)
CHA(MD)
ITW(MD)
STT(MD)
RTE(MD)
LTA(MD)
ITE(MD)

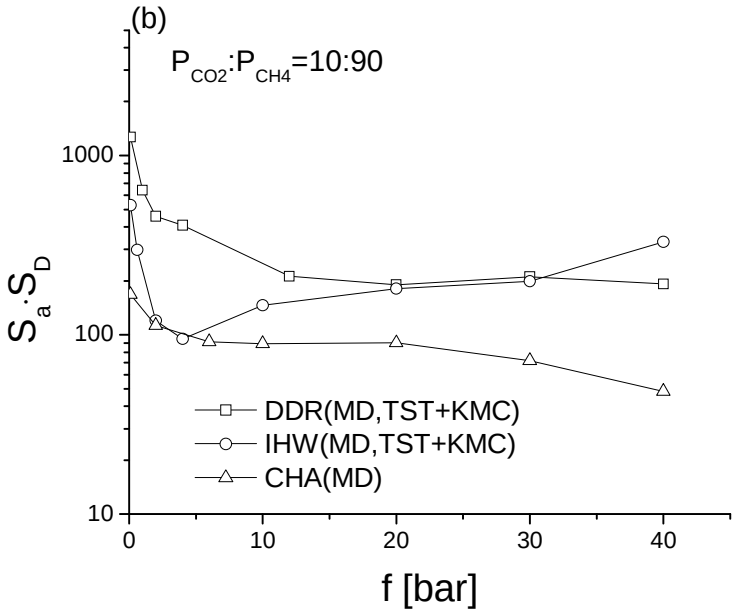
(b)
P_{CO2}:P_{CH4}=10:90
S_a·S_D
f [bar]
DDR(MD,TST+KMC)
IHW(MD,TST+KMC)
CHA(MD)

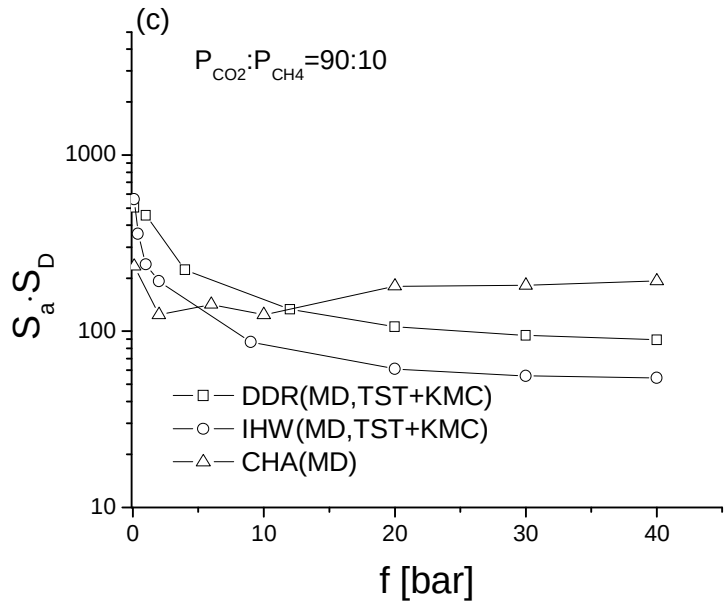

Figure 6.18: Selectivities of CO_2/CH_4 separation at various conditions $Sa \cdot S_D$ is calculated from the equation (6.3). CO_2/CH_4 diffusivities for CHA and CO_2 diffusivities for DDR and IHW were calculated using MD, while CH_4 diffusivities for DDR and IHW were calculated from TST-KMC.

REFERENCES

(1) Gies, H. *Z. Kristallogr.* **1986**, *175*, 93.
(2) Gramlich, V.; Meier, W. M. *Z. Kristallogr.* **1971**, *133*, 134.
(3) Calligaris, M.; Nardin, G.; Randaccio, L. *Zeolites* **1983**, *3*, 205.
(4) Cantin, A.; Corma, A.; Leiva, S.; Rey, F.; Rius, J.; Valencia, S. *J. Am. Chem. Soc.* **2005**, *127*, 11560.
(5) Camblor, M. A., Corma, A., Lightfoot, P., Villaescusa, L.A. and Wright, P.A. *Angew. Chem. Int. Ed.* **1997**, *36*, 2659.
(6) Yang, X. B.; Camblor, M. A.; Lee, Y.; Liu, H. M.; Olson, D. H. *J. Am. Chem. Soc.* **2004**, *126*, 10403.
(7) Barrett, P. A.; Diaz-Cabanas, M.-J.; Camblor, M. A. *Chem. Mater.* **1999**, *11*, 2919.
(8) Marler, B.; Stroter, N.; Gies, H. *Micropor. Mesopor. Mater.* **2005**, *83*, 201.
(9) Wragg, D. S.; Morris, R.; Burton, A. W.; Zones, S. I.; Ong, K.; Lee, G. *Chem. Mater.* **2007**, *19*, 3924.
(10) Camblor, M. A.; Diaz-Cabanas, M.-J.; Perez-Pariente, J.; Teat, S. J.; Clegg, W.; Shannon, I. J.; Lightfoot, P.; Wright, P. A.; Morris, R. E. *Angew. Chem. Int. Ed.* **1998**, *37*, 2122.
(11) Marler, B.; Grunewald-Luke, A.; Gies, H. *Zeolites* **1995**, *15*, 388.
(12) Keskin, S.; Sholl, D. S. *Langmuir* **2009**, *25*, 11786.
(13) Vasenkov, S.; Schuring, A.; Fritzsche, S. *Langmuir* **2006**, *22*, 5728.
(14)Kukla, V.; Kornatowski, J.; Demuth, D.; Girnus, I.; Pfeifer, H.; Rees, L. V. C.; Schunk, S.; Unger, K. K.; Karger, J. *Science* **1996**, *272*, 702.
(15) Palomino, M.; Cantin, A.; Corma, A.; Leiva, S.; Rey, F.; Valencia, S. *Chem. Commun.* **2007**, 1233.
(16) Liu, B.; Smit, B.; Rey, F.; Valencia, S.; Calero, S. *J. Phys. Chem. C* **2008**, *112*, 2492.
(17) Rahmati, M.; Modarress, H. *J. Mol. Struct.: THEOCHEM* **2009**, *901*, 110.
(18) Skoulidas, A. I.; Sholl, D. S.; Krishna, R. *Langmuir* **2003**, *19*, 7977.
(19) Skoulidas, A. I.; Sholl, D. S. *J. Phys. Chem. A* **2003**, *107*, 10132.
(20) Skoulidas, A. I.; Sholl, D. S. *J. Phys. Chem. B* **2002**, *106*, 5058.
(21) Krishna, R.; van Baten, J. M.; Garcia-Perez, E.; Calero, S. *Chem. Phys. Lett.* **2006**, *429*, 219.
(22) Krishna, R.; van Baten, J. M. *Chem. Eng. Sci.* **2008**, *63*, 3120.
(23) Poshusta, J. C.; Tuan, V. A.; Pape, E. A.; Noble, R. D.; Falconer, J. L. *Ind. Eng. Chem. Res.* **1998**, *37*, 3924.
(24) Li, S. G.; Falconer, J. L.; Noble, R. D. *Adv. Mater.* **2006**, *18*, 2601.
(25) Li, S. G.; Falconer, J. L.; Noble, R. D. *J. Membr. Sci.* **2004**, *241*, 121.
(26) Carreon, M. A.; Li, S.; Falconer, J. L.; Noble, R. D. *J. Am. Chem. Soc.* **2008**, *130*, 5412.

CHAPTER 7

CONCLUSIONS

In this thesis, we examined the effect of the pore dimension of zeolites on the separation of gas mixtures using atomistic simulation methods. Among the large number of zeolite structures, zeolites with small pores are considered as particularly good candidates for separation of light gas mixtures based on the idea that having pores with a similar size to the size of the species being separated could lead to large differences in diffusion rates, and therefore high selectivities. In this thesis, we studied two categories of the zeolites with small pores: pore modified silicalite for H_2/CH_4 separation and small pore silica zeolites for CO_2/CH_4 separation.

Although zeolites are widely used, their transport properties are not entirely understood. The diffusion properties of adsorbed molecules, which are expected to be a key factor in determining the flux of molecules through small pore zeolites, are very difficult to measure experimentally. Molecular simulation methods can play an important role in understanding of the physical origins of high separation selectivities for zeolites with specific pore dimensions and consequently, aid in the identification of additional materials for related applications.

In the first section of this thesis, the effect of pore modification of silicalite on the H_2/CH_4 separation was examined. We developed methods to mimic the chemical vapor deposition of Si and O atoms near the surface of a silicalite crystal, and examined the flux of CH_4 and H_2 through the resulting materials using the Local Equilibrium Flux Method. Under some degrees of surface modification, the CH_4 flux was reduced much more than the H_2 flux, resulting in high ideal selectivities. This observation indicates that careful control of surface modifying layers may be a useful means of tailoring the performance of zeolite membranes for H_2 separations.

In the remainder of the thesis, the use of small pore zeolites for CO_2/CH_4 separations was examined. First, we examined the transport properties of these two species in DDR. Our simulations introduced a new forcefield for DDR, which is transferrable to other small pore zeolites, that for the first time gives results that are consistent with experimental measurements of single component adsorption and diffusion. Diffusivities obtained from previous simulations greatly overestimated the transport rates of CH_4, and to a lesser extent, CO_2. Since CH_4 diffuses extremely slowly in DDR, we developed a Binary Kinetic Monte Carlo scheme to accurately describe the diffusion transport of CO_2/CH_4 mixtures. The most important observation from our calculations is that the characteristics of CO_2/CH_4 diffusion in DDR are very different from the usual situation in nanoporous materials, where the presence of a slowly diffusing species retards transport of a more rapidly diffusing species. In DDR, we showed that CO_2 diffusion rates are only weakly affected by the presence of CH_4, even though the latter molecules diffuse very slowly. Consequently, therefore, the permeance of CO_2 in the equimolar mixtures is similar to the permeance for pure CO_2, while the CH_4 permeance in the mixture is greatly reduced relatively to the pure component permeance. The calculated CO_2/CH_4 separation selectivities are higher than 100 for a wide range of feed pressure, indicating excellent separation capabilities of DDR based membranes. The physical origins of this unusual behavior are explained by different adsorption sites for CO_2 and CH_4 and diffusion mechanism for each species. Good agreement between our predictions and experimentally measured selectivities from the literature confirmed that our description of the transport properties of molecules in DDR is reasonable.

Inspired by the fact that the small pores of DDR is the main factor that makes it possible to to achieve high separation selectivities with this zeolite, we also examined the

separation capabilities of 10 additional pure silica small pore zeolites for CO_2/CH_4 separations. To model these small pore zeolites we used the forcefields derived from our initial work on DDR. By adapting screening methods that have been developed for other crystalline nanoporous materials, we identified a number of interesting materials which are predicted to have high separation selectivities based on calculations for equimolar bulk mixtures. Based on this screening method, the silica zeolites SAS, MTF, RWR, CHA and IHW were identified as potentially giving high selectivities for CO_2/CH_4 separations. The separation abilities of these materials at various conditions were then described using more detailed calculations using the GCMC, MD and TST-KMC methods we developed for DDR. From these considerations, we predict that SAS, MTF and RWR will exhibit high separation selectivities because of their very high adsorption selectivities for CO_2 over CH_4. CHA and IHW, which have similar pore structures to DDR, showed comparable separation selectivities to DDR. That is, these zeolites are predicted to have moderate adsorption selectivity but a high overall selectivity when used as membranes because of large differences in the diffusion rates of CO_2 and CH_4. These calculations are a useful example of using atomically-detailed molecular simulations to focus experimental efforts on materials that have potential value for chemical separations with large-scale applications.